A COMPARISON OF THEORETICAL AND EXPERIMENTAL REDUCTION FACTORS FOR LOCATIONS IN THE BASEMENT OF A TYPICAL HOUSE

by

CHARLES ARTHUR BURRE

B.S., University of Kansas, 1967

A MASTER'S THESIS

submitted in partial fulfillment of the

requirements for the degree

MASTER OF SCIENCE

Department of Nuclear Engineering

KANSAS STATE UNIVERSITY

Manhattan, Kansas

1970

Approved by

M. John Robinson

Richard E. Faw

Major Professors

TABLE OF CONTENTS

ILLEGIBLE DOCUMENT

THE FOLLOWING DOCUMENT(S) IS OF POOR LEGIBILITY IN THE ORIGINAL

THIS IS THE BEST COPY AVAILABLE

THIS BOOK CONTAINS NUMEROUS PAGES WITH DIAGRAMS THAT ARE CROOKED COMPARED TO THE REST OF THE INFORMATION ON THE PAGE.

THIS IS AS RECEIVED FROM CUSTOMER.

LIST OF TABLES

LIST OF FIGURES

1.0 INTRODUCTION

The threat of nuclear warfare has prompted many people to investigate the problem of protecting a civilian population from the wide-ranging effects of nuclear weapons. Most of these investigations have been encouraged, financed, and coordinated by the Office of Civil Defense (OCD). A unique characteristic of nuclear-weapons effects is radioactive fallout which can be a hazard to life many miles from any physical damage produced by the weapon. If a population is to be protected, it must be shielded from fallout radiation. Rather than constructing shelters for this express purpose, economic and other considerations have led to the philosophy of seeking sheltered areas in existing buildings.

The study of buildings with respect to the penetration of fallout radiation is referred to as structure shielding. A remarkably flexible methodology has been developed which enables one to evaluate the protection afforded by almost any type of structure. Data from involved radiation transport calculations have been reduced to a set of simple functions which are presented as graphs. The procedure specifies how these functions are used to give an estimate of the relative value of a structure as a fallout shelter. This methodology is referred to as the "Engineering Manual" and is fully described in an OCD publication [1].

Experiments have, in general, verified the predictions of the Engineering Manual with one notable exception. The protection in the basement of some structures seems to be overestimated. Whether or not the current theory is valid for a location in the basement of a residential structure is a vital question in civil defense planning. To obtain more information on this question, a contract was let to Kansas State University by OCD. The contract

(OCD Contract DAHC20-67-C-0196) called for 1) the construction of a typical one-story, 30×40 ft, house with a full basement and 2) a thorough experimental study inside the house with simulated fallout radiation. The design of the house was such that the thickness of the exterior walls, the heights of the floor and exposed foundation walls, and the position of the interior partitions could be varied.

The relative protection afforded at a particular location inside a structure is expressed quantitatively by a number called the reduction factor, which is defined in Section 2.0. There have been a number of proposed modifications to the Engineering Manual which are designed to give better agreement between experiment and theory for basement locations. The main objective of this work is a comparison of the results of the various theoretical models with the reduction factors measured in the test house. Comparison is made with the experimental results from two configurations of the house. In one series of experiments the exterior walls had a mass thickness of 5.5 pounds per square foot, while in the other the mass thickness of the exterior walls was 45.5 pounds per square foot. Both house configurations featured the floor at ground-level and no interior partitions. The reduction factor was measured at nineteen locations in the basement of the house.

Since the Engineering Manual theory is a refinement of concepts familiar to the nuclear engineer or physicist, an attempt, though incomplete, has been made to explain some of the notation peculiar to this theory. Much of Section 2.0 is devoted to explaining the underlying assumptions and basic approaches of the theory.

Incidental to this work was the development of a computer code which

could perform Engineering Manual calculations for any location in the test house for any proposed combination of the house parameters. A description of this code is included as an appendix to this work.

2.0 ENGINEERING MANUAL THEORY

2.1 Idealization of the Problem

The fundamental question in structure shielding is how much protection will a given building provide from fallout radiation. To formulate a general methodology for answering such a question, it is necessary to idealize the problem with respect to the radiation sources and geometry.

Radioactive fallout consists of small particles of debris which have been contaminated with, or are composed entirely of, fission products arising from the detonation of a nuclear warhead. These particles are carried about by air currents and eventually settle to the ground. Predicting the distribution of fallout is a complex problem involving many variables (e.g., type of burst, distance from ground-zero, and wind conditions). For the purpose of structure analysis, it is assumed that the fallout is uniformly distributed over all surfaces in proportion to the horizontal projection of the surface.

Fission products emit alpha, beta, and gamma radiation. However, the ranges of alpha and beta particles are so small that these radiations can be neglected in the structure shielding problem. The radiation to be considered is the gamma spectrum from mixed fission products. Mixed fission products are composed of isotopes of many elements, most of which are unstable and reach stability through a series of nuclear transformations. This causes the gamma-ray energy spectrum to change in shape as well as intensity as the various isotopes decay. To reduce the complexity of the problem, an energy spectrum at a fixed time after fission is chosen to characterize fallout radiation. The spectrum chosen, for reasons given in the references [1, 2], is the gamma-ray spectrum of 1.12 hour-old fission products.

The immediate surroundings of the structure affect the radiation field

in which the structure exists. As a standard location it is assumed that the building is situated in an infinite, flat field. The Engineering Manual takes into account such things as isolated areas of contamination, ground roughness, and mutual shielding of adjacent buildings; however, these techniques are not dealt with in this work.

2.2 The Radiation Field from a Plane Isotropic Source

Having specified the source type and the geometry of the idealized problem, one can proceed with the description of the resulting radiation field. The concept of detector response is used to describe quantitatively the various components of the radiation. This, of course, implies integration over the photon energies. Specifically, the quantity exposure, in units of roentgens, is used since this is the quantity usually measured in experiments.

The Boltzmann transport equation describes the transport, diffusion, and energy loss of gamma radiation. Solutions to this equation can be obtained by the method of moments for infinite media cases and by Monte Carlo methods for finite media. Using the former method, Spencer [2] has generated sets of data which are numerical solutions to the transport equation. From his results the structure-shielding methodology of the Engineering Manual (EM) has been formulated.

The response of a directional detector located a height d above the source plane is expressed by means of a "dose angular distribution" $\ell(d,\cos\theta)$. The angle θ is the polar angle, where the polar axis is the perpendicular line from the detector to the source plane. Since there is azimuthal symmetry, $\ell(d,\cos\theta)$ refers to the response from all azimuthal directions at a fixed polar angle. The function $\ell(d,\cos\theta)$ is normalized such that the integral over all θ at a detector height of three feet in air (at 20°C and 760 mm of Hg) is unity. The un-normalized value of this integral is referred to as D_o

the standard, or reference, dose rate. Thus $D_o \times \ell(d,\cos\theta)\sin\theta d\theta$ is the dose rate, in roentgens per unit time, from gamma photons reaching the detector between the polar directions θ and $\theta+d\theta$. Figure 1 is a plot of this function for various heights in air.

The radiation which contributes to the portion of the dose angular distribution from $\cos\theta=0$ to $\cos\theta=1$ is referred to an direct radiation, while that from $\cos\theta=-1$ to $\cos\theta=0$ is referred to as skyshine. Direct radiation includes not only the unscattered photons but also any photon which reaches the detector after suffering its last scattering interaction below the detector plane. The skyshine component is composed entirely of scattered photons reaching the detector after suffering their last scattering interaction above the detector plane.

2.3 Essentials of Engineering Manual Theory

2.3.1 Solid Angle Fractions

An important quantity in dealing with the directional response of a detector inside a structure is the solid angle fraction ω. It is defined as the solid angle subtended by a surface in units of 2π steradians. The formulas for computing the solid angle fractions at a point D subtended by two frequently encountered surfaces are shown in Fig. 2 along with the necessary geometry. These formulas are obtained by integration in spherical polar coordinates [3(Vol. III)].

2.3.2 Effective Mass Thickness

A characteristic of the attenuation of gamma radiation proved fortunate in the application of the transport calculations. This characteristic is

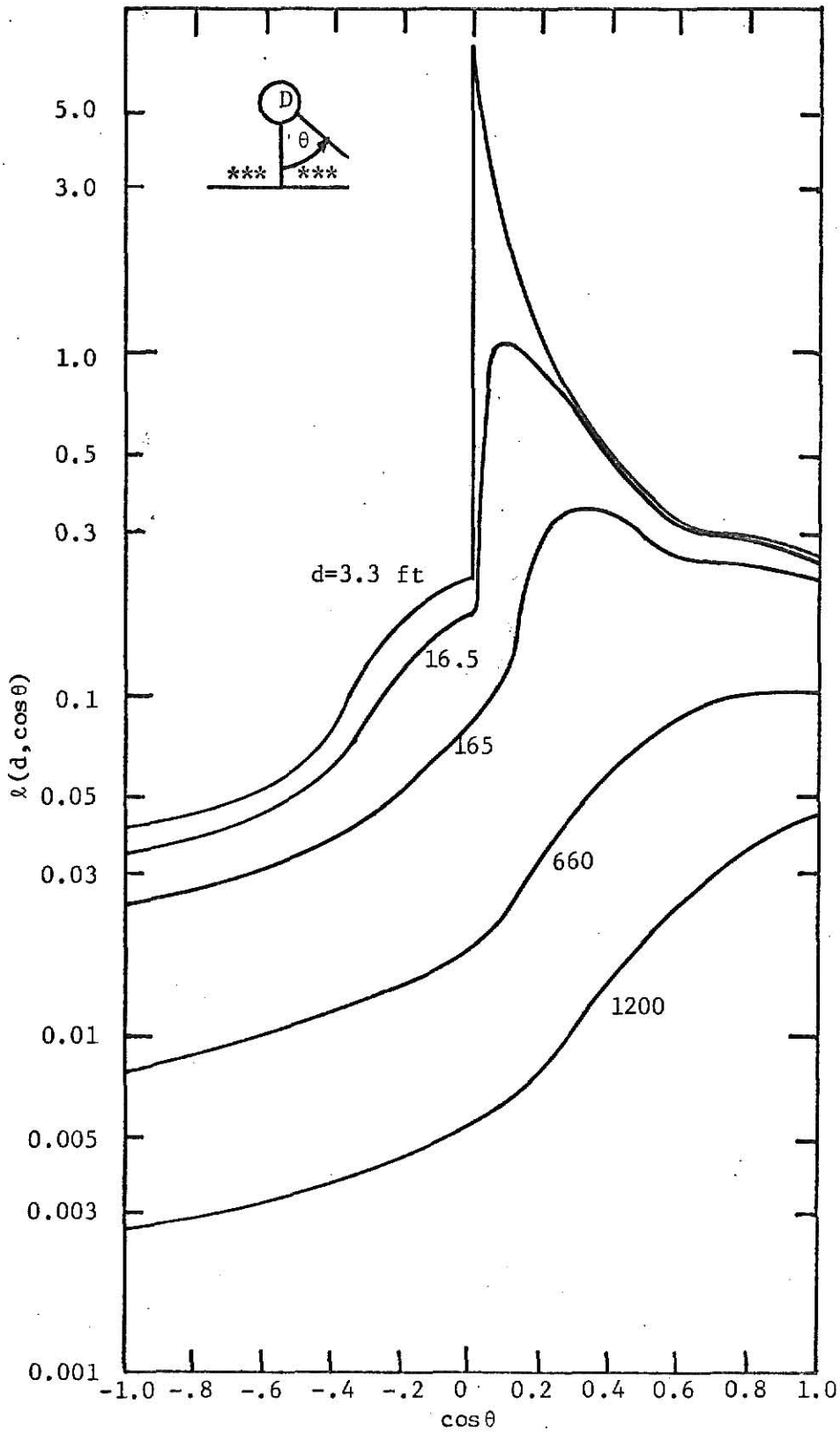

Figure 1. The dose angular distribution $\ell(d,\cos\theta)$ from a plane isotropic source of fallout radiation at different heights d in air.

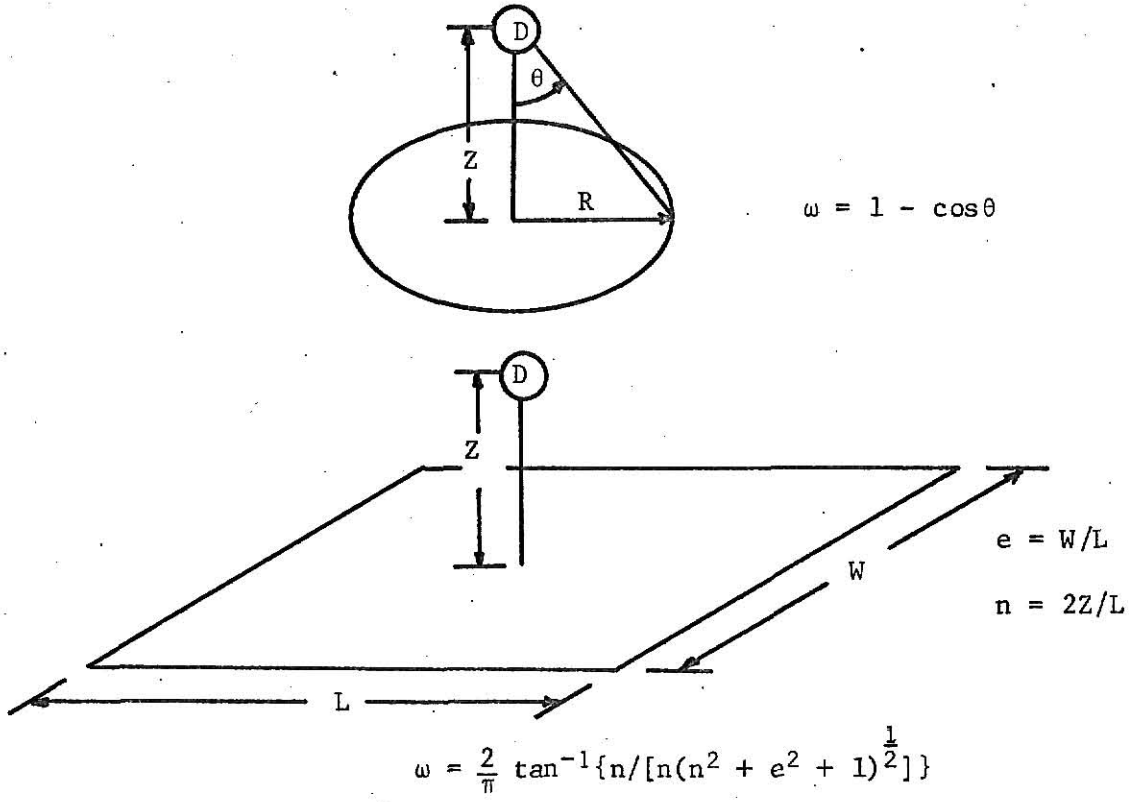

Figure 2. Solid angle fractions for a circular area and a rectangular area.

that attenuation in different materials of low atomic mass is nearly the same when distances are scaled by the corresponding electron densities. For a given material, the electron density is proportional to $\rho Z/A$, where ρ is the density, Z is the atomic number, and A is the atomic weight. The values of $2Z/A$ for materials important to structure shielding are 1.0 (air, concrete, and brick), 1.06 (wood), 1.1 (water), and 0.931 (steel) [2]. A scaled quantity called effective mass thickness enables one to apply the results of calculations performed in one medium to other media. The effective mass thickness X of a barrier of linear thickness Δx is given by

$$X = 2(Z/A)\rho\Delta x \qquad (1)$$

where ρ is the density of the material in pounds per cubic foot, Δx is in feet,

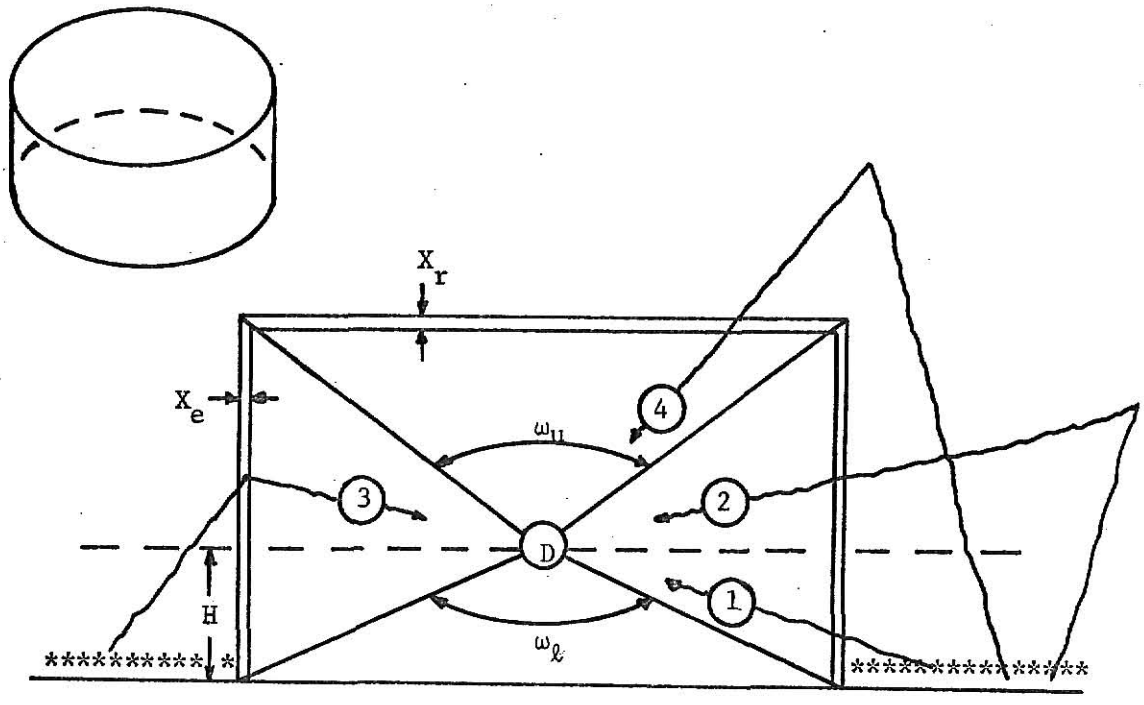

Figure 3. The contributions from ground sources to a detector inside a simplified building.

and X is in pounds per square foot (psf).

2.3.3 The Reduction Factor

Figure 3 shows a simple "pill box" building which is situated in a fallout field* A detector is located in the center of this building at a height H above grade. The solid angle fractions ω_u and ω_ℓ indicate those directions which intercept the roof and the floor, respectively. There are four significant categories of paths which the radiation can take to reach the detector: 1) it can pass through the walls coming from a direction below the plane of the detector, 2) it can pass through walls from a direction above the detector plane after having scattered in the air, 3) it can scatter in the walls

* Normally the roof of the building would be covered with fallout. However, since the experiments were conducted with ground sources only, the contribution from roof sources will not be discussed in this work.

emerging in a direction towards the detector, or 4) it can pass through the roof. The detector response D may be written as the sum of these four contributions;

$$D = D_1 + D_2 + D_3 + D_4 \ . \tag{2}$$

Each of these responses, or dose rates, depend linearly on the intensity of the source. This dependency may be eliminated by dividing each term by the standard dose rate D_o (see Section 2.2). The resulting terms are of the form (D/D_o) and are called reduction factors. In terms of reduction factors, Eq. (2) becomes

$$R_f = R_{f_1} + R_{f_2} + R_{f_3} + R_{f_4} . \tag{3}$$

This equation summarizes the basic approach of the EM. The contribution to the detector response is expressed as a sum of partial contributions, each of which has peculiar characteristics. Generally, each partial contribution is expressed as the product of geometry and barrier factors which are defined below.

2.3.4 Geometry Reduction Factors

A geometry reduction factor for a given contribution represents the ratio of the detector response from the allowable directions for that contribution to the response from all directions. For D_1 in Fig. 3, the allowable directions are those in the lower hemisphere between the horizontal plane and the solid angle fraction ω_ℓ. The geometry reduction factor for direct radiation is labelled $G_d(\omega_\ell, H)$ and is defined by

$$G_d(\omega_\ell, H) = \frac{\int_0^{1-\omega_\ell} \ell(H, \cos\theta)\, d(\cos\theta)}{\int_{-1}^{1} \ell(H, \cos\theta)\, d(\cos\theta)} . \tag{4}$$

The dependence on H, the detector height, is necessary because the shape of the dose angular distribution for direct radiation changes markedly with height, which can be seen in Fig. 1. Since the shape of the skyshine distribution is relatively insensitive to variations in height, the geometry reduction factor for skyshine $G_a(\omega)$ is defined for a height of three feet and assumed to be independent of height;

$$G_a(\omega) = \frac{\int_{-1-\omega_u}^{0} \ell(3', \cos\theta)\, d(\cos\theta)}{\int_{-1}^{1} \ell(3', \cos\theta)\, d(\cos\theta)} + \alpha(\omega) \qquad (5)$$

where $\alpha(\omega)$ is a small correction factor for the reflection of radiation from the ceiling. Since there are no theoretical data for the angular distribution of the scattered radiation emergent from a vertical wall, it is assumed that the θ dependence of this distribution is identical to that of skyshine for either direction about the horizontal. The geometry factor for wall-scattered radiation is labelled $G_s(\omega)$ and represents the response from those directions, in either the upper or lower hemisphere, defined by the detector plane and the solid angle fraction ω.

The functions $G_d(\omega,H)$ and $G_a(\omega)$ represent the response from non-wall-scattered radiation. When the walls of a structure have nonzero mass thickness, these functions must be weighted by the fraction of radiation which has not been scattered in the walls. This weighting factor is of the form $[1-S_w(X_e)]$; where $S_w(X_e)$ represents the ratio of the scattered to the total dose rate for a barrier of mass thickness X_e. The scattered fraction has been derived from buildup factor calculations. Since $G_s(\omega)$ represents the response to wall-scattered radiation, it must be weighted by $S_w(X_e)$.

When the plan of the structure is rectangular rather than circular, the functions $G_d(\omega_\ell,H)$ and $G_a(\omega_u)$ should adequately describe the directional

response when the solid angle fractions ω_ℓ and ω_u are defined by the rectangular areas of the floor and ceiling, respectively. However, if the angular distribution of the wall-scattered radiation is not isotropic in the azimuthal directions (angles in the horizontal plane with respect to the normal to the wall), the shape of the wall plan will affect the detector response. Since this azimuthal distribution is known to be peaked about the normal, Eisenhauer has derived a shape correction factor based on the assumption that the distribution is proportional to the cosine of the azimuthal angle [4]. The factor is labelled E(e) and has the analytic form

$$E(e) = (1 + e)/(1 + e^2)^{\frac{1}{2}} \tag{6}$$

where e is the ratio of width to length of the rectangle. For a circular wall plan, $E = \pi/2$. This correction factor must be applied to the geometry factor $G_s(\omega)$.

2.3.5 Barrier Reduction Factors

The magnitude of the incident spectrum and the absorption in the mass of the exterior walls is taken into account by a barrier reduction factor labelled $B_e(X_e,H)$. It is derived from the infinite medium calculations of Spencer. The dependence on the detector height reflects 1) the decrease in the magnitude of the incident spectrum due to absorption in the intervening layer of air and 2) the increased effective thickness of the walls due to changing incident angular distribution (see Fig. 1). It is normalized such that its value is unity at X_e=0 and H=3 ft.

The absorption in other types of barriers, such as floors, ceilings, and interior walls, is taken into account by attenuation factors which depend only on the mass thickness of the barrier. An attenuation factor is defined

as the ratio of the detector response with the given barrier in place to the response when the barrier is removed.

2.3.6 The Functional Expression

When the factors described above are appropriately combined, an expression for the reduction factor is obtained in terms of the EM functions. For the situation pictured in Fig. 3, the functional expression is

$$R_f = \{[G_d(\omega_\ell,H) + G_a(\omega_u)][1 - S_w(X_e)] + [G_s(\omega_\ell) + G_s(\omega_u)]S_w(X_e)E(e)\}B_e(X_e,H) + R_{f_4} . \quad (7)$$

The last term in Eq. (7) is the reduction factor for the skyshine contribution through the decontaminated roof. Its discussion is deferred until Section 2.4.2.

2.4 The Ground Contribution to the Reduction Factor at a Basement Location.

2.4.1 Terminology

The primary interest of this work is attenuation in the floor slab separating the basement from the first story of a simplified one-story structure. This effect was originally taken into account in the first editions of the EM [1,5] by a simple attenuation factor labeled $B'_o(X'_o)$, where X'_o refers to the mass thickness of the basement ceiling (the floor of the first story). It was renamed $B_c(X_c)$ in the July 1967 edition of the EM and modified to include a solid angle dependence, $B_c(X_c,\omega)$, in the July 1969 edition. The original factor and subsequent modifications of it have been referred to as "overhead barrier factor," "ceiling barrier factor," "floor barrier factor," and "ceiling attenuation factor." The last term is used herein when a verbal reference is required, while the symbolic references are $B'_o(X_c)$ for the

original factor and $B_c(X_c,\omega_u)$ for the modified factor.

2.4.2 The Functional Expression with the Original Ceiling Attenuation Factor

Figure 4 shows the simplified structure and detector location with the appropriate solid angle fractions and mass thicknesses. Since this work is restricted to the ground contribution, the roof of the structure is considered free of any contamination. The expression for the reduction factor is

$$R_f = \{[G_a(\omega_u') - G_a(\omega_u)][1 - S_w(X_e)] + [G_s(\omega_u') - G_s(\omega_u)] \times S_w(X_e)E(e)\}\, B_e(X_e,3')B_o'(X_c) + A_a(\omega_u')B_o'(X_o) \qquad (8)$$

where $X_o = X_c + X_r$, the total overhead mass thickness. The detector height is taken to be 3 ft for below grade cases in the function B_e. The two differences of the geometry factors G_a and G_s limit the response of the detector to those directions between ω_u and ω_u'.

The last term in Eq. (8) represents the contribution through the roof and requires some explanation. For a decontaminated roof and a total overhead mass thickness of less than 25 psf, the EM has a table of reduction factors for this contribution at various values of the solid angle fractions subtended by the roof. The values in this table are taken from the function $A_a(\omega)$* which is recommended for use in determining the skyshine contribution to a detector located in an open vertical shaft. The function $A_a(\omega)$ is equivalent to the function $G_a(1-\omega)$ without the correction for ceiling reflection. To account for the absorption in roof and basement ceiling, the author has chosen to multiply this geometry factor by the attenuation factor $B_o'(X_o)$ for the total overhead mass thickness.

---

* This is the notation of the May 1964 edition of the EM and is more specific than the current notation $C_s(\omega)$.

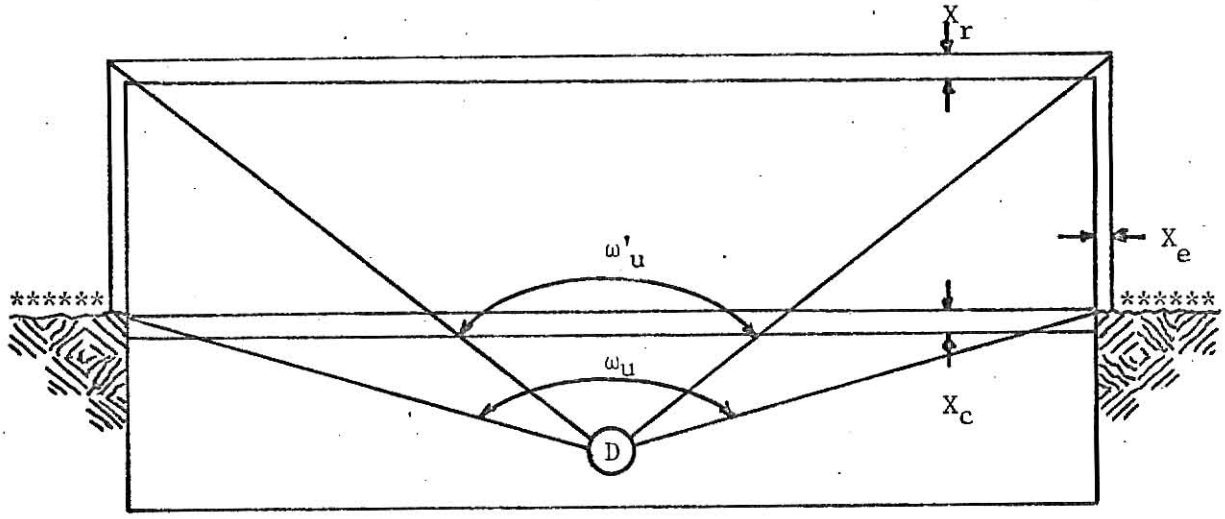

Figure 4. A basement detector location in a simplified structure.

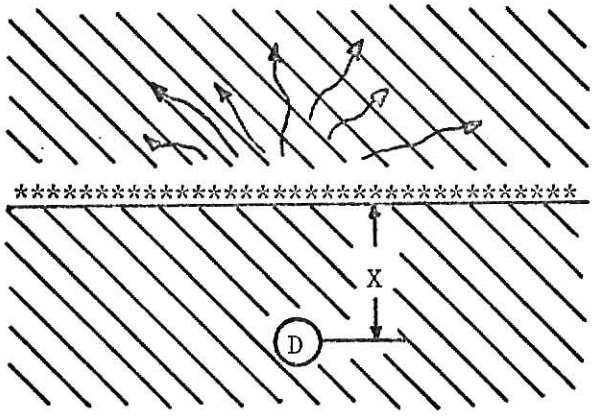

Figure 5. Detector-source-medium arrangement for the function S'(X).

The ceiling attenuation factor was taken to be equal to one of the functions calculated by Spencer, namely, S'(X). The function S'(X) represents the response from a detector imbedded a depth, corresponding to a mass thickness X, below an infinite plane source which emits radiation isotropically but only in the upper hemisphere. This configuration is pictured in Fig. 5. The radiation arriving at the detector has been back-scattered in the medium above the source plane. The function is normalized to unity at X = 0.

The dose angular distribution immediately below the source plane in Fig. 5 is approximately that of skyshine. As can be seen in Fig. 1, the skyshine distribution is peaked in the horizontal direction. Since penetration through a vertical wall tends to collimate the radiation in the horizontal direction, the angular distribution incident on the basement ceiling is approximately that of skyshine. In addition, the energy spectra are similar because in both cases the radiation has been scattered. For these reasons the function S'(X) was originally selected to represent the attenuation in the basement ceiling.

2.4.3 The Modified Ceiling Attenuation Factor of Eisenhauer

In the latest edition of the EM (July 1969), the ceiling attenuation factor $B'_o(X_c)$ in Eq. (8) is replaced by a modified factor $B_c(X_c,\omega_u)$. The additional variable implies that the attenuation in the basement ceiling not only depends on the ceiling thickness X_c but also on the solid angle fraction subtended by the ceiling. The factor is presented in the EM as a family of curves of attenuation versus mass thickness for various values of ω_u. These curves have been calculated from an empirical formula due to Eisenhauer [6]:

$$B_c(X,\omega) = (1 - 3.5e^{-2.3\omega})e^{-0.10X} + 3.5e^{-2.3\omega}e^{-0.040X}. \quad (9)$$

Equation (9) is essentially a fit to data from an experiment conducted at the Nuclear Defense Laboratory [6, 7]. The experimental structure was a 20×10 ft rectangular basement, 7 ft deep, which could either be covered by a ceiling of variable thickness or left uncovered. An above-grade story was simulated by erecting walls of heights 2, 4, or 8 ft. With this type of structure, the attenuation factor for the basement ceiling could be obtained directly by taking the ratio of the results of two experiments: one experiment with the barrier in place and the other with no barrier. Attenuation factors were measured for mass thicknesses of 46, 69, and 92 psf and at solid angle fractions in the range 0.3 - 0.9.

This factor is the only EM function which is based on experimental results rather than theoretical calculations.

3.0 THREE PROPOSED MODIFICATIONS TO ENGINEERING MANUAL THEORY FOR A BASEMENT DETECTOR LOCATION

In this section are described three modifications to the EM theory which were designed to give better agreement with certain sets of data for basement reduction factors. These methods were proposed prior to the adoption of Eisenhauer's formula by the OCD. The criteria which were used to select Eisenhauer's method in preference to any of these is given in [6].

3.1 The Method of Kaplan

Kaplan's modification [8] is similar to that of Eisenhauer's, since it involves the substitution of a solid-angle-dependent attenuation factor $\hat{B}_c(X_c,\omega_u)$ for the original factor $B'_o(X_c)$ in Eq. (8). His factor is the result of an empirical fit to data taken in a small cylindrical steel structure [9]. The structure consisted of a cylindrical basement 2 ft in diameter and 4 ft deep. Walls of the first story were simulated by steel cylinders 2 ft in diameter and 2 ft high. The basement ceiling was simulated by various thicknesses of steel.

Measurements of the ceiling attenuation factor were obtained for mass thickness of 0 to 40 psf and solid angle fractions of 0.05 to 0.8. The data were observed to approach the EM functions $B'_o(X_c)$ as ω_u approached zero. The variation of the data with ω_u was similar to that of $S_a(d=X_c,\omega_u)$, where S_a is one of the functions of Spencer [2]. The function S_a is unity for $\omega = 1$ and zero for $\omega = 0$; its significance here is numerical rather than physical. Using these functions, Kaplan formulated an empirical equation for the ceiling attenuation factor which fit his data:

$$\hat{B}_c(X_c,\omega_u) = B_e(X_c,3')[1 - S_a(X_c,\omega_u)] + B'_o(X_c)S_a(X_c,\omega_u) \quad . \qquad (10)$$

3.2 The Method of Batter and Starbird

The discrepancies between experimental and theoretical results for basement reduction factors have been attributed to the perturbation of the angular distribution of the radiation as it scatters from the walls of the structure into the basement - often referred to as the "in-and-down" effect. Investigations by Batter and Starbird [10] have led to an attenuation factor based on calculations of the in-and-down effect. In their calculations they have divided the scattering wall into differential areas, computed the incident uncollided dose rate from a differential area in the contaminated plane, and, using Compton-scattering probabilities, computed the dose rate at a basement location. The attenuation in the basement ceiling was determined from Monte Carlo transmission data for a monodirectional beam incident to a slab. After the necessary integrations were performed, a set of attenuation factors $\tilde{B}_c(X_c,\bar{\omega})$ was determined for wall sections of incremental heights

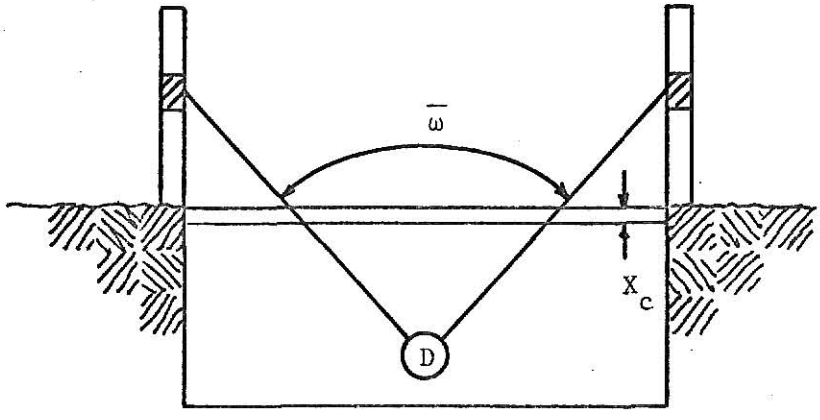

Figure 6. Geometry for the ceiling attenuation factor $\tilde{B}_c(X_c,\bar{\omega})$ of Batter and Starbird.

(refer to Fig. 6). The values of the attenuation factor are presented as a family of curves of attenuation versus mass thickness for various values of $\bar{\omega}$.

To use this factor precisely, one would have to divide the walls of a structure into a number of horizontal layers and determine a separate reduction factor for each. However, Batter and Starbird do not recommend this procedure. They say that sufficient accuracy is obtained when just one value of $\tilde{B}_c(X_c,\bar{\omega})$ is used for the entire contribution from the first-story walls. For the situation shown in Fig. 4, $\bar{\omega}$ is defined by the average value of ω_u and ω_u'. When the factor $B_o'(X_c)$ is replaced by $\tilde{B}_c(X_c,\bar{\omega})$, Eq. (8) gives the reduction factor for this method.

3.3 The Method of French

French [11] has attributed the discrepancies between the original EM theory and experiments to scattering in the basement ceiling. He has devised a method in which the contributions to the reduction factor are split into two components: one for the radiation which has scattered in the basement ceiling and the other for that which has not.

The structure of Section 2.4.2 is shown again in Fig.7 to define a new solid angle fraction. The non-ceiling-scattered contribution is similar to Eq. (8) with a weighting factor for the fraction of radiation not scattered in the ceiling:

$$R_f' = \Big[\{[G_a(\omega_u') - G_a(\omega_u)][1 - S_w(X_e)] + [G_s(\omega_u') - G_s(\omega_u)]S_w(X_e) \times E(e)\}\, B_e(X_e,3')B_o'(X_c) + A_a(\omega_u')B_o'(X_o)\Big][1 - S_w(X_c)] \quad . \tag{11}$$

The expression for the ceiling scattered component is written

$$R_f'' = \Big[\{G_a(\omega_u'')[1 - S_w(X_e)] + G_s(\omega_u'')S_w(X_e)E(e)\}\, B_e(X_e,3') \times B_o'(X_c) + A_a(\omega_u'')B_o'(X_o)\Big]S_w(X_c)G_b(\omega_u) \tag{12}$$

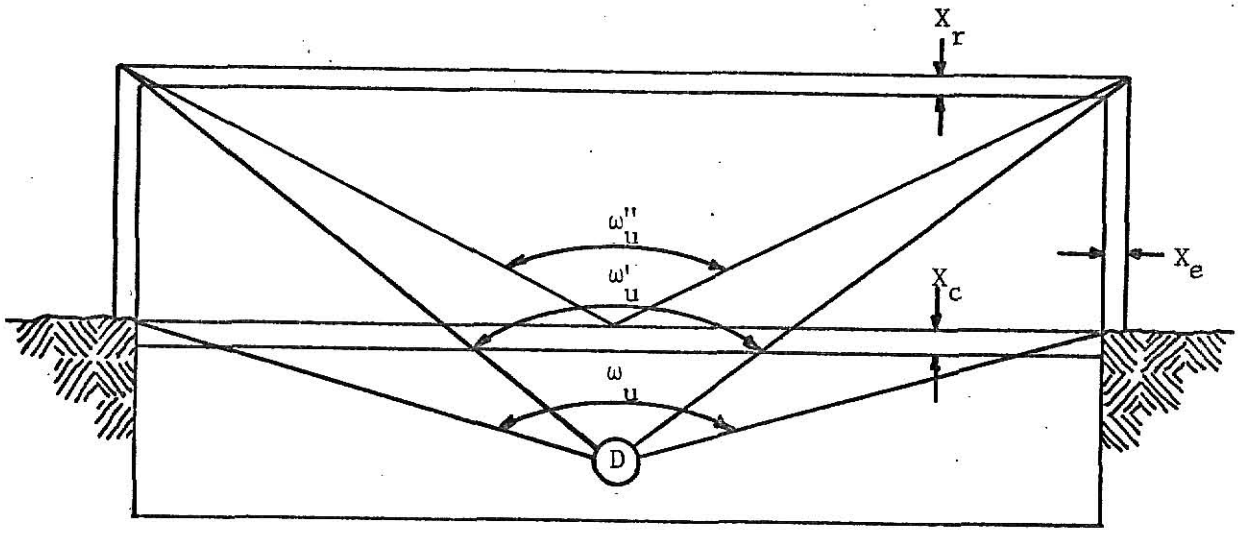

Figure 7. A basement detector location in a simplified structure with solid angle fractions for French's method.

where the geometry factors, whose arguments are ω_u'', indicate the amount of radiation which is incident on the basement ceiling and, hence, has the potential for scattering into the detector. The factor $G_b(\omega_u)$ is the directional response for the ceiling scattered radiation. It was derived under the assumption that the scattered radiation emerges from the ceiling with an angular distribution proportional to $\cos\theta$, where θ is the angle with respect to the downward normal. It can be expressed as an analytic function of ω_u:

$$G_b(\omega_u) = 1 - (1 - \omega_u)^2 \ . \qquad (13)$$

The total reduction factor is the sum of Eqs. (11) and (12).

4.0 EXPERIMENTAL FACILITIES AND PROCEDURE

4.1 Safety Considerations

The experimental results cited in this work were obtained at the Kansas State University Nuclear Engineering Shielding Facility (KSUNESF). The KSUNESF is a 180 acre plot of land which is located five miles west of the campus in a sparsely inhabited area. During experiments which required the exposure of multi-curie ^{60}Co sources, perimeter guards were stationed around the test area to prohibit access to high-radiation areas. All personnel were equipped with radiation survey meters, film badges, and self-reading pocket dosimeters. Remote handling techniques permitted the experimenters to remain safe distances away from the sources.

4.2 The Test House

The test house is a 30×40 ft structure, with full basement, whose construction resembles that of a typical American home. Figure 8 is a complete copy of the working drawings of the house and associated materials. The most unusual feature of the house is the floor panel separating the basement from the upper story. The floor is unattached to the exterior walls and can be raised to a maximum height of three feet above grade by means of hydraulic jacks. In addition to the permanent wood-frame shell of the house, there are concrete blocks and panels which can be placed around the outside of the house. The panels are used to simulate a house with masonry walls; when the floor is raised, the blocks are used to simulate an exposed foundation. There is also a set of wooden partitions which can be placed inside the house to simulate interior walls according to the scheme shown in the drawings.

Random samples of the various construction materials were weighed, and

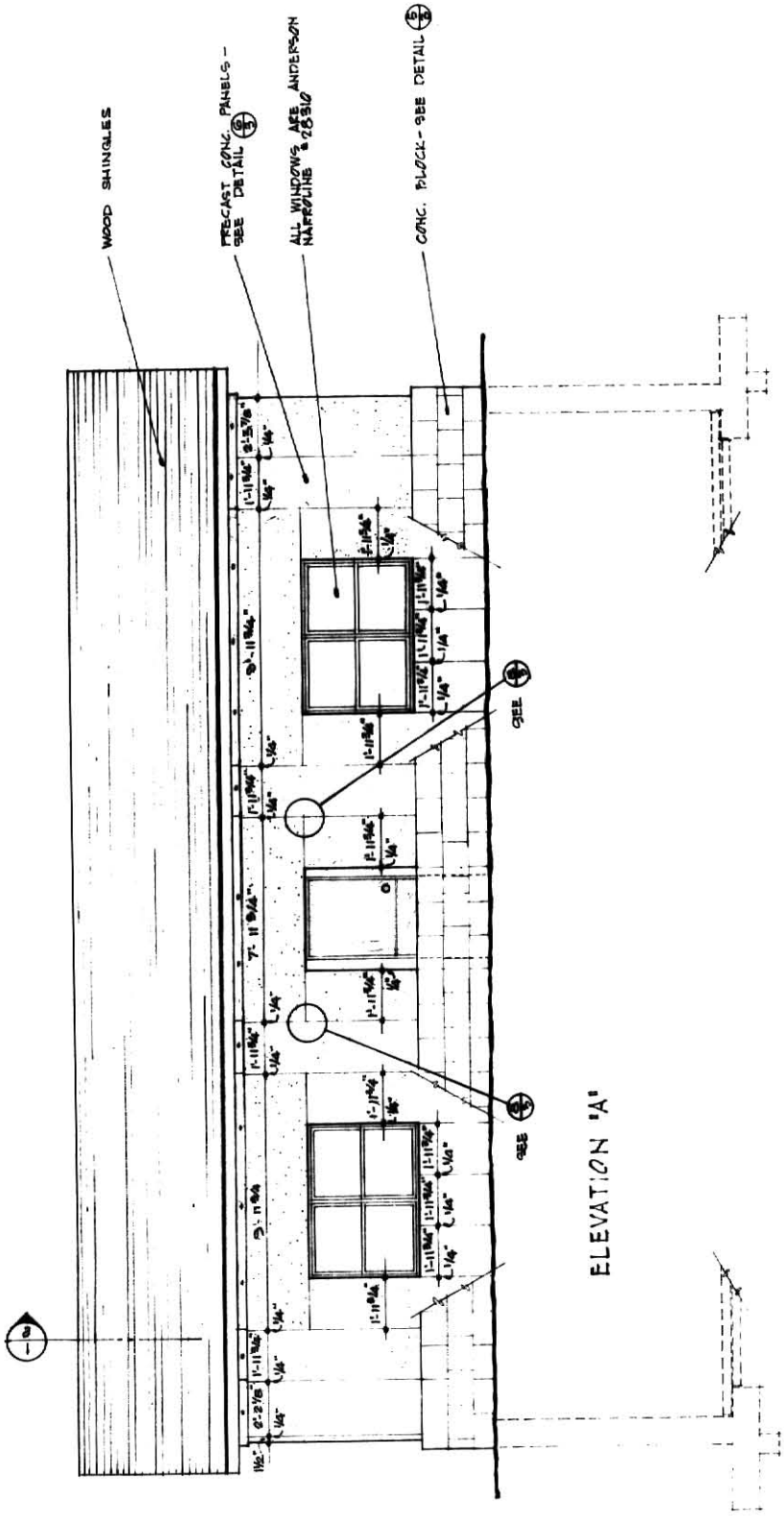

Figure 8. Working drawings of the test house.

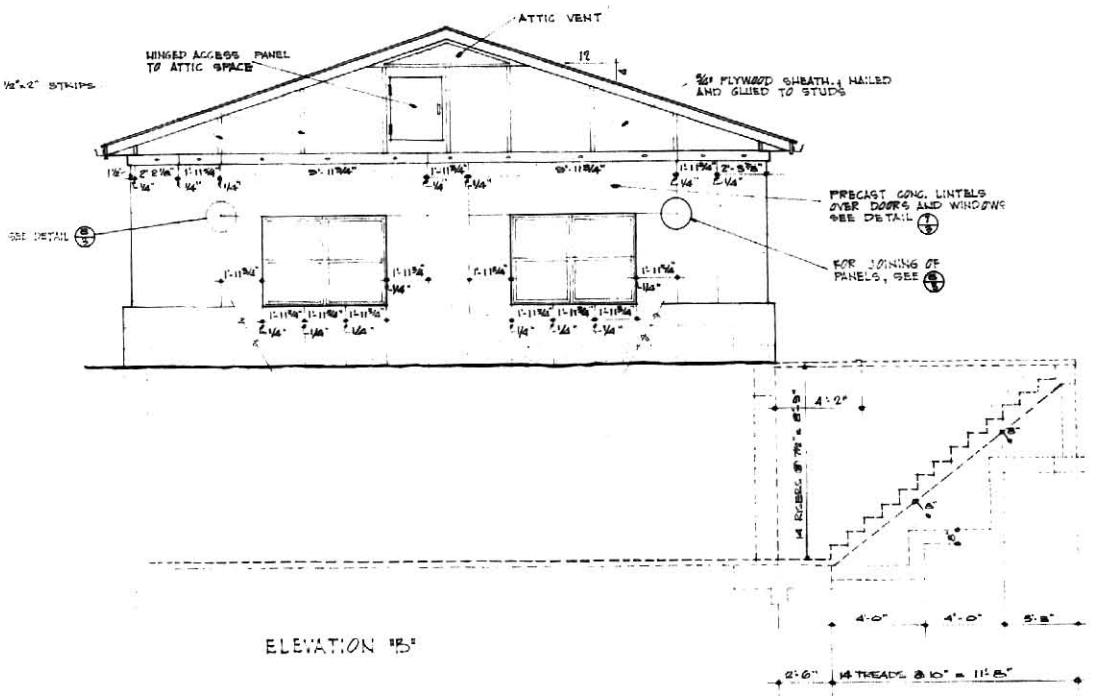

GENERAL NOTES:

1. ALL VERTICAL JOINTS ON EXTERIOR SHEATHING TO BE COVERED WITH 1/2"x 2" WOOD STRIPS.
2. ALL INTERIOR AND EXTERIOR SHEATHING TO BE GLUED TO FRAMING WITH RESORCINOL GLUE SIMILAR TO "PELIACOLITE G-1620" MORRELL CO.
3. NAIL PLYWOOD AND BATTENS ON EXTERIOR WALLS WITH "STRONGHOLD" 2"x 0.148 HI-LOAD SHEAR RESISTANT GALVANIZED NAILS.
4. NAIL PLYWOOD ON INTERIOR WALLS WITH "STRONGHOLD" 1 1/2"x 0.135 HI-LOAD SHEAR RESISTANT NAILS.
5. ALL CONCRETE: 6 SACKS/CU. YD. 80% CRUSHED ROCK/CU. YD.

Figure 8. (continued)

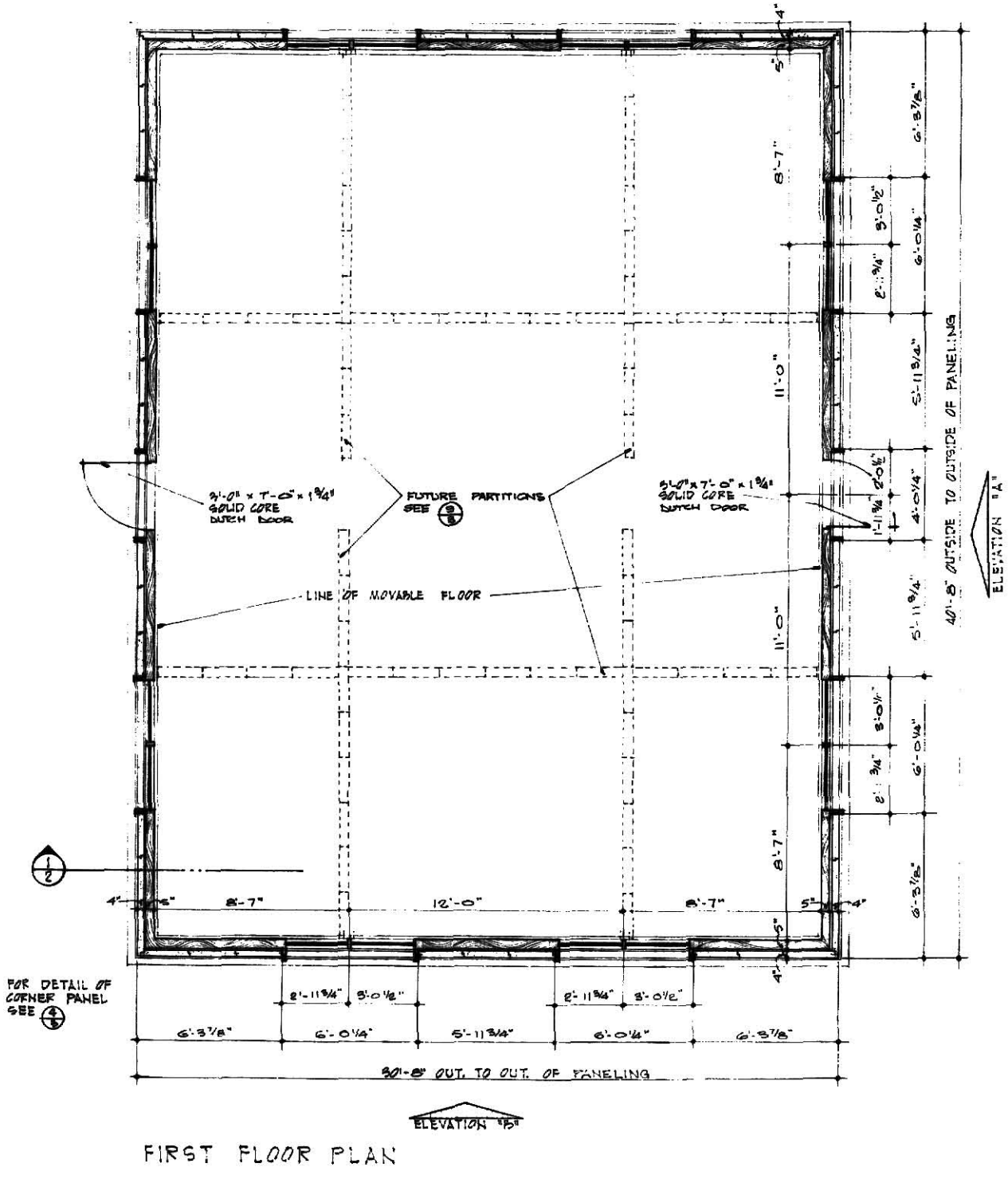

FIRST FLOOR PLAN

Figure 8. (continued)

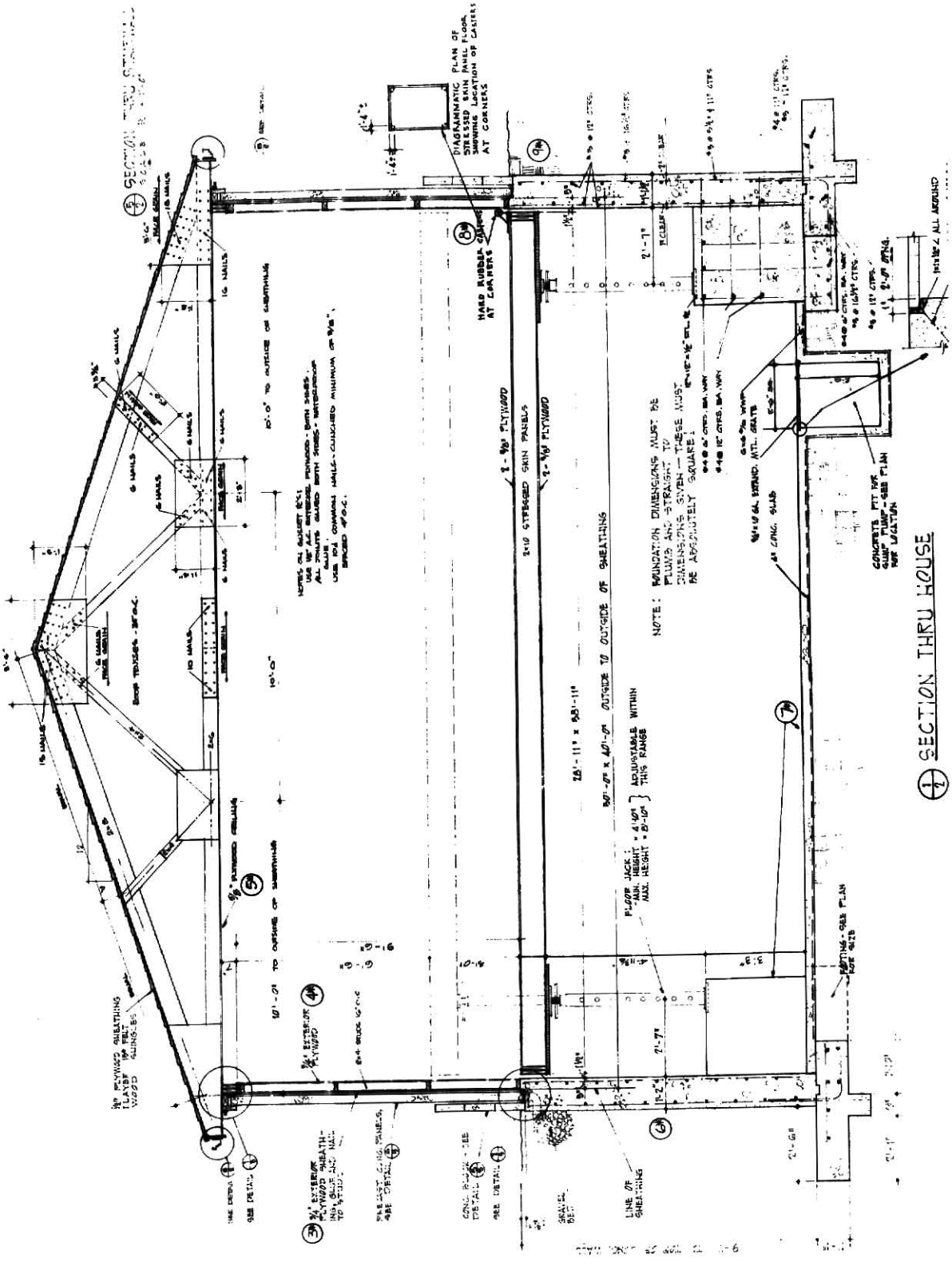

Figure 8. (continued)

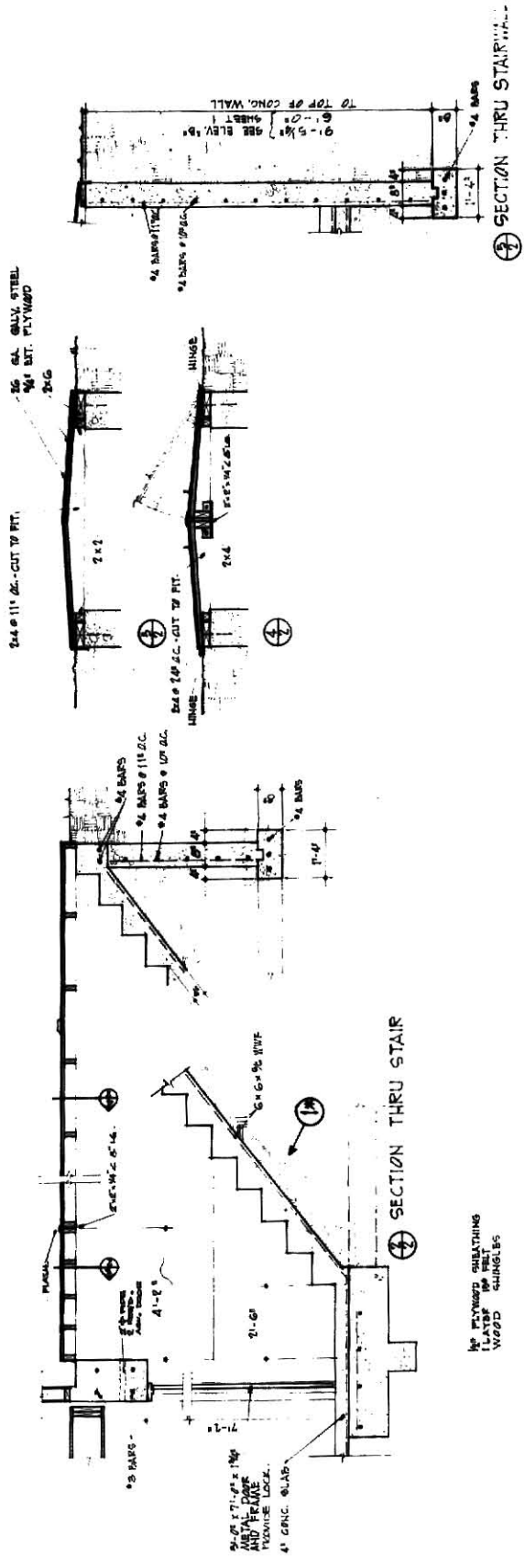

Figure 8. (continued)

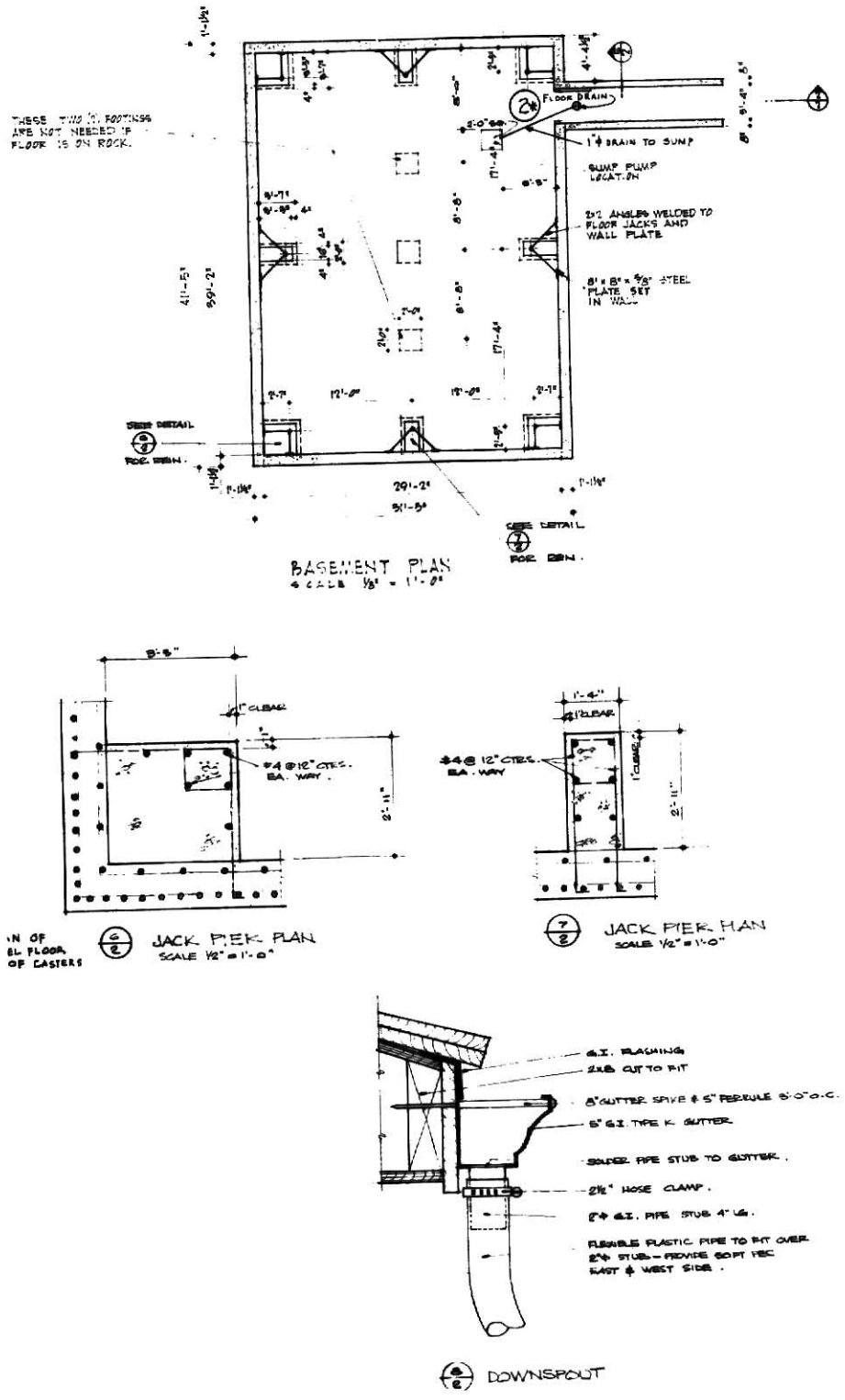

Figure 8. (continued)

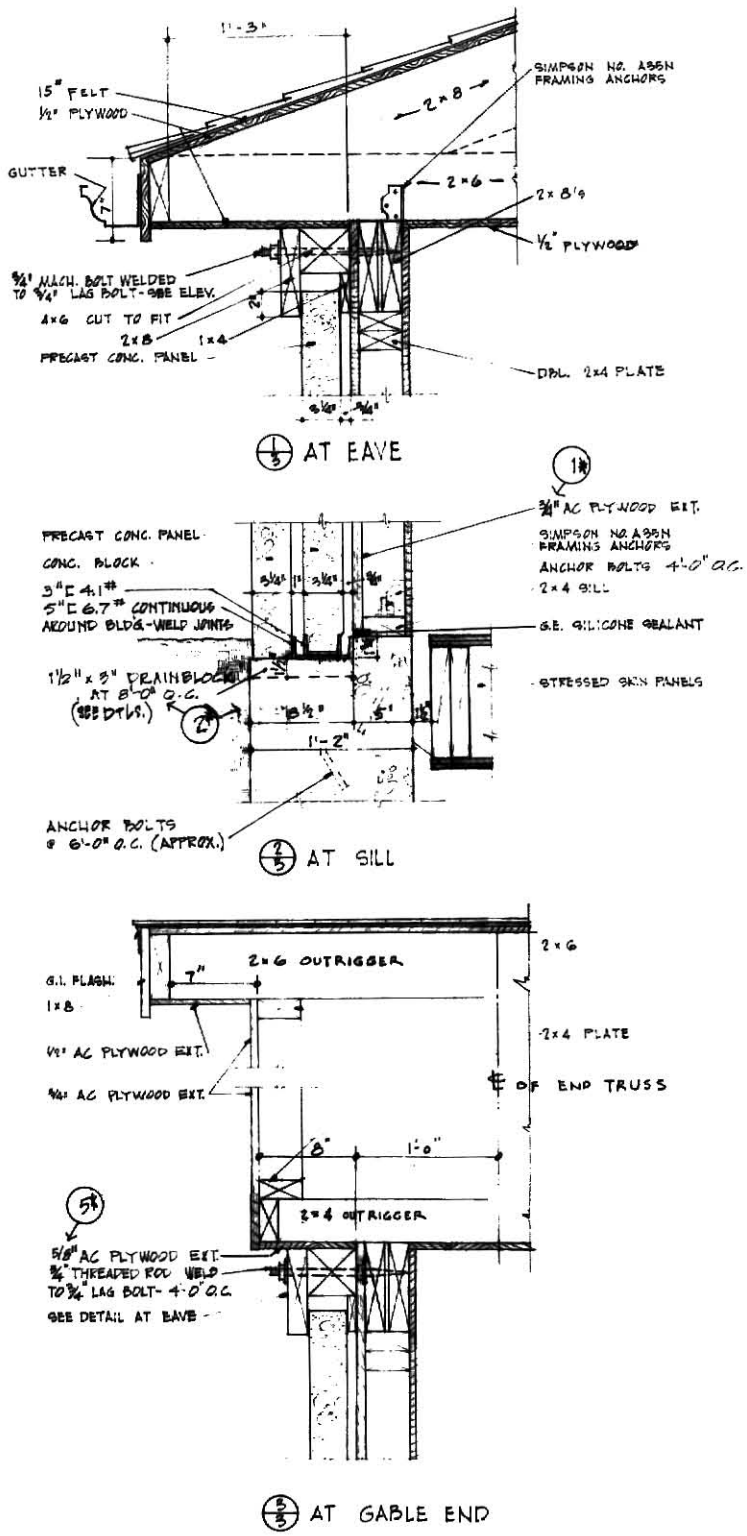

WALL DETAILS

Figure 8. (continued)

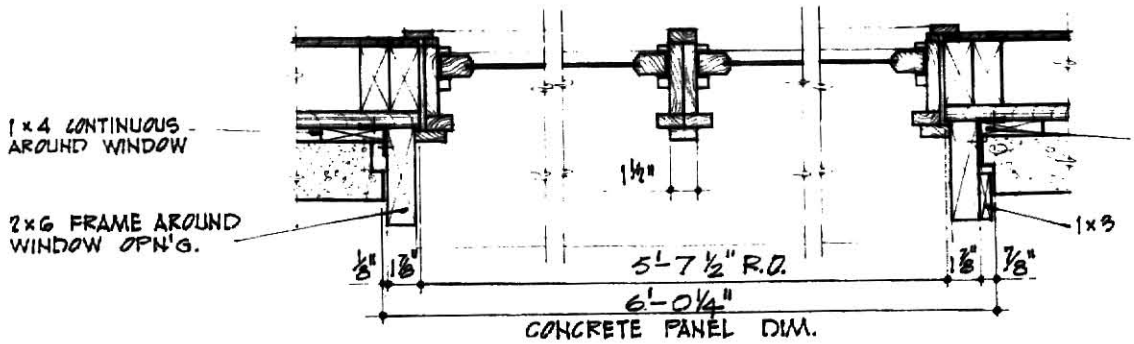

JAMB DETAILS

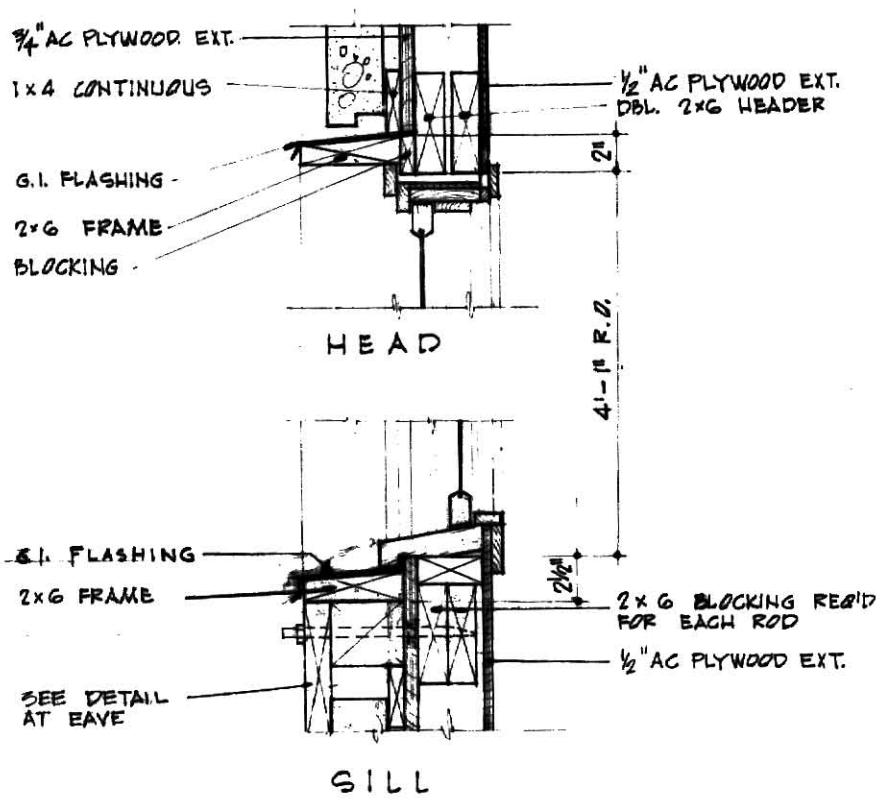

WINDOW DETAILS

Figure 8. (continued)

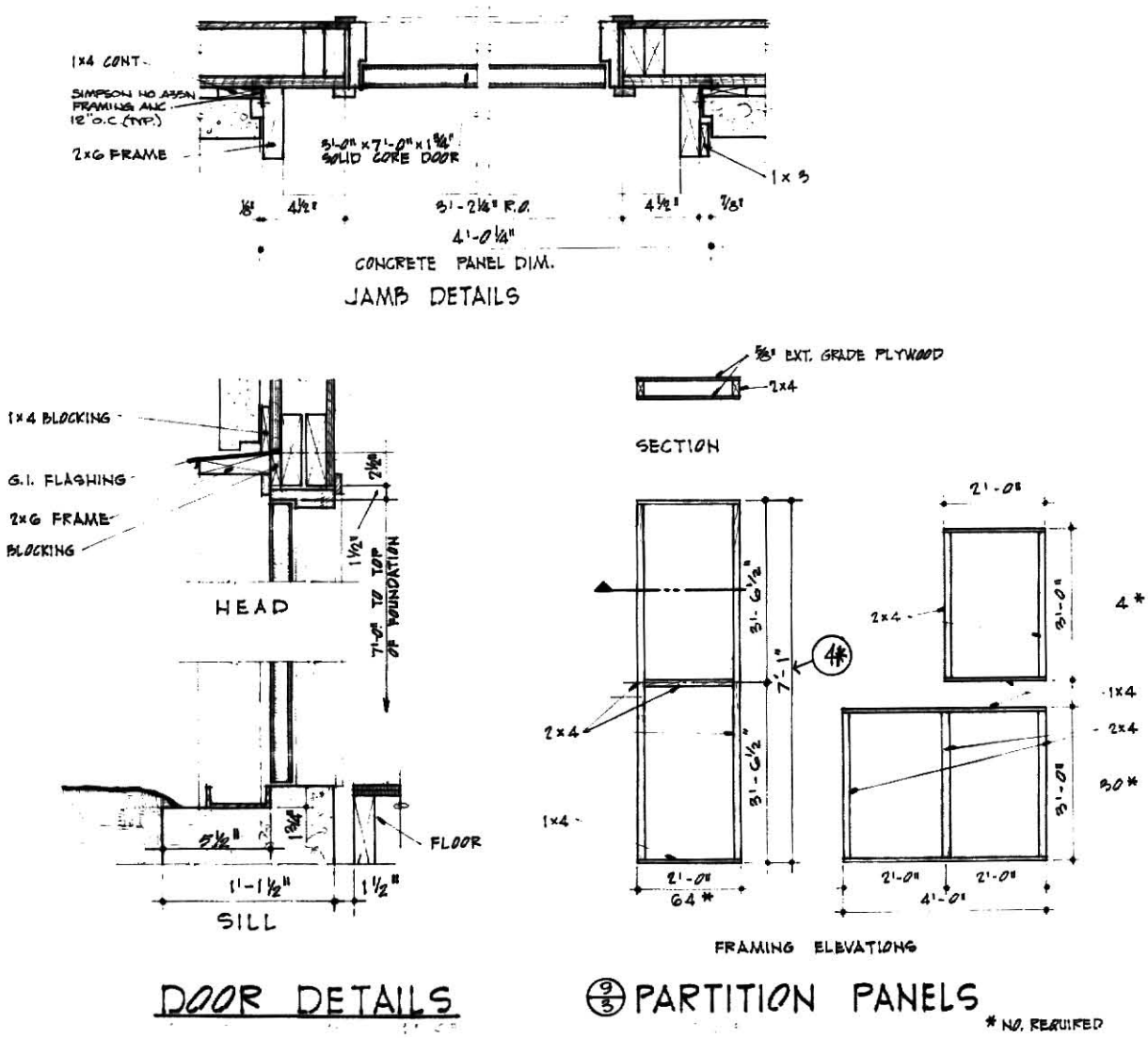

Figure 8. (continued)

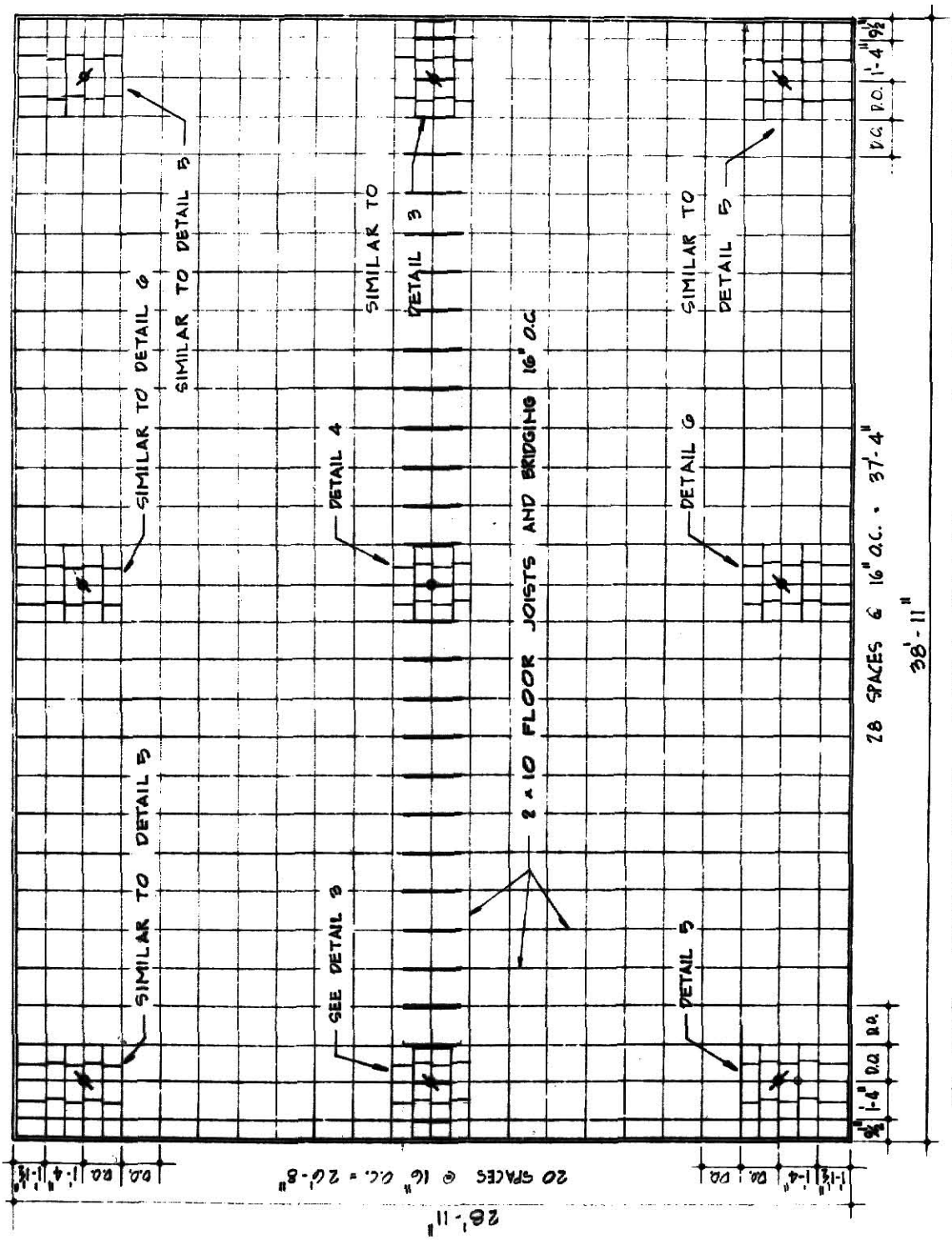

Figure 8. (continued)

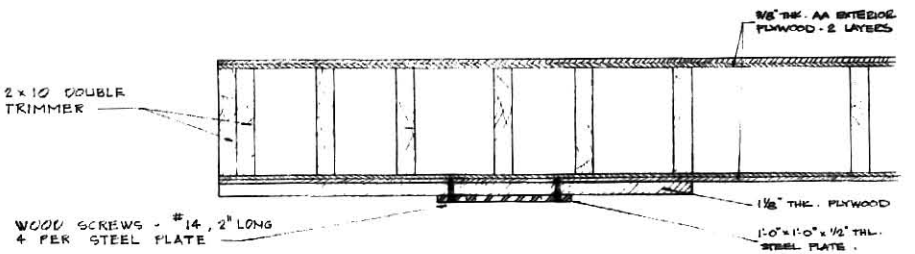

DETAIL 1

NOTES:

1. ALL 2x10 FRAMING LUMBER IN STRESSED SKIN PANEL TO BE WEST COAST DOUGLAS FIR, DENSE SELECT STRUCTURAL SURFACED 4 SIDES, KILN DRIED.
2. ALL PLYWOOD FOR STRESSED SKIN PANEL TO BE A-A FIR PLYWOOD EXTERIOR GRADE.
3. ALL 2x10 FRAMING LUMBER, INCLUDING BLOCKING, SHALL BE SQUARE CUT WITH FIRM CONTACT OVER ENTIRE JOINT WITH ADJOINING PIECES. PIECES NOT FITTING PERFECTLY WITH ADJOINING PIECES SHALL BE REJECTED.
4. ENTIRE STRESSED SKIN PANEL MUST BE GLUED & NAILED, INCLUDING 2x10 FRAMING & PLYWOOD SKINS.
5. ALL GLUE TO BE A RESORCINOL GLUE SIMILAR TO KOPPERS CO. "PELLACOLITE G-1260".
6. EACH LAYER OF PLYWOOD SHALL BE GLUED CONTINUOUS OVER ALL JOINTS & SOLID BRIDGING. TOP LAYER OF PLYWOOD SHALL BE GLUED SOLID TO UNDERLAYER. EACH LAYER OF PLYWOOD SHALL BE NAILED 4"O.C. OVER ALL JOISTS & ALL BRIDGING WITH "STRONGHOLD" THREADED NAIL 2" x 0.148 " HI-LOAD" SHEAR RESISTANT STEEL NAILS.
7. GLUE DOUBLE TRIMMERS.

Figure 8. (continued)

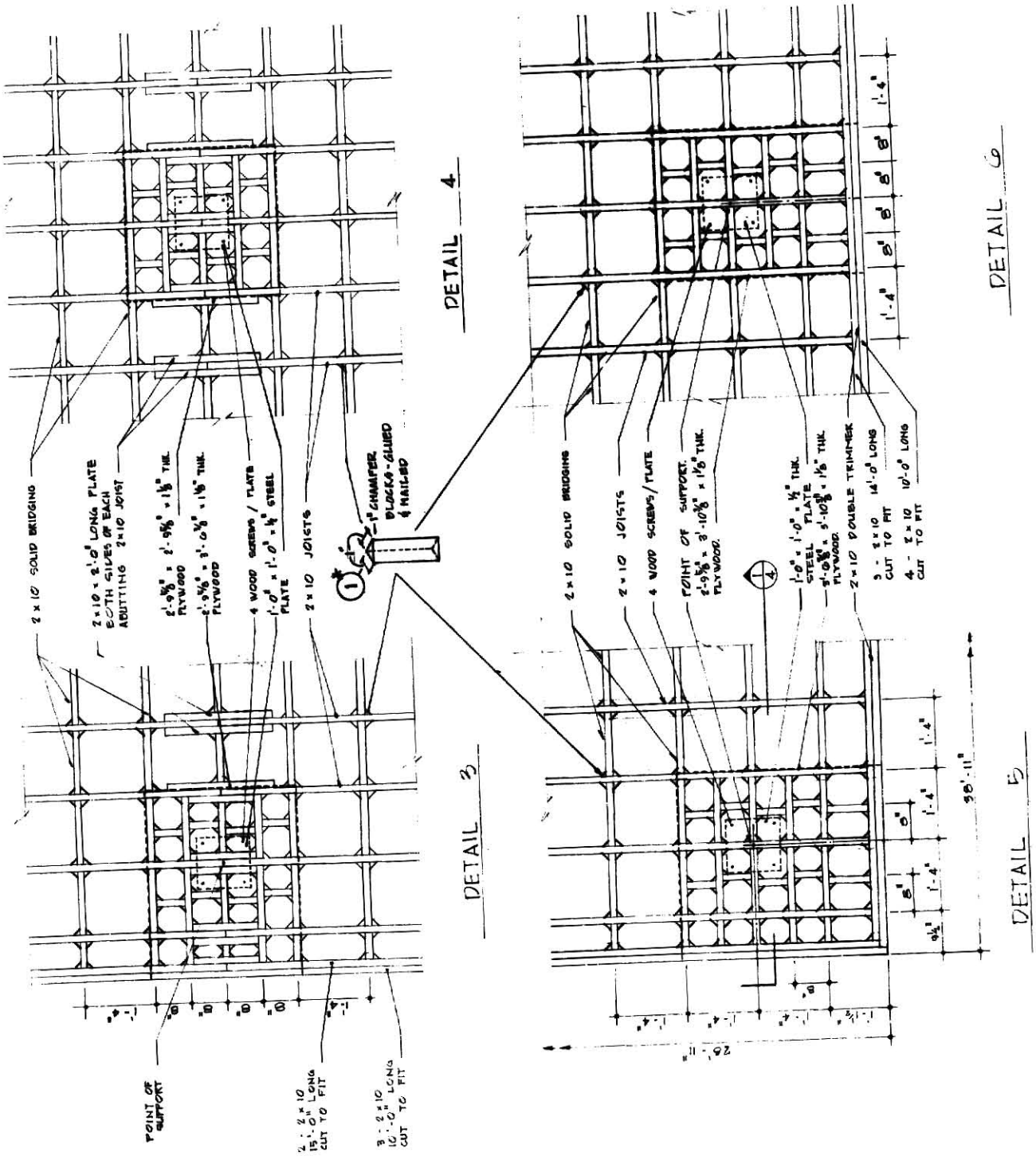

Figure 8. (continued)

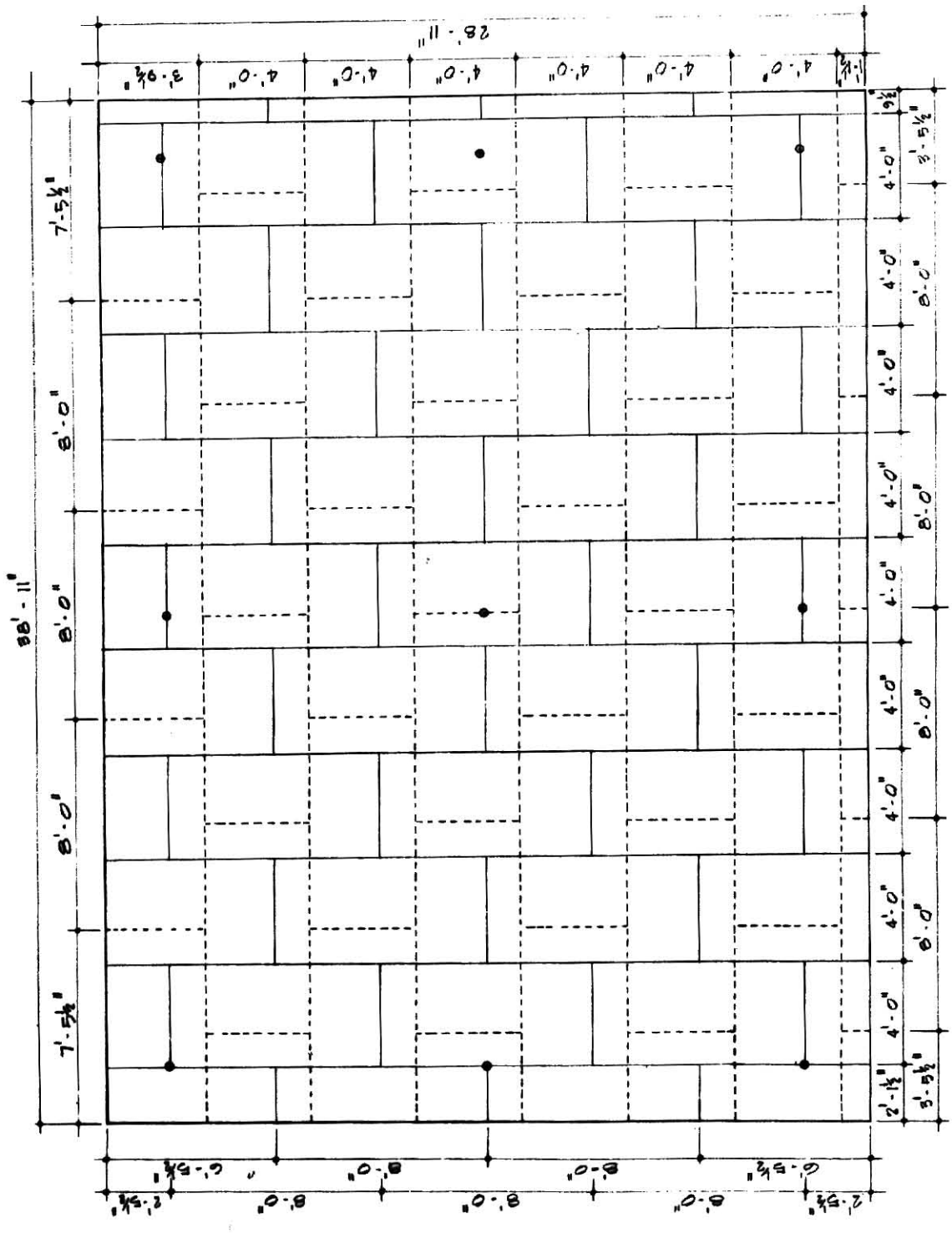

Figure 8. (continued)

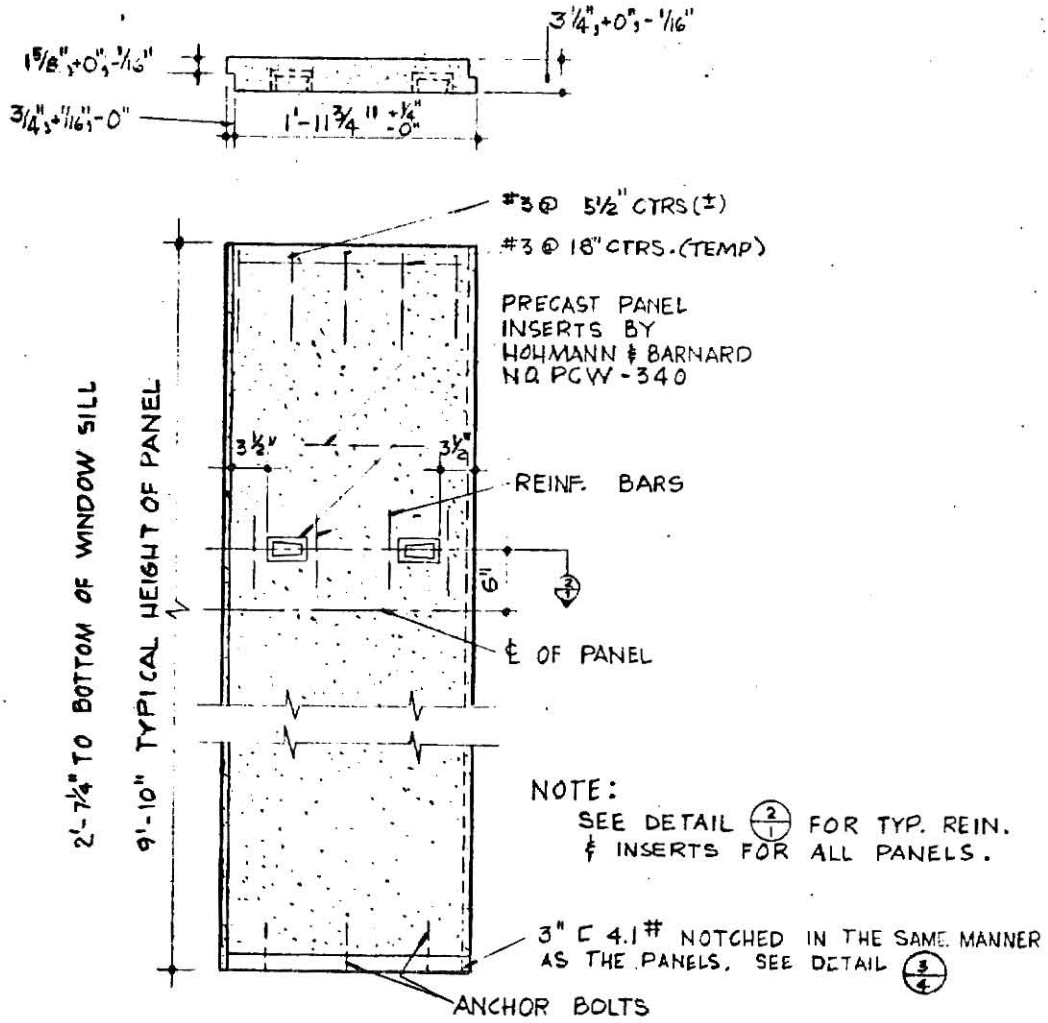

1/1 CONC. PANEL DTL.
SCALE 3/4" = 1'-0"

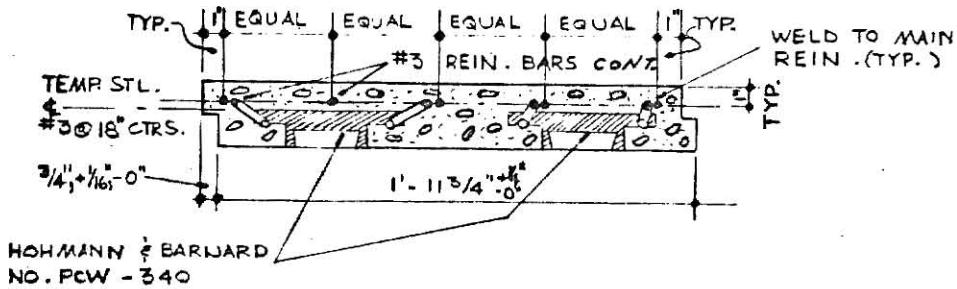

2/1 TYPICAL PANEL REIN.
SCALE 1½" = 1'-0"

Figure 8. (continued)

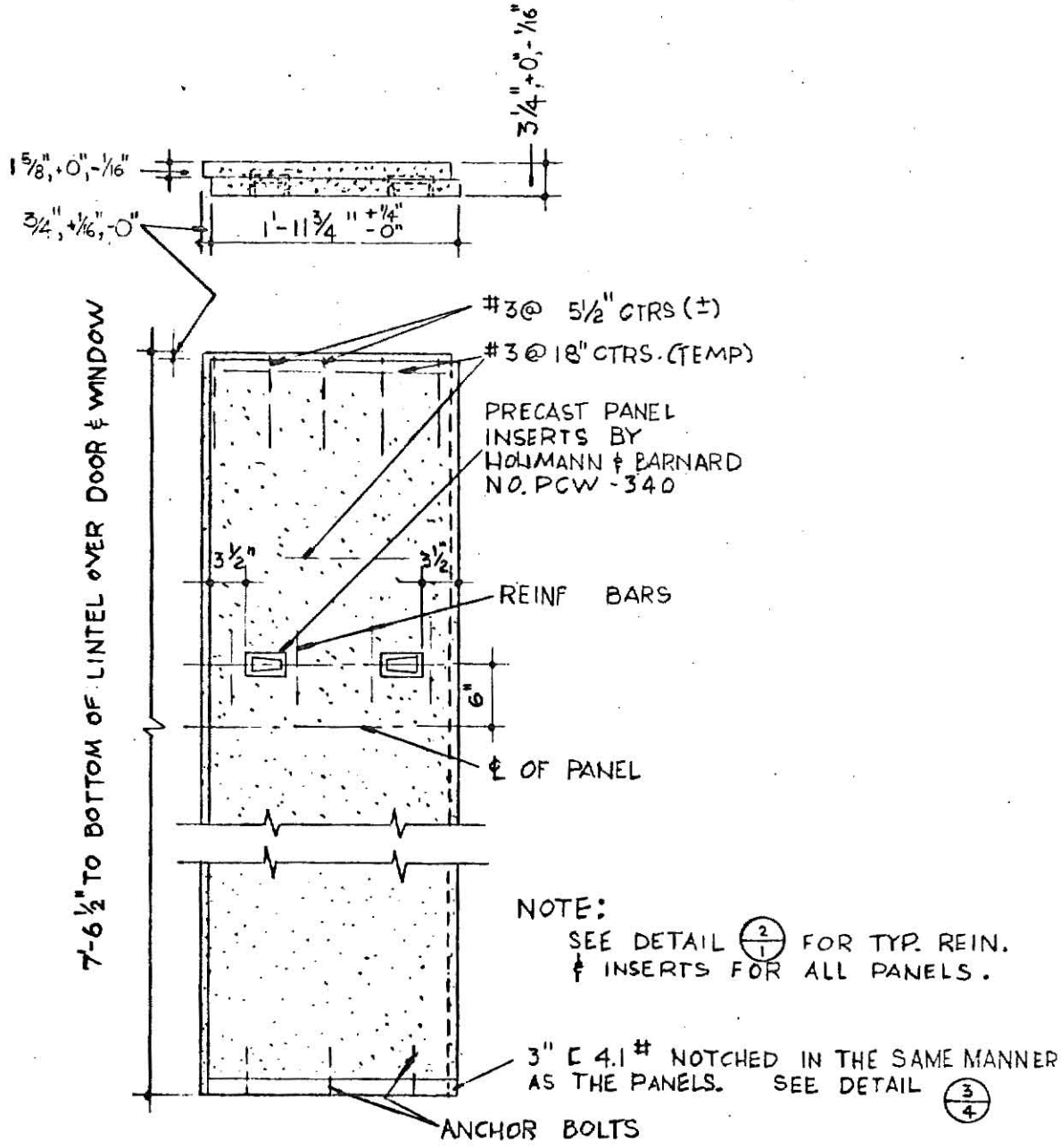

(1/2) CONC. PANEL DTL. (NOTCHED TOP)
SCALE 3/4" = 1'-0"

Figure 8. (continued)

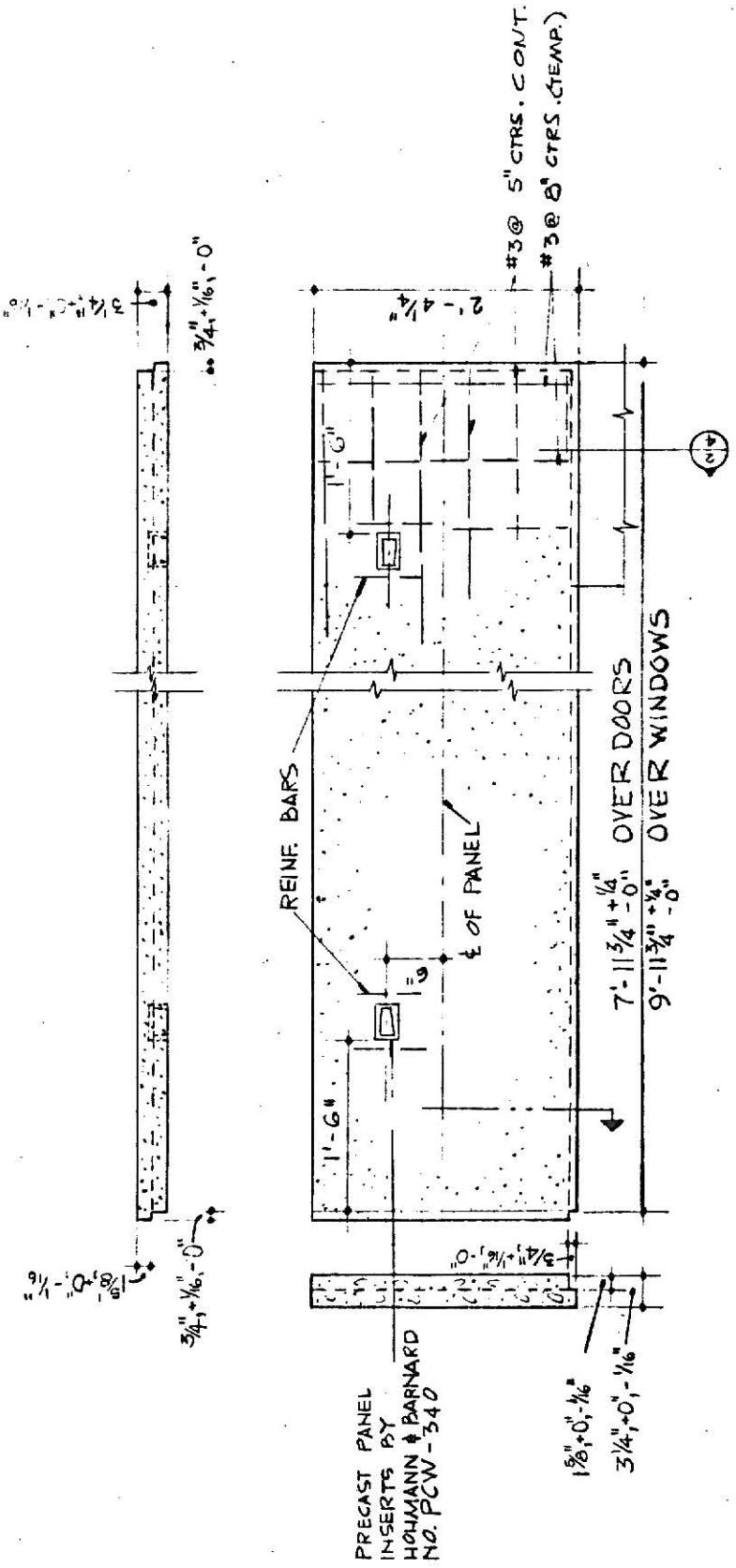

Figure 8. (continued)

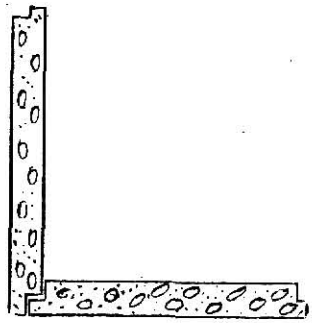

1/4 CORNER PANELS
SCALE 3/4" = 1'-0"
(ASSEMBLY)

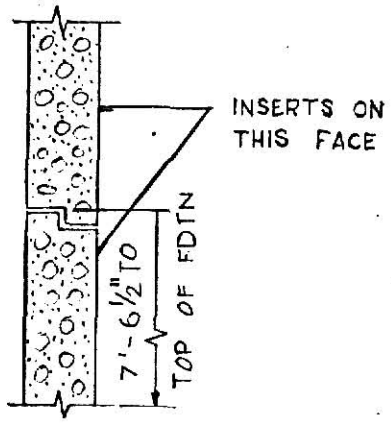

2/4 JOINT DETAIL
FOR LINTEL PANELS
SCALE 1 1/2" = 1'-0"
(ASSEMBLY)

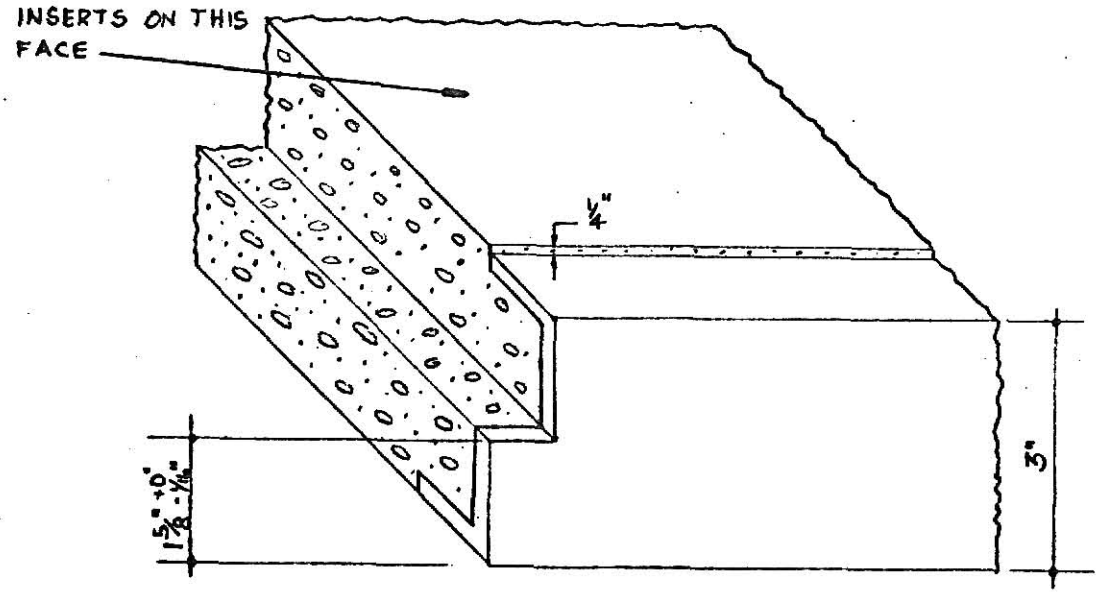

3/4 BOTTOM CHANNEL DTL.
1/2" SCALE

Figure 8. (continued)

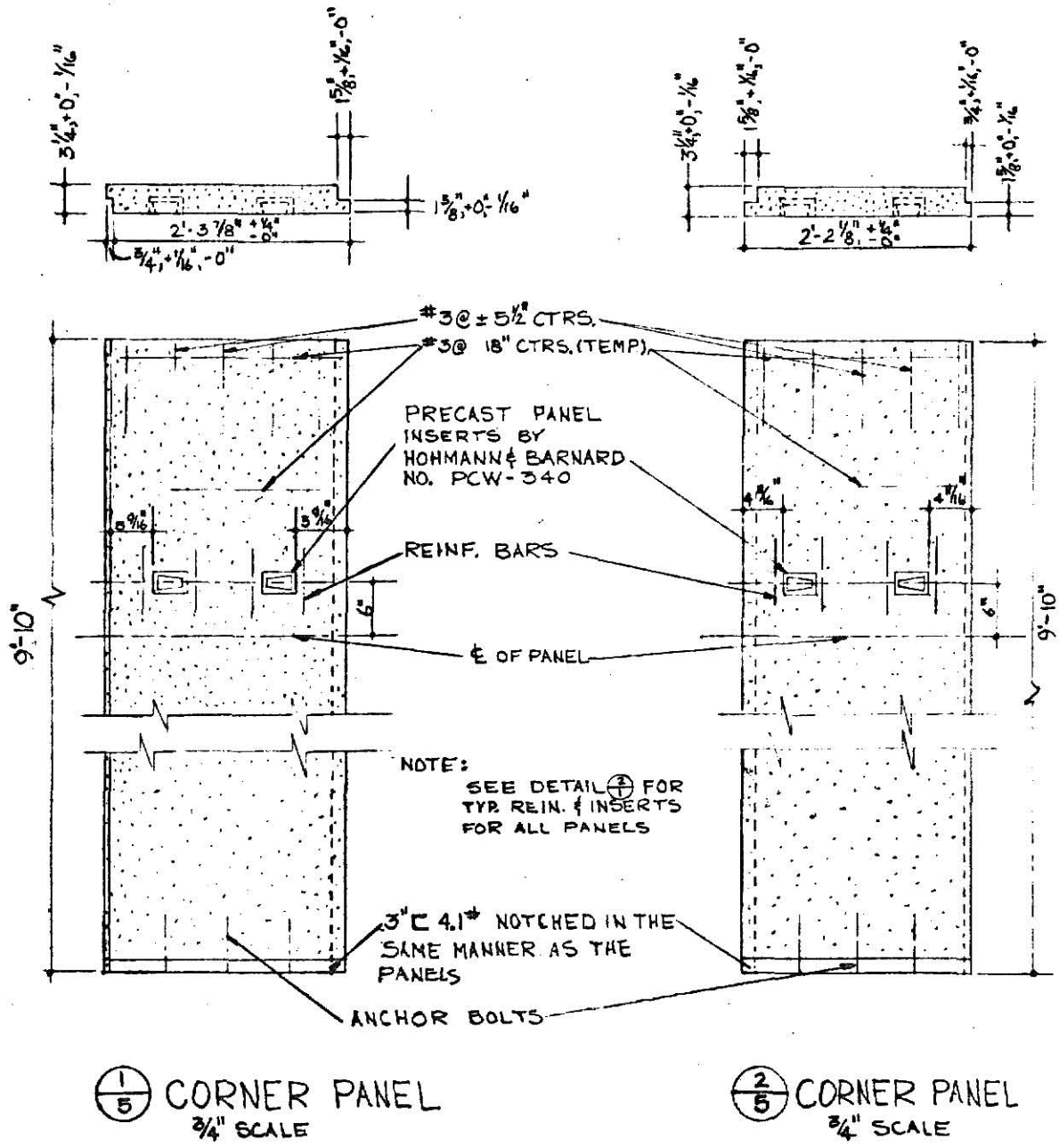

Figure 8. (continued)

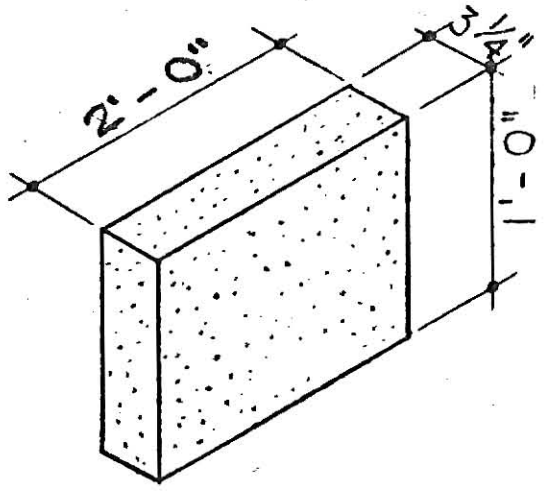

1/1 CONC. BLOCK DTL.

ALL DIMENSIONS ± 1/8"

Figure 8. (continued)

an average density for each was determined. The observed densities are listed below with estimates of the range of variations.

Material	Density (lb/ft^3)
plywood	33.4 ± 10%
2×10 (structural grade)	35.0 ± 10%
other lumber	30.7 ± 10%
concrete	148 + 5%, - 10%

After determining a weight per unit area for each barrier, the effective mass thicknesses were computed by multiplying by the factor 2(Z/A) for the material in question. The resulting values are shown in Table I.

Since the primary interest of this work is the attenuation in the floor (basement ceiling), the data chosen for analysis were those taken with two

Table I. Effective mass thicknesses for the test house.

Barrier	Effective mass thickness (psf)
Exterior walls	5.5
Roof	8.8
Floor	12.0
Door	5.5
Interior partitions	5.3
Concrete panels	40.0
Concrete blocks	40.0

configurations of the test house which featured the floor at grade and no interior partitions. This provided for the cleanest possible measurements of the reduction factor in the basement. One house configuration, referred to as House 1, featured bare wood-frame walls; the other configuration, referred to as House 12, had the concrete panels in place.

4.3 Simulation of the Fallout Field

The standard technique of simulating a fallout field consists of circulating a point ^{60}Co source through tubing placed uniformly on the ground adjacent to the test structure. If a source of C curies travels at a constant rate of speed through tubing, which uniformly covers an area of A square feet, in a time T, then the response of a detector in roentgens times A/(CT) is equivalent to the dose rate which would be observed if the given area were a plane source of 1 Ci/sq ft. Since the test house was symmetric in each quadrant, only one quarter of the contaminated plane had to be simulated. Measurements for full symmetry were obtained by placing the dosimeters at symmetric points in each quadrant of the house and adding the response from each.

The area adjacent to the test house was graded to the dimensions shown in Fig. 9 with a negative 1.5 percent slope (outward from the house). Three tubing areas were marked off and approximately 5000 ft of polyethylene tubing was laid out in concentric arcs in each area with the spacing indicated in Fig. 9. The outer radius was restricted by 1) the limit of the graded area, 2) the amount of tubing available, 3) the source strengths available, and 4) the sensitivity of the dosimeters. Figure 10 is a photograph of the test house and tubing field.

The source was driven through the tubing by water-pressure supplied by an electric pump. The source assembly, pump, and lead storage container

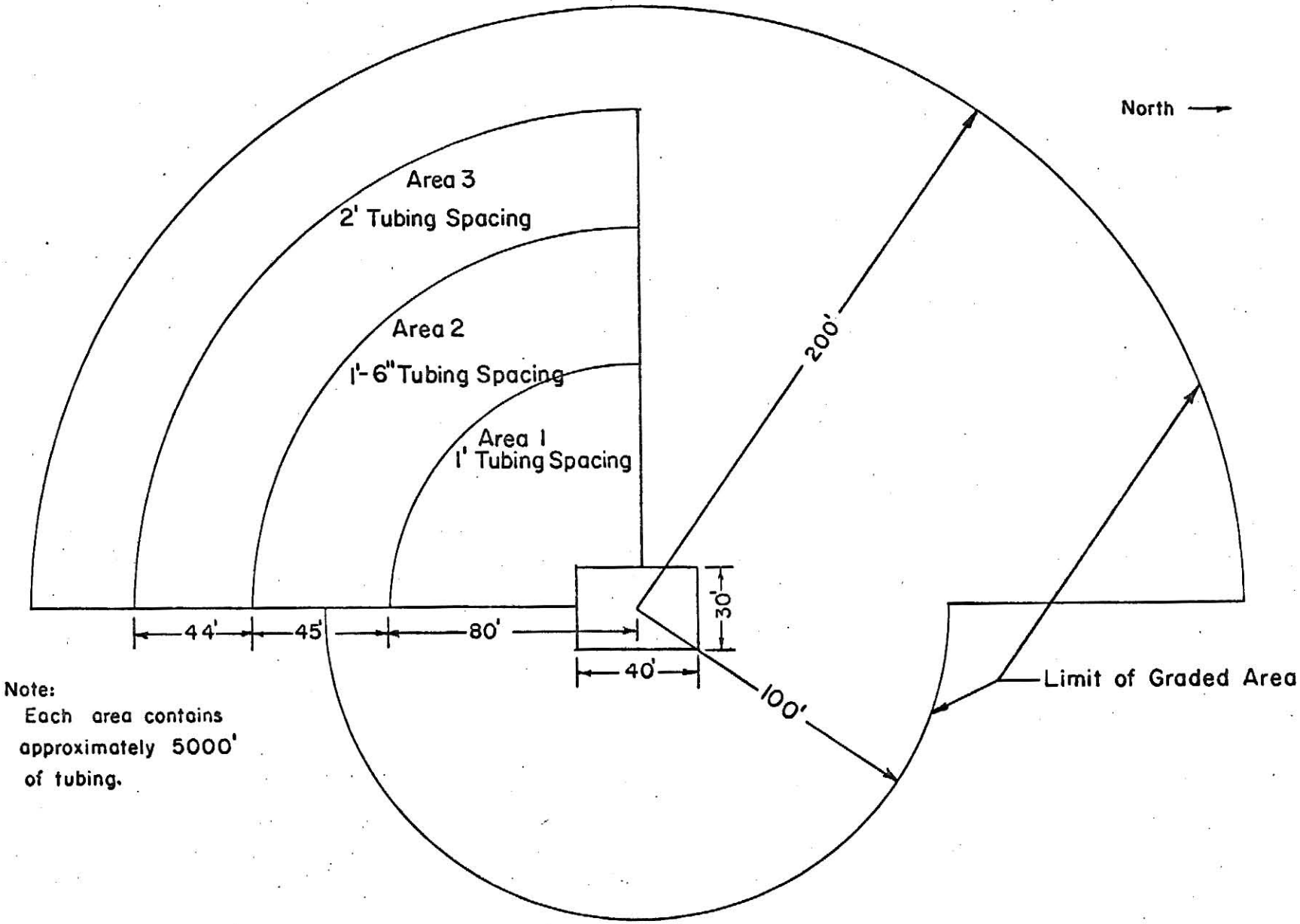

Figure 9. Tubing areas for the simulation of the fallout field.

Figure 13. The test house and tubing field at the KSUNESF.

were components of the Technical Operations, Inc. (Tech/Ops) Duplex Hydraulic Source Circulation System, Model 539. There were two sources available with this system which had been calibrated in previous work at the KSUNESF. The source strengths of each were 83.8±1.3 Ci and 7.38±0.10 Ci on August 10, 1965 [12].

4.4 Dosimetry

Two types of dosimeters were used to measure the accumulated doses in the basement of the test house. One type was the air-equivalent ionization chamber, and the other was a thermoluminescent detector (TLD). The dosimeters were calibrated before measurements were taken in the test house, and subsequent calibration checks were made throughout the course of the experiments. The procedure for the calibration is detailed in Appendix C.

The ionization chambers were Victoreen Instrument Co. Stray-Radiation Chambers, Model 239. They have an over-all length of 4.5 in., a diameter of 2 in., and bakealite walls 0.0625 in. thick. A charger-reader, made by Tech/Ops specifically for these dosimeters, was used to charge and read the dosimeters. The full-scale reading for these dosimeters occurs at an approximate exposure of 10 milliroentgens; hence, they are referred to as 10-mR chambers.

The thermoluminescent dosimeters were Edgerton, Germeshausen, and Grier, Inc. (EG&G) Model TL-12 dosimeters. The dosimeter consists of two components: 1) a detector (Model TL-32) of manganese-activated calcium floride (CaF_2:Mn) bonded to a helical heating element which was enclosed in an evacuated glass envelope and 2) an energy compensating shield (Model TL-52) of aluminum, tin, and lead. The TL-52 is a cylindrical capsule, about 2 in. long and 0.5 in. in diameter. An EG&G Model-3B reader was used to obtain readings from these

dosimeters after irradiation. During readout, the TL-32 was heated to ∿350°C by the reader and the amount of light given off by the TLD material, which is proportional to the amount of energy absorbed, was measured by a photo multiplier tube and recorded on a strip chart. The range of these dosimeters is 0.5mR to 50,000R.

Both types of dosimeters have a flat energy response from 1.25 MeV to 100 keV. There were 51 10-mR chambers and 66 TL-12 dosimeters available for the experiments.

4.5 Data Acquisition

A plan of the detector positions in the basement of the test house is shown in Fig. 11. Data were taken at the twenty-one positions at heights of three and six feet above the floor. In addition, dosimeters were placed at one foot intervals at the center of the basement from heights of two to eight feet. In all, 47 detectors were required for a complete series of measurements. Detector racks were made of four pieces of nylon cord to which were glued squares of lucite at the appropriate heights. A hole was drilled in the lucite which would accomodate either type of dosimeter. The racks were hung from the basement ceiling at the positions shown in Fig. 11.

One experiment, or run, consisted of zeroing the dosimeters, placing them in position, driving the source through one of the three tubing areas, and reading and recording the accumulated doses. The time required for the source to traverse 5,000 ft of tubing was about one hour, while the time required for reading and replacing the dosimeters was 70 to 90 min. A minimum of three runs was performed in each tubing area.

The large pumped source (∿60Ci) was used in all three areas for House 1. Generally, TL-12 dosimeters were used at all detector positions when the source was driven through Area 1. For Areas 2 and 3, the 10-mR chambers

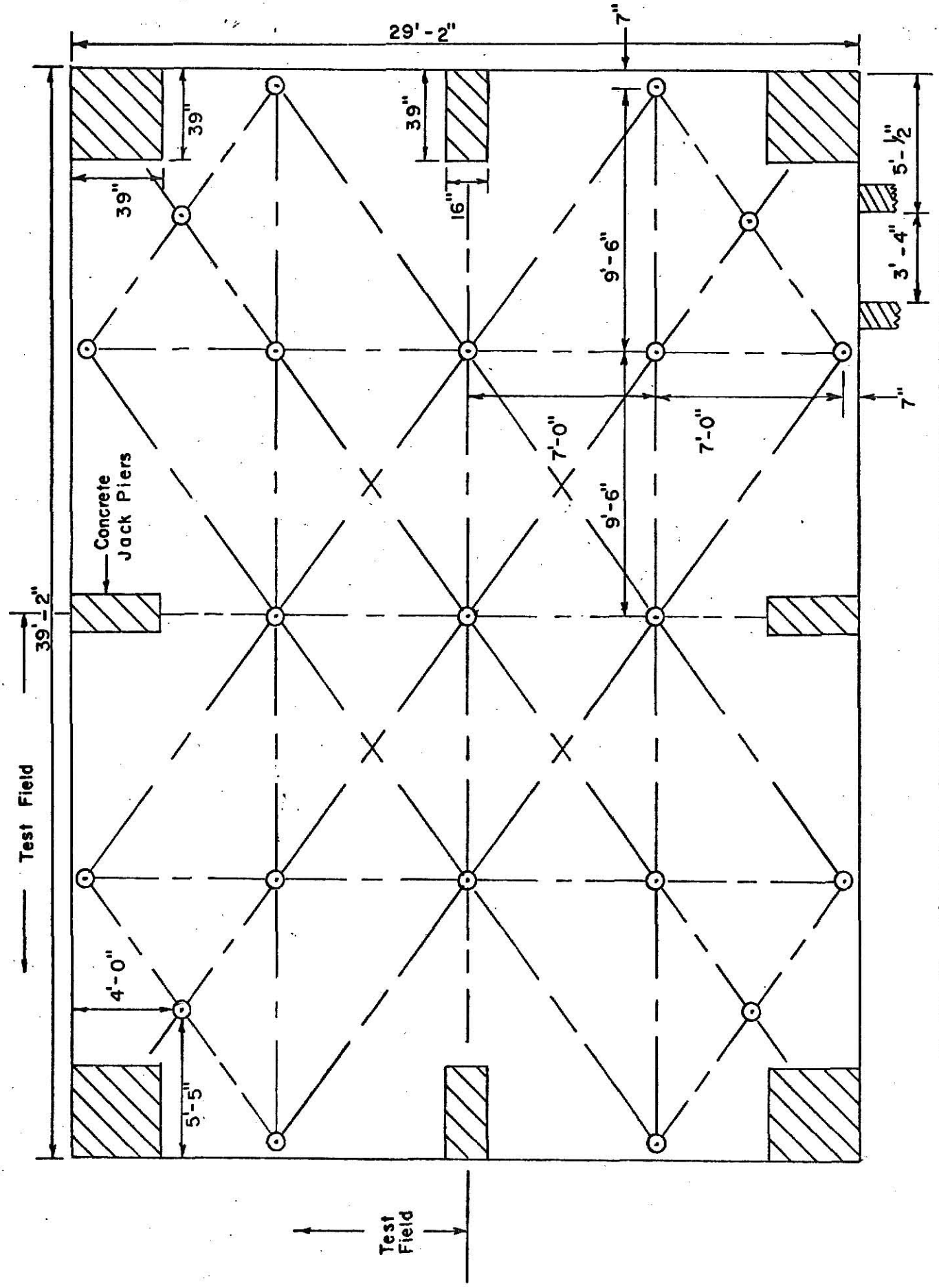

Figure 11. Plan of the detector positions in the basement of the test house.

were used. The resulting average exposures in House 1 were ∿9 mR (Area 1), ∿2.5 mR (Area 2), and ∿1.0 mR (Area 3). In an effort to minimize the turn-around time between runs, the small pumped source (∿6 Ci) was used in Area 1 for House 12. This allowed for the use of the 10-mR chambers which could be read more rapidly. The observed average exposures in House 12 were ∿1 mR (Area 1), ∿1.5 mR (Area 2), and ∿1 mR (Area 3).

Details of the data reduction are given in Appendix D.

5.0 PRESENTATION OF THE DATA

5.1 Calculated Results ^{60}Co Radiation

Since the fallout field was simulated with ^{60}Co radiation, it was desirable to have theoretical results which are based on ^{60}Co radiation rather than the fallout spectrum. It is reasonable to assume that any conclusions drawn from the comparison of theoretical and experimental results based on the ^{60}Co spectrum will be applicable to results from the 1.12 hour fission spectrum, since the average photon energies of both spectra are nearly the same. Spencer has published a set of data for ^{60}Co radiation [2] which is analogous to the fission data from which the EM functions were derived. The construction of EM functions for the ^{60}Co data is discussed in Appendix B. Eisenhauer's ceiling attenuation factor has the following form for ^{60}Co radiation:

$$B_c(X,\omega) = (1 - 3.0e^{-2.3\omega})e^{-0.12X} + 3.0e^{-2.3\omega}e^{-0.042X} \quad . \tag{14}$$

Batter and Starbird have presented a separate set of curves for their factor $\tilde{B}_c(X,\bar{\omega})$ for ^{60}Co radiation. Hence, the required functions for ^{60}Co radiation were available for each method.

The functional expressions for the test house are somewhat more complicated than those in Section 2.4.2 due to the windows and doors of the house. The exact expressions used for the EM reduction factors are given in Appendix A. Although they are not explicitly written out, the expressions for modified methods may be inferred from Section 3.0.

The calculated reduction factors at the same location in Houses 1 and 12 nearly indistinguishable. This fact is due to the following relationship:

$$\{\Delta G_a[1 - S_w(5.5)] + \Delta G_s S_w(5.5)E(e)\}\, B_e(5.5,3')$$

$$\simeq \{\Delta G_a[1 - S_w(45.5)] + \Delta G_s S_w(45.5)E(e)\}\, B_e(45.5,3') \quad (15)$$

where $\Delta G_a = G_a(\omega_u') - G_a(\omega_u)$ and $\Delta G_s = G_s(\omega_u') - G_s(\omega_u)$. Figure 12 shows the variation in the reduction factor at two basement detector locations as a function of the mass thickness of the exterior walls of the test house. The physical interpretation of this effect is that, as the thickness of the walls is increased, the amount of skyshine which is attenuated in the wall mass is more than compensated by radiation which is scattered towards the detector by the wall. At a certain mass thickness ($\sim$20 psf in this case) the absorption in the wall becomes dominant, and reduction factor in the basement begins to decrease. The two mass thicknesses of the exterior walls of the test house are such that the reduction factors are nearly equal.

The reduction factors along the basement centerline for both houses and each method are listed in Table II. The maximum discrepancy between the results for both houses at any given location is about 8 percent. Similar observations were made on the calculations for off-center locations. Because of these similarities, only the calculated results for House 1 were used in the succeeding comparisons with the experimental values.

5.2 The Experimental Results

When the results from the symmetric points in each quadrant of the dosimeter layout of Fig. 11 were combined, a seven-point grid was obtained. The detector positions on this grid were numbered as shown in Fig. 13.

The contribution to the reduction factor from that portion of the infinite plane source which was not simulated in the experiments was estimated by the method of Kaplan [13]. This contribution is referred to as the far field, and the estimation of it is discussed in Appendix E.

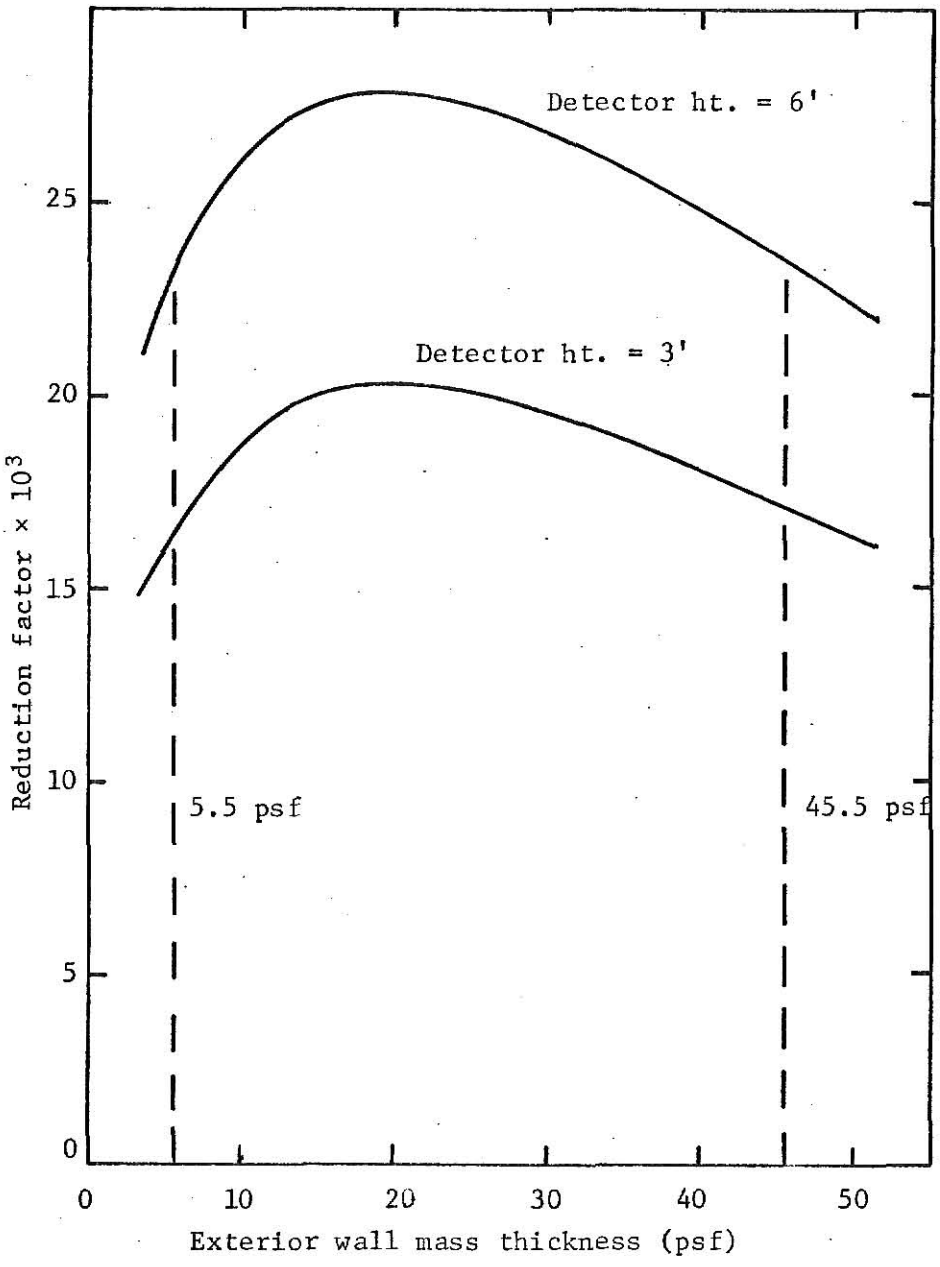

Figure 12. Theoretical variation of the reduction factor with exterior wall mass thickness for two heights along the basement centerline.

Table II. Calculated reduction factors along the basement centerline in House 1 and House 12.

Height (ft)	House No.	Reduction factor × 10^3				
		Old EM	New EM	Kaplan	Batter-Starbird	French
0	1	8.0	12.5	13.1	14.5	13.5
	12	8.5	13.4	14.0	15.4	13.5
1	1	9.0	13.6	14.5	15.7	14.6
	12	9.5	14.4	15.3	16.7	14.6
2	1	10.3	15.0	16.2	17.3	15.9
	12	10.8	15.7	17.0	18.1	15.9
3	1	11.7	16.3	17.8	18.8	17.2
	12	12.1	17.0	18.5	19.6	17.1
4	1	13.7	18.5	20.2	21.2	19.0
	12	14.1	19.1	20.8	21.8	18.9
5	1	15.9	20.6	22.5	23.2	20.9
	12	16.2	21.0	22.9	23.7	20.7
6	1	18.5	23.1	24.6	24.7	23.1
	12	18.7	23.3	24.8	24.9	22.8
7	1	22.2	26.7	27.8	26.6	26.1
	12	22.0	26.5	27.5	26.4	25.5
8	1	27.1	31.4	31.1	28.7	29.9
	12	26.3	30.5	30.1	27.9	28.8

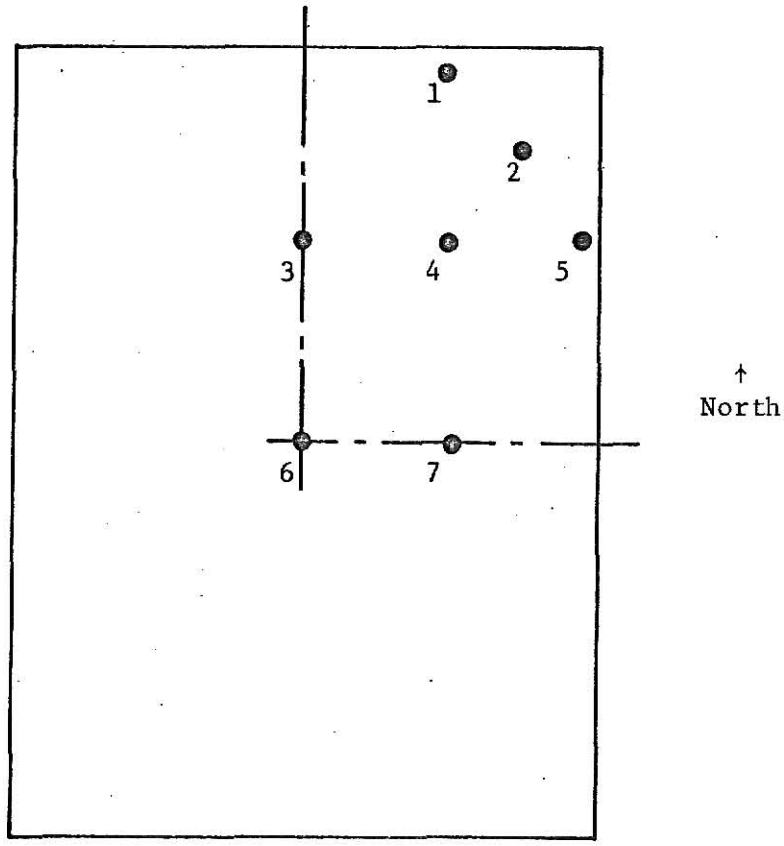

Figure 13. Key to grid point numbers.

The measured reduction factors for each tubing area, the far field estimates, and the total experimental reduction factors are presented in Tables III and IV. The reduction factors are based on a reference dose rate of 480 R/hr for 1 Ci/ft^2 [14]. The uncertainties indicated are estimates of the standard deviation, and the methods used to obtain these estimates are detailed in Appendices C, D, and E.

5.3 Comparison of the Calculated and Measured Reduction Factors

A comparison of the theoretical and experimental results for the reduction factors along the basement centerline is shown in Fig. 14. The large error bars on the experimental points are due mainly to the uncertainties in

Table III. Measured reduction factors for House 1.

	Reduction factor × 10^3				
	Area 1	Area 2	Area 3	Far Field	Total
Grid height = 3 ft					
Grid pt.					
1	3.60±0.12	1.37±0.08	0.96±0.08	7.66±1.03	13.58±1.13
2	3.82±0.14	1.51±0.06	1.14±0.08	9.55±0.99	16.02±1.13
3	5.43±0.15	2.10±0.10	1.52±0.11	12.39±1.34	21.53±1.53
4	5.05±0.13	1.95±0.09	1.42±0.08	11.48±1.11	19.90±1.30
5	3.60±0.15	1.29±0.07	1.02±0.09	7.48±1.13	13.38±1.22
6	5.68±0.27	2.23±0.26	1.60±0.20	13.12±2.76	22.64±2.89
7	5.23±0.14	1.95±0.16	1.50±0.12	11.82±1.61	20.50±1.76
Grid height = 6 ft					
Grid pt.					
1	4.49±0.12	1.71±0.13	1.24±0.10	9.28±1.33	17.26±1.46
2	6.08±0.17	2.06±0.13	1.51±0.09	10.42±1.28	20.07±1.46
3	6.36±0.37	2.60±0.18	1.84±0.12	15.38±2.04	26.18±2.25
4	6.63±0.12	2.47±0.22	1.66±0.21	12.79±2.54	23.54±2.67
5	4.43±0.17	1.63±0.12	1.16±0.07	8.68±1.16	15.89±1.29
6	6.09±0.20	2.52±0.31	1.64±0.18	13.39±2.56	23.63±2.71
7	6.10±0.20	2.62±0.18	1.90±0.11	16.79±1.64	27.41±1.89
Centerline data					
Height (ft)					
2	5.32±0.17	2.12±0.55	1.51±0.25	12.25±3.75	21.21±3.86
3	5.66±0.23	2.23±0.26	1.60±0.20	13.18±2.72	22.67±2.84
4	5.93±0.17	2.32±0.32	1.45±0.39	12.39±4.20	22.07±4.29
5	6.04±0.20	2.42±0.35	1.78±0.18	14.79±2.60	25.03±2.76
6	6.01±0.18	2.37±0.22	1.64±0.18	13.41±2.34	23.43±2.48
7	5.38±0.25	2.54±0.58	1.69±0.43	16.28±5.73	25.89±5.84
8	5.93±0.21	1.90±0.40	1.29±0.27	12.54±3.74	19.66±3.82

Table IV. Measured reduction factors for House 12.

	Reduction factor × 10^3				
	Area 1	Area 2	Area 3	Far Field	Total
Grid height = 3 ft					
Grid pt.					
1	3.88±0.39	1.18±0.06	0.81±0.10	4.40±1.72	10.27±1.79
2	4.66±0.40	1.29±0.07	0.86±0.09	3.52±1.72	10.33±1.80
3	6.84±0.75	1.83±0.08	1.14±0.16	3.58±3.13	13.39±3.25
4	6.50±0.41	1.77±0.07	1.11±0.10	3.85±1.80	13.24±1.90
5	3.74±0.40	1.03±0.06	0.69±0.15	2.56±1.97	8.03±2.03
6	6.95±0.90	2.10±0.14	1.35±0.26	6.82±4.17	17.21±4.31
7	6.61±0.65	1.89±0.10	1.37±0.15	6.72±2.78	16.58±2.91
Grid height = 6 ft					
Grid pt.					
1	4.71±0.39	1.37±0.08	0.94±0.13	4.38±1.04	11.39±2.02
2	6.55±0.67	1.76±0.12	1.15±0.12	4.33±2.63	13.79±2.76
3	7.38±0.65	2.30±0.12	1.55±0.15	8.74±2.81	19.97±2.96
4	7.84±0.69	2.20±0.10	1.48±0.14	6.41±2.83	17.93±2.97
5	4.35±0.47	1.28±0.06	0.79±0.13	3.62±2.14	10.04±2.22
6	7.39±0.84	2.34±0.16	1.54±0.21	8.80±3.75	20.06±3.90
7	7.76±0.65	2.36±0.10	1.59±0.16	8.45±2.89	20.15±3.04
Centerline data					
Height (ft)					
2	7.09±1.17	2.04±0.14	1.30±0.16	5.73±4.06	16.16±4.26
3	6.95±0.90	2.10±0.14	1.35±0.26	6.82±4.17	17.21±4.31
4	7.81±1.17	2.17±0.15	1.39±0.22	5.47±4.63	16.84±4.81
5	7.67±0.83	2.24±0.19	1.53±0.28	7.30±4.21	18.74±4.34
6	7.39±0.84	2.34±0.16	1.54±0.21	8.80±3.75	20.07±3.91
7	6.59±0.91	2.15±0.30	1.40±0.20	8.22±3.90	18.37±4.06
8	4.72±0.86	1.64±0.13	1.16±0.16	8.10±3.41	15.62±3.56

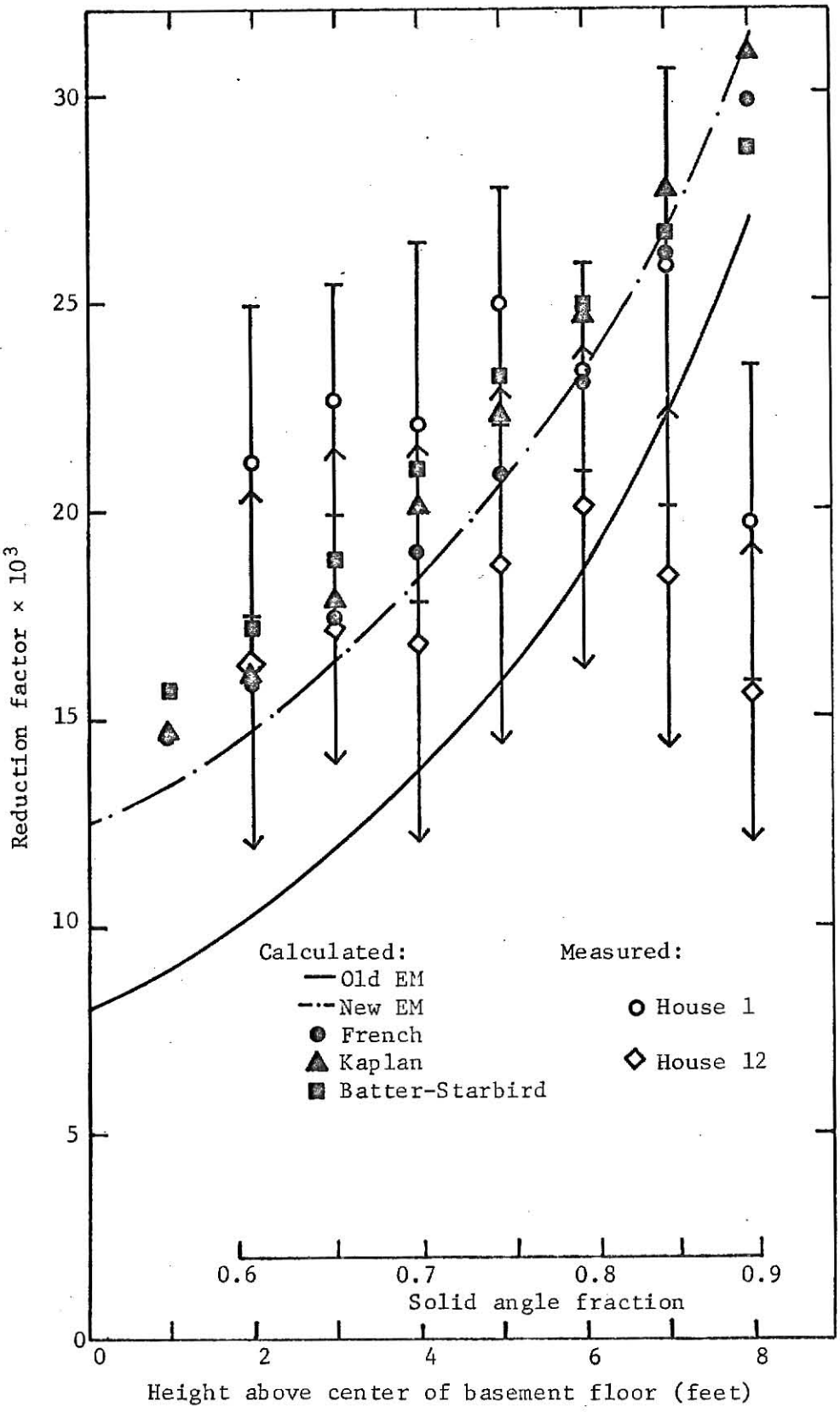

Figure 14. Calculated and measured reduction factors for a vertical traverse at the center of the basement.

the far field estimates. Since the far field contribution was about half of the total, the magnitude of these uncertainties is not unreasonable.

The data from the grid points are compared to the theoretical values in a series of horizontal traverses. Three traverses are presented for each grid height. One traverse is along the diagonal from the center to the corner of the basement, Figs. 15 and 16; another is along the northerly direction from grid point 7 to the wall, Figs. 17 and 18; and the third is along the easterly direction from grid point 3 to the wall, Figs. 19 and 20. Each traverse passes through three detector locations.

The error bars on the off-center points are smaller because these values are the sum of results from four detector locations and, consequently, are based on four times as much data as are the centerline points. Although the error bars for the results from Houses 1 and 12 overlap in Fig. 14, they, in general, do not at the off-center points.

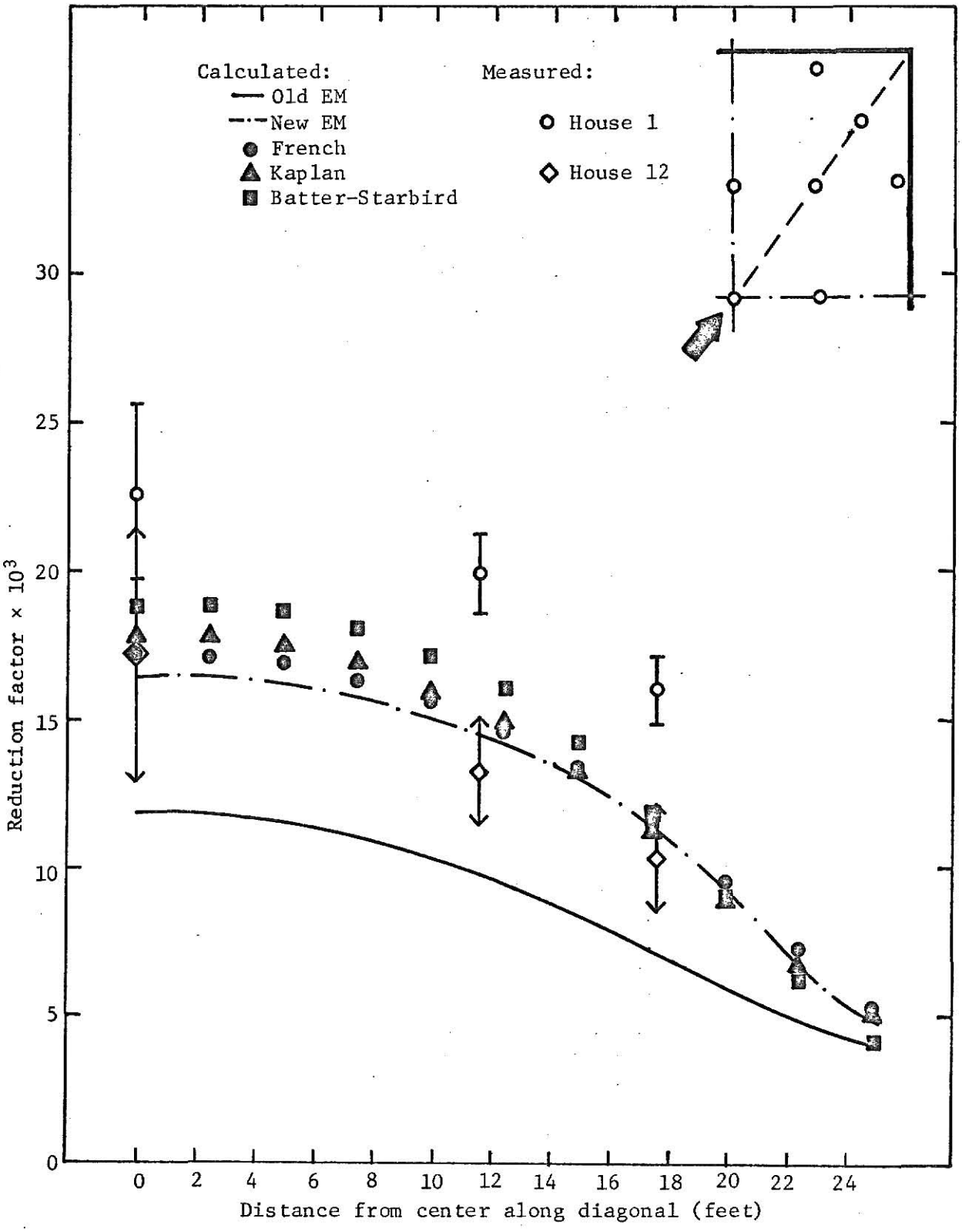

Figure 15. Calculated and measured reduction factors for a horizontal traverse along the diagonal 3 ft above the basement floor.

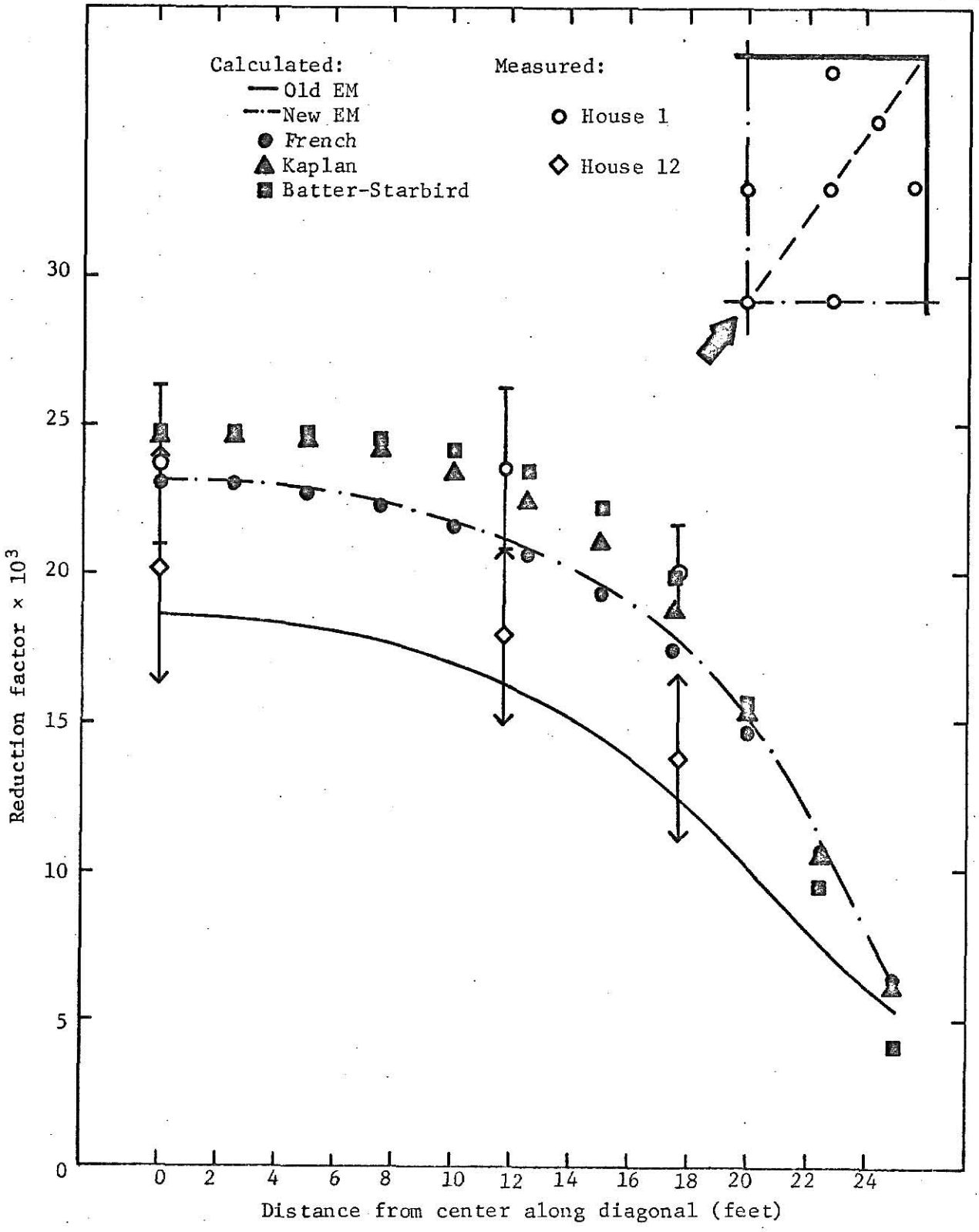

Figure 16. Calculated and measured reduction factors for a horizontal traverse along the diagonal 6 ft above the basement floor.

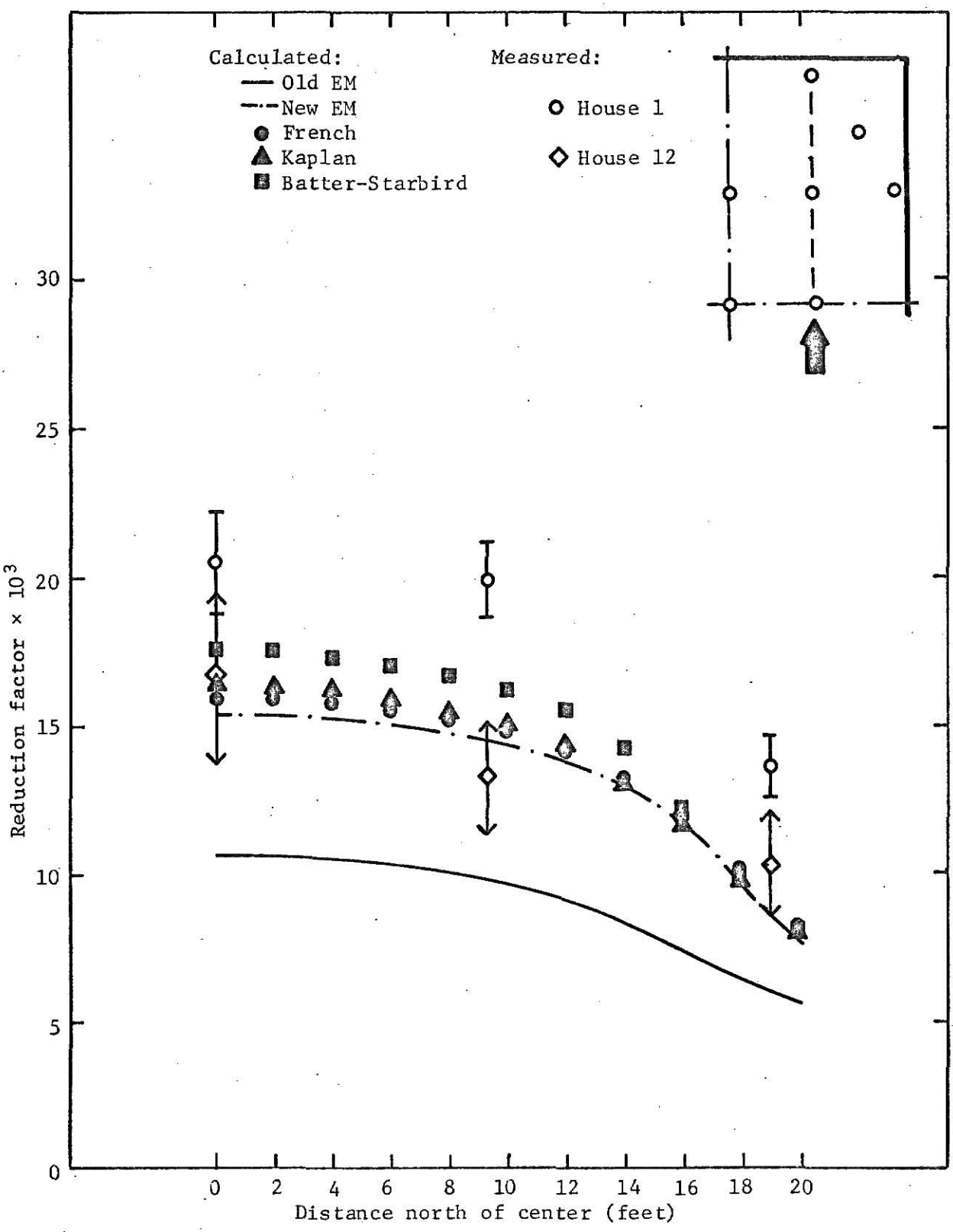

Figure 17. Calculated and measured reduction factors for a north-south traverse 3 ft above the basement floor 7 ft east of center.

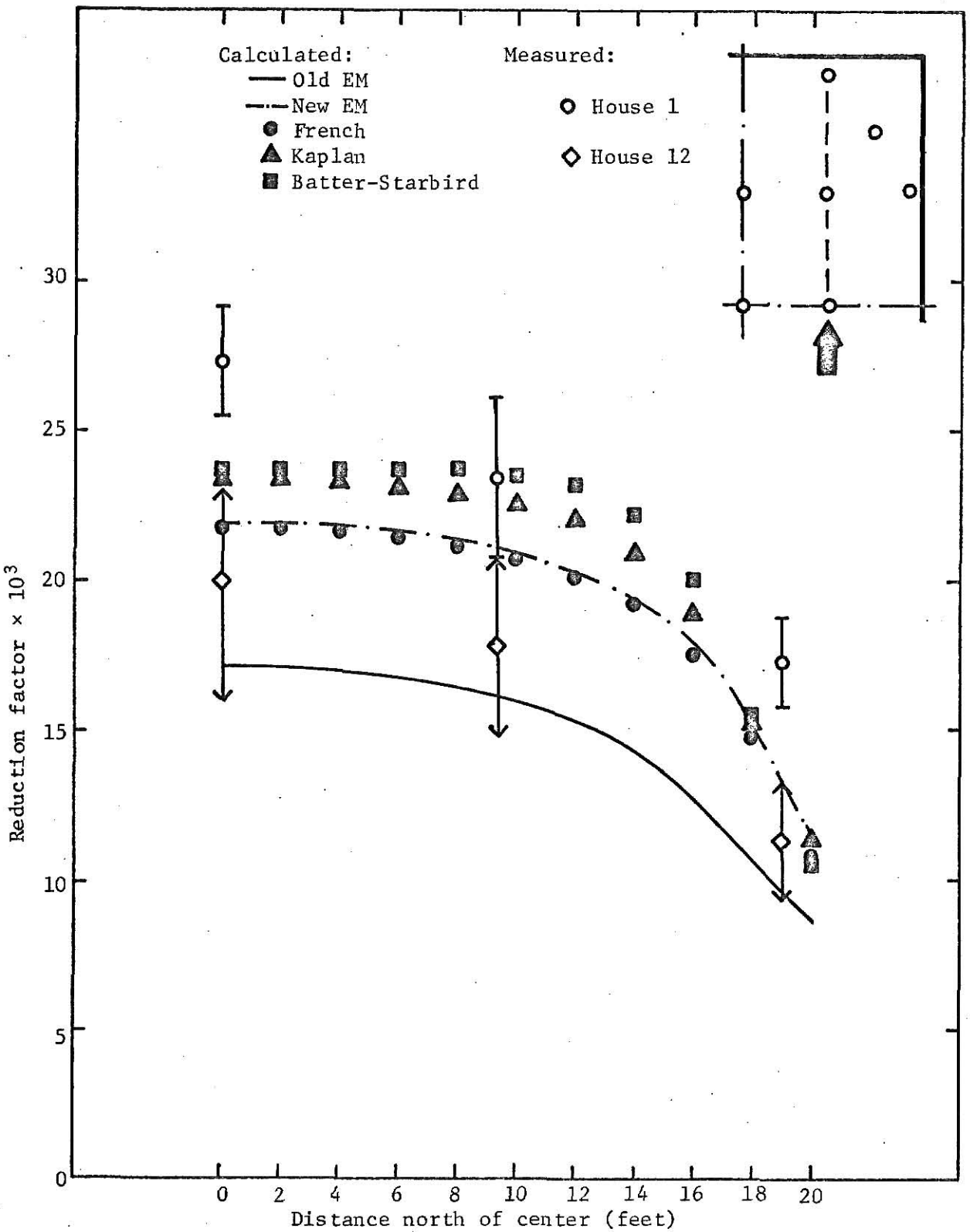

Figure 18. Calculated and measured reduction factors for a north-south traverse 6 ft above the basement floor 7 ft east of center.

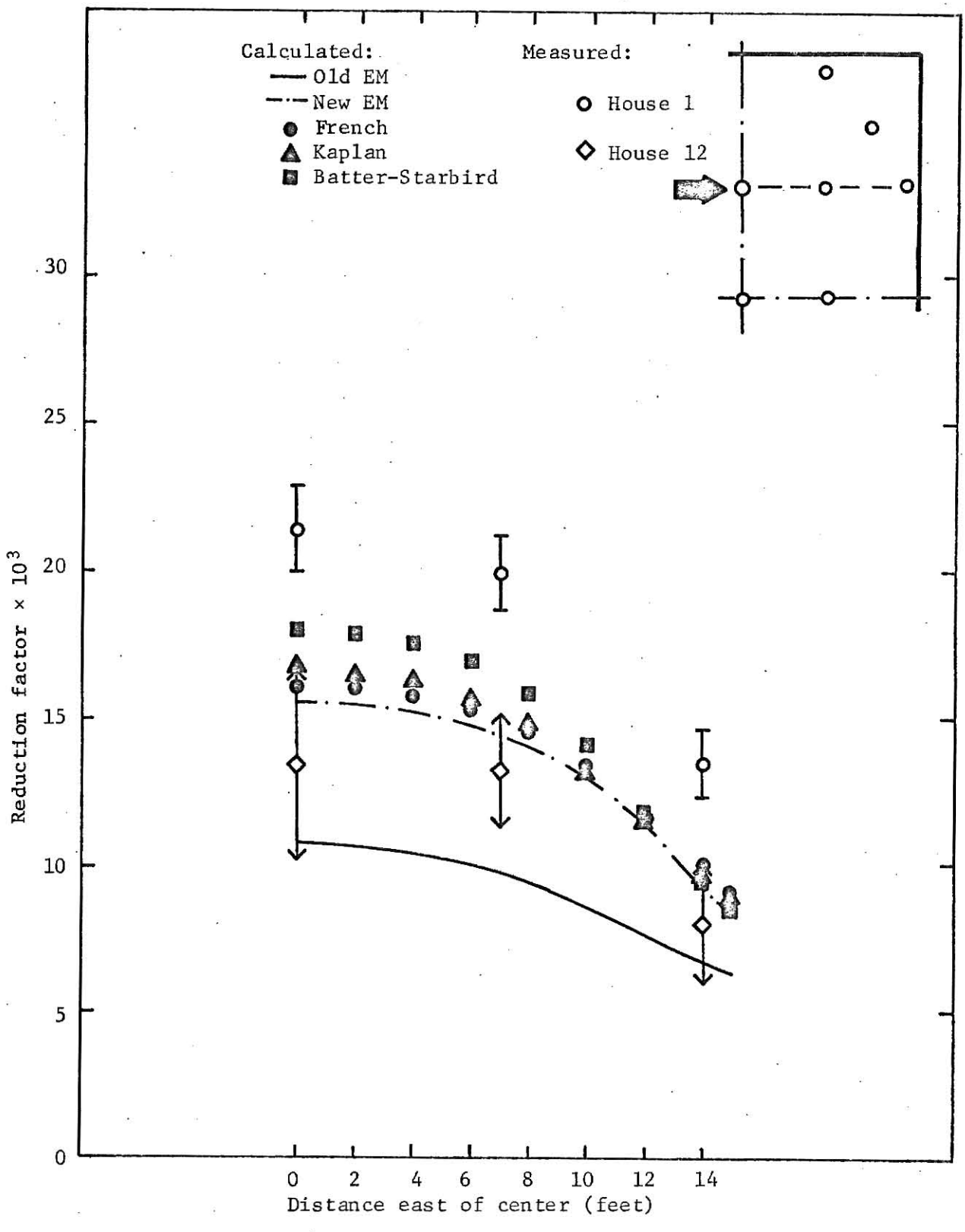

Figure 19. Calculated and measured reduction factors for an east-west traverse 3 ft above the basement floor 9.3 ft north of center.

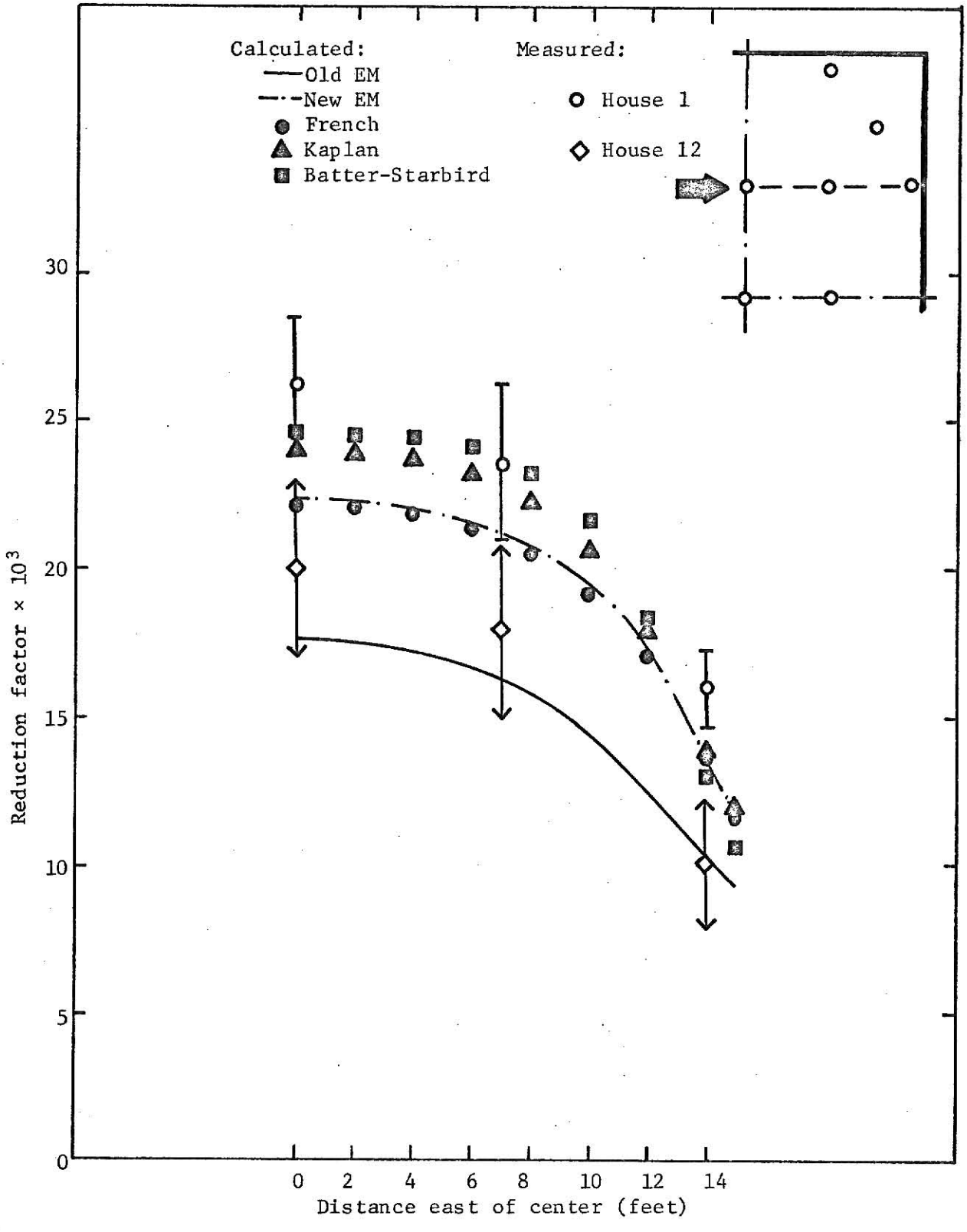

Figure 20. Calculated and measured reduction factors for an east-west traverse 6 ft above the basement floor 9.3 ft north of center.

6.0 CONCLUSIONS

Considering the many simplifying assumptions inherent in the EM, the over-all agreement between the calculated and measured reduction factors is satisfactory. The use of the EM for surveys of residential buildings of the type which was studied in this work should give results within an accuracy of 50 percent.

Because of the low mass thickness of the basement ceiling, no significant differences were observed between the results of any of the modified methods for calculating the reduction factor. However, the predictions of the original EM were 15 to 40 percent below those of the modified methods

The shape of the calculated curves for the various horizontal traverses was generally verified by the experimental points for both house configurations. Since the variations in the calculated values, as the detector is moved horizontally across the basement, are due to different contributions from the geometry factors, the preceding observation would seem to verify the geometry functions $G_a(\omega)$, $G_s(\omega)$, and $E(e)$. Although the calculations predicted almost identical results for the two thicknesses of the exterior walls, the experimental results indicated that the reduction factors for the thick-wall case were about 30 percent lower than those of the thin-wall case. This discrepancy is probably due to some error in one or both of the EM functions $B_e(X_e,3')$ and $S_w(X_e)$ for low mass thickness.

The most significant deviation of experiment from theory is that observed in the vertical traverse at the center of the basement. The measured reduction factors do not increase as rapidly as do the calculated values as the basement ceiling is approached. At a height of about six feet ($\omega_u \simeq 0.8$) both sets of measured values go through maxima while the calculated values continue

to rise sharply. The inability to predict this effect is an acknowleged weakness in the current EM ceiling attenuation factor [6]. Although it is not important in small structures, in the basement of large buildings, where the ceiling subtends a large solid angle fraction ($\omega_u > 0.9$), the result could lead to the over-estimation of the exposure by a factor of 2 or more.

7.0 SUGGESTIONS FOR FURTHER WORK

Since the largest contribution to the experimental uncertainties was that from the estimation of the far field, an effort should be made in any further studies in the test house to reduce this contribution. The author believes that the method of Kaplan is basically sound, although it is quite sensitive to small fluctuations in the data. Improved accuracy could be obtained by dividing the three existing tubing areas into, say, five areas. Kaplan's method could then be applied to the data from the outer four areas.

Most of the measured exposures from the second and third tubing areas were below 2 mR which resulted in a 10 percent, or greater, uncertainty in the measurements. If a new source could be obtained of 100 to 150 Ci, more reliable dosimeter readings could be obtained.

It was assumed that the dosimeters behaved as isotropic detectors. The response of the 10-mR chambers is known to vary with the direction of the incident radiation; however the angular response of the TL-12 dosimeters is not known. Data should be taken to determine the exact nature of the angular dependence for each dosimeter, and investigations should be carried out, if necessary, to determine how the data might be corrected for this effect.

8.0 ACKNOWLEDGEMENTS

The author is indebted to Professors R. E. Faw and M. J. Robinson for their guidance in the planning and completion of this work; Mr. R. S. Reynolds, who directed the experiments which have been cited in this work; and the Office of Civil Defense, whose fellowship program has provided financial support. A special thanks is expressed to the author's mother who has helped in preparing the manuscript.

9.0 REFERENCES

1. Office of Civil Defense
   Shelter Design and Analysis, Vol. 1, Fallout Radiation Shielding, TR-20, July 1969.

2. Spencer, L. V.
   Structure Shielding against Fallout Radiation from Nuclear Weapons, NBS Monograph 42, June 1962.

3. Kimel, W. R. et al.
   Radiation Shielding, Analysis and Design Principles as Applied to Nuclear Defense Planning, TR-40, U. S. Government Printing Office, Nov. 1966.

4. Eisenhauer, C.
   An Engineering Method for Calculating Protection Afforded by Structures against Fallout Radiation, NBS Monograph 76, Jan. 1964.

5. Office of Civil Defense
   Design and Review of Structures for Protection from Fallout Gamma Radiation, Interim Edition, OCD PM-100-1, Feb. 1965.

6. Eisenhauer, C. E. and Kaplan, A. L.
   Evaluation of the Reduction Factor in the Basement of a Structure, NBS Report 10 037, May 16, 1969.

7. Schumchyk, M. J. et al.
   Scattered Radiation (Skyshine) Contribution to a Concrete-Covered Basement Location in a Simulated Fallout Field, Nuclear Defense Laboratory, NDL-TR-69, July 1967.

8. Kaplan, A. L.
   "Investigation of the Floor-Barrier Reduction Factor Used in Structure Shielding Theory," Nucl. Sci. Eng., 27, p. 388, Feb. 1967.

9. Kaplan, A. L. et al.
   Final Report Phase II: Structure Shielding from Simulated Fallout Gamma Radiation, Technical Operation Research Report TO-B65-123, June 1966.

10. Batter, J. F. and Starbird, A. W.
    The Preparation of Simplified Manuals for Shielding Analysis, Supplement One: "In and Down Scattering", Conesco Report No. 4848-2, March 1967.

11. French, R. L.
    An Extension of the Engineering Method to Improve Fallout Protection Factor Calculations for Basements, Radiation Research Associates Report RRA-M75, Nov. 1967.

12. Rubin, R. M.
Personal Communication, Dept. Nuc. Engg., Kansas State University, 1968.

13. Kaplan, A. L.
Final Report: Analysis of Data from Structure Shielding Experiments, Technical Operation Research Report No. TO-B 68-39. June 1968.

14. Eisenhauer, C. E.
"Some Benchmark Experiments in Fallout Sheilding," Proceedings of the Special Panel Discussion on Shielding Standards, ANS-SD-6, June 1967.

15. Office of Civil Defense
PFCOMP-Computer Program, "Fallout Protection Factor Analysis of Buildings," April 1968.

16. Blizard, E. P.
Reactor Handbook, Vol. III, Part B: Shielding, Interscience Publishers, New York, 1962.

17. Storm, E. and Israel, H. J.
Photon Cross-Sections from 0.001 to 100 MeV for Elements 1 to 100, Los Alamos Report LA-3753, Nov. 1967.

18. Chilton, A. B. et al.
Determination of Parameters in an Empirical Function for Buildup Factors for Various Photon Energies, U. S. Naval Civil Engineering Laboratory Technical Note N-389, Aug. 1960.

19. Fu,C. Y. and Chilton, A. B.
Exposure Field from a Point Isotropic Source Located at the Surface of a Thick Concrete Slab, University of Illinois Report NRSS-2, July 1966.

20. Brownlee, K. A.
Statistical Theory and Methodology in Science and Engineering, John Wiley and Sons, Inc., New York, 1965.

21. Melissinos, A. C.
Experiments in Modern Physics, Academic Press, New York 1966.

10.0 APPENDICES

10.1 Appendix A: Engineering Manual Calculations for the KSUNESF Test House

10.1.1 Introduction

This appendix outlines Engineering Manual (EM) calculations for the KSUNESF test house according to TR-20, Vol. 1 [1]. An attempt has been made to stay within the bounds of the EM theory in cases where the procedure was not explicitly described in the EM. A FORTRAN IV program called ENGMAN was written to carry out calculations for almost any combination of detector location and floor height. No explanation of the EM functions is given here; it is assumed that the reader has a knowledge of EM theory. The purpose of this appendix is to document the exact functional expressions used.

10.1.2 Nomenclature

The reduction factor for the ground contribution, C_g, has been separated into three contributions: 1) the contribution from non-structure-scattered radiation reaching the detector from directions below the detector plane; 2) the contribution from non-structure-scattered radiation reaching the detector from directions above the detector plane (air-scattered radiation, or skyshine); and 3) the structure scattered contribution. These contributions are identified with the following superscripts: D, A, S, respectively. The contributions are further broken down according to the various external surfaces of the house through which the radiation passes. These surfaces are as follows: 1) the exposed basement walls, 2) the solid walls of the first story, 3) the windows, 4) the roof, 5) the doors of the first story. They are identified by the following second-superscripts: 1, 2, 3, 4, d, respectively. Thus, C_g^{A3}

would be the skyshine contribution through the windows, while C_g^{S1} would be the wall-scattered contribution from the exposed basement walls.

The mass thickness of the various barriers in the house are given the following labels: exposed basement walls, X_w; first story walls, X_e; doors, X_d; floor slab, X_f; roof, X_r; and interior partitions, X_i. The mass thickness of the floor slab will always be labeled X_f, regardless of whether the detector is above or below it.

10.1.3 First-Story Detector Locations

The most general case is for a detector located above the window sill height and below the top of the windows. Refer to Figures A-1 and A-2 for dimensions and solid angles. Note that P_a, the "perimeter ratio", is actually an azimuthal sector as defined in Figure A-1. Note also that the doors are considered in a separate azimuthal sector. Refer to Figure A-3 for the fictitious building used to determine the contribution through the doors. The functional expressions and diagrams below are for a detector located on the centerline of the house. Applications to off-center locations will be discussed later.

$$C_g^{D1} = [G_d(\omega_\ell',H) - G_d(\omega_\ell,H)][1-S_w(X_w)]B_e(X_w,H)B_f(X_f) \qquad \text{(A-1)}$$

$$C_g^{S1} = [G_s(\omega_\ell') - G_s(\omega_\ell)]\, S_w(X_w)\, E(e)\, B_e(X_w,H)\, B_f(X_f) \qquad \text{(A-2)}$$

$$C_g^{D2} = \{[G_d(\omega_\ell,H) - G_d(\omega_{a\ell},H)][1-A_{z_D}] + G_d(\omega_{a\ell},H)[1-P_a-A_{z_D}]\}$$

$$\times [1-S_w(X_e)]B_e(X_e,H) \qquad \text{(A-3)}$$

$$= \{G_d(\omega_\ell,H)[1-A_{z_D}] - P_a\, G_d(\omega_{a\ell},H)\}[1-S_w(X_e)]B_e(X_e,H)$$

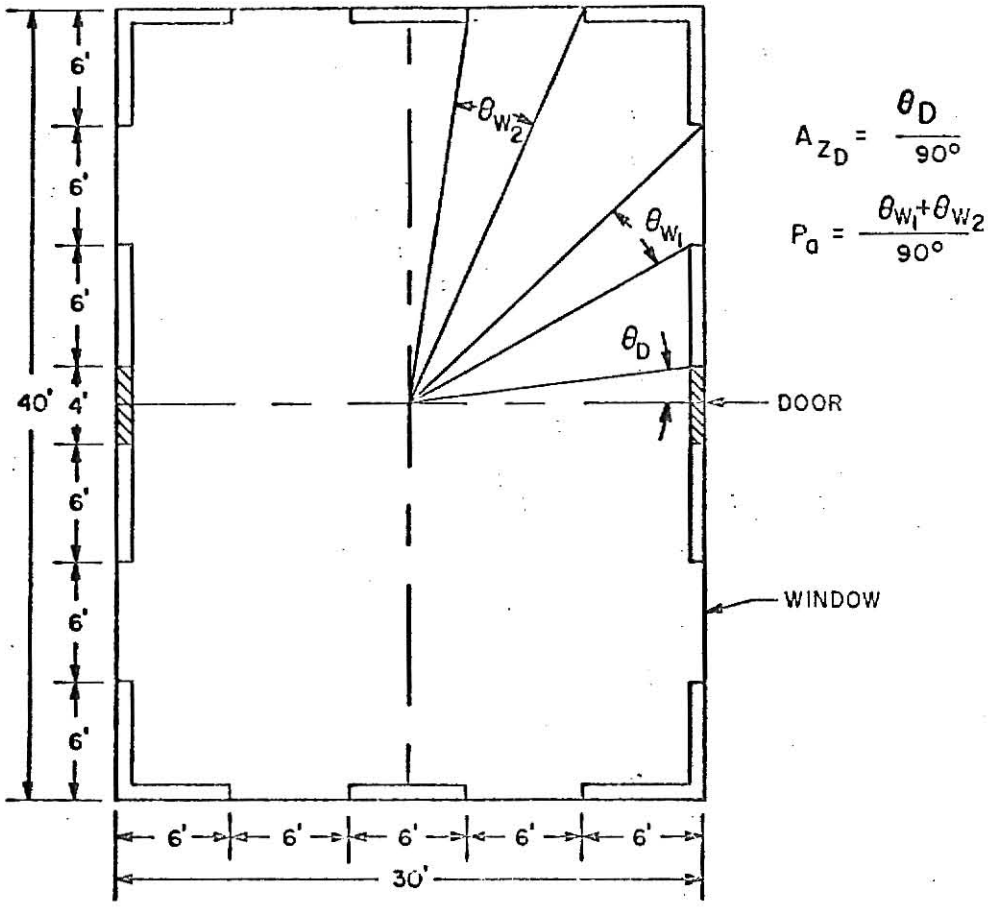

Figure A-1. Plan of the test house showing azimuthal sectors for doors and windows.

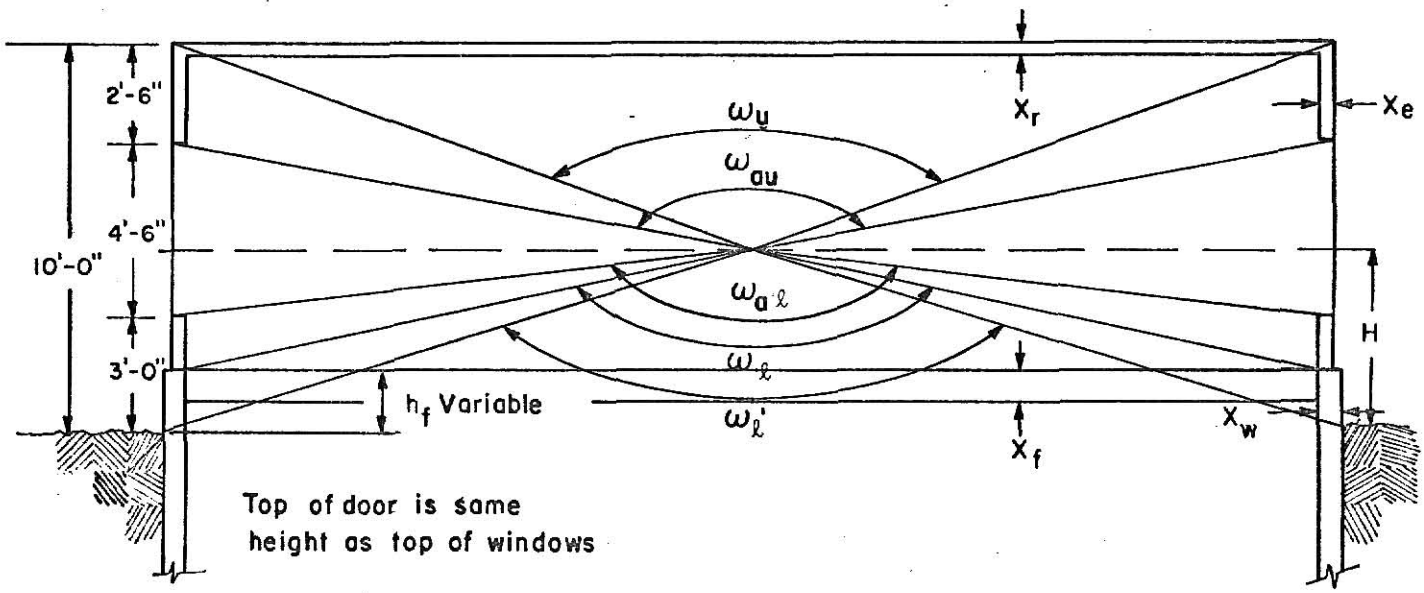

Figure A-2. Elevation of the test house with solid angle fractions for a first-story detector location.

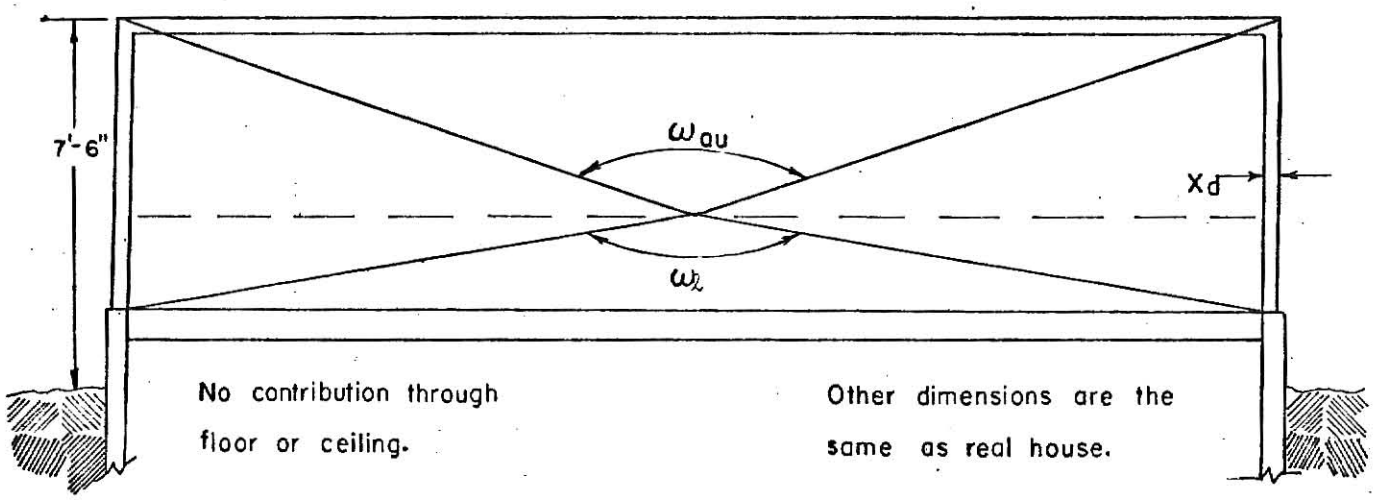

Figure A-3. Fictitious building for the contribution through the doors to a first-story detector location.

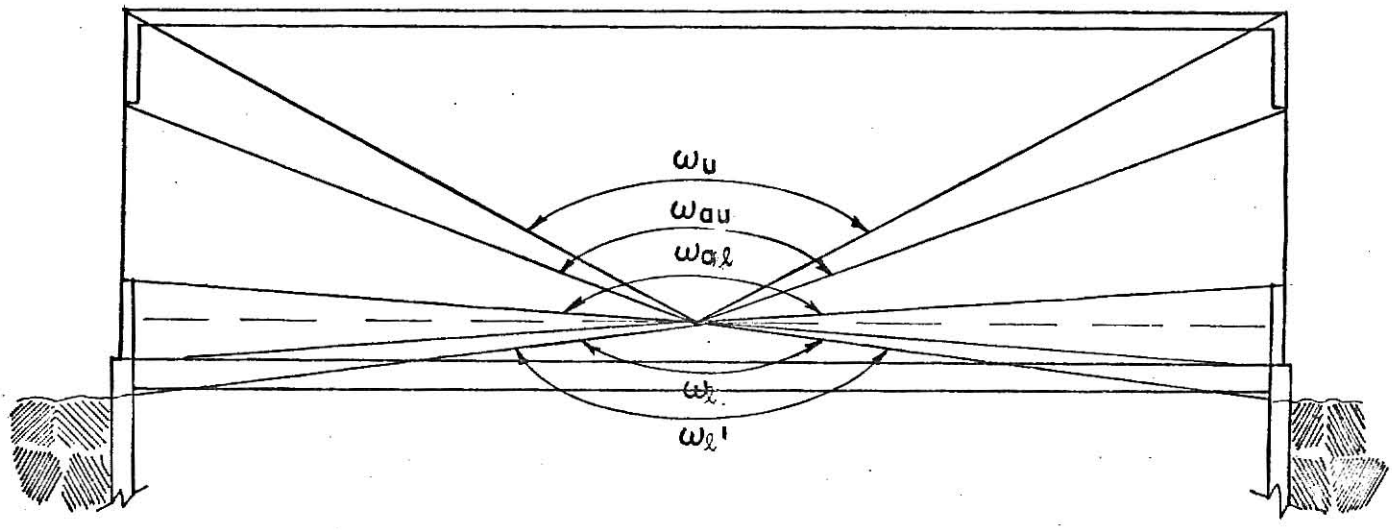

Figure A-4. Solid angle fractions for a first-story detector below window sill height.

$$C_g^{S2} = \{[G_s(\omega_u) - G_s(\omega_{a\ell})] + [G_s(\omega_\ell) - G_s(\omega_{a\ell})][1-A_{z_D}]$$

$$+ [G_s(\omega_{au}) + G_s(\omega_{a\ell})][1-P_a-A_{z_D}]\} S_w(X_e)E(e) B_e(X_e,H) \quad (A-4)$$

$$= \{G_s(\omega_u) - G_s(\omega_{au}) [P_a + A_{z_D}] - P_a G_s (\omega_{a\ell}) + G_s(\omega_\ell)[1-A_{z_D}]\}$$

$$\times S_w(X_e) E(e) B_e(X_e,H)$$

$$C_g^{A2} = \{G_a(\omega_u) - G_a(\omega_{au})[P_a + A_{z_D}]\}[1-S_w(X_e)]B_e(X_e,H) \quad (A-5)$$

$$C_g^{D3} = G_d (\omega_{a\ell},H) P_a B_e(0,H) \quad (A-6)$$

$$C_g^{A3} = G_a(\omega_{au}) P_a B_e(0,H) \quad (A-7)$$

$$C_g^{A4} = A_a(\omega_u) B'_o(X_r)^* \quad (A-8)$$

$$C_g^{Dd} = G_d(\omega_\ell,H) [1-S_w(X_d)]B_e(X_d,H) A_{z_D} \quad (A-9)$$

$$C_g^{Sd} = [G_s(\omega_\ell) + G_s(\omega_{au})] S_w(X_d)E(e) B_e(X_d,H) A_{z_D} \quad (A-10)$$

$$C_g^{Ad} = G_a(\omega_{au})[1-S_w(X_d)] B_e(X_d,H) A_{z_D} \quad (A-11)$$

---

* This is the notation of the May 1964 edition of the Engineering Manual and is most common in the literature. In the July 1968 edition the ceiling attenuation factor is labeled $B_c(X)$.

It was determined that the wall-scattered contribution from the gable walls was at most one percent of the total contribution. Hence, the flat roof configuration of Figure A-2 is justified.

Note that Eq. (A-8) is the expression for a decontaminated roof contribution for below grade detector locations. It is used here as the best approximation for the skyshine contribution through the roof since the detector heights are small.

For the cases when the detector is below the sill height, the contribution through the first story walls and windows are slightly different. Refer to Figure A-4.

$$C_g^{D2} = G_d(\omega_\ell, 3')\ [1-S_w(X_e)]B_e(X_e,3')[1-A_{z_D}] \tag{A-12}$$

$$C_g^{S2} = \{G_s(\omega_u)-G_s(\omega_{au}) + [G_s(\omega_\ell) + G_s(\omega_{a\ell})][1-A_{z_D}]$$

$$+ [G_s(\omega_{au}) - G_s(\omega_{a\ell})][1-P_a-A_{z_D}]\}S_w(X_e)E(e)B_e(X_e,3') \tag{A-13}$$

$$= \{G_s(\omega_u) -G_s(\omega_{au})[P_a + A_{z_D}] + G_s(\omega_{a\ell})P_a + G_s(\omega_\ell)[1-A_{z_D}]$$

$$\times S_w(X_e)E(e)B_e(X_e,3')$$

$$C_g^{A2} = \{G_a(\omega_u) - G_a(\omega_{au}) + G_a(\omega_{a\ell})[1-A_{z_D}] + [G_a(\omega_{au}) - G_a(\omega_{a\ell})]$$

$$\times [1-P_a-A_{z_D}]\}\ \ [1-S_w(X_e)]\ B_e(X_e,3') \tag{A-14}$$

$$= \{G_a(\omega_u) - G_a(\omega_{au})[P_a + A_{z_D}] + P_aG_a(\omega_{a\ell})\}[1-S_w(X_e)]B_e(X_e,3')$$

$$C_g^{D3} = 0 \tag{A-15}$$

$$C_g^{A3} = [G_a(\omega_{au}) - G_a(\omega_{a\ell})]P_a B_e(0,3') \qquad \text{(A-16)}$$

10.1.4 Case with Interior Partitions

The configuration for the interior partitions is shown in Fig. A-5. The azimuthal sectors containing zero, one, and two partitions are also defined in Fig. A-5. A separate azimuthal aperture fraction P_a, is defined for each sector. This factor is defined as the ratio of the azimuthal angle subtended by the windows in the sector to the total azimuthal angle of the sector in question.

Sector A:

$$A_{z_A} = \frac{10.93}{90} = 0.121 \qquad P_{a_A} = 0$$

Sector B:

$$A_{z_B} = \frac{8.18 + 9.63 + 8.53 + 8.17}{90} = 0.383$$

$$P_{a_B} = \frac{8.18 + 8.17}{34.52} = 0.474$$

Sector C:

$$A_{z_C} = \frac{7.53 + 22.75 + 6.77}{90} = 0.412$$

$$P_{a_C} = \frac{7.53 + 6.77}{37.05} = 0.386$$

Since each azimuthal fraction will appear with the barrier factor for the mass thickness of partitions in that sector, the following weighted azimuthal fractions are defined:

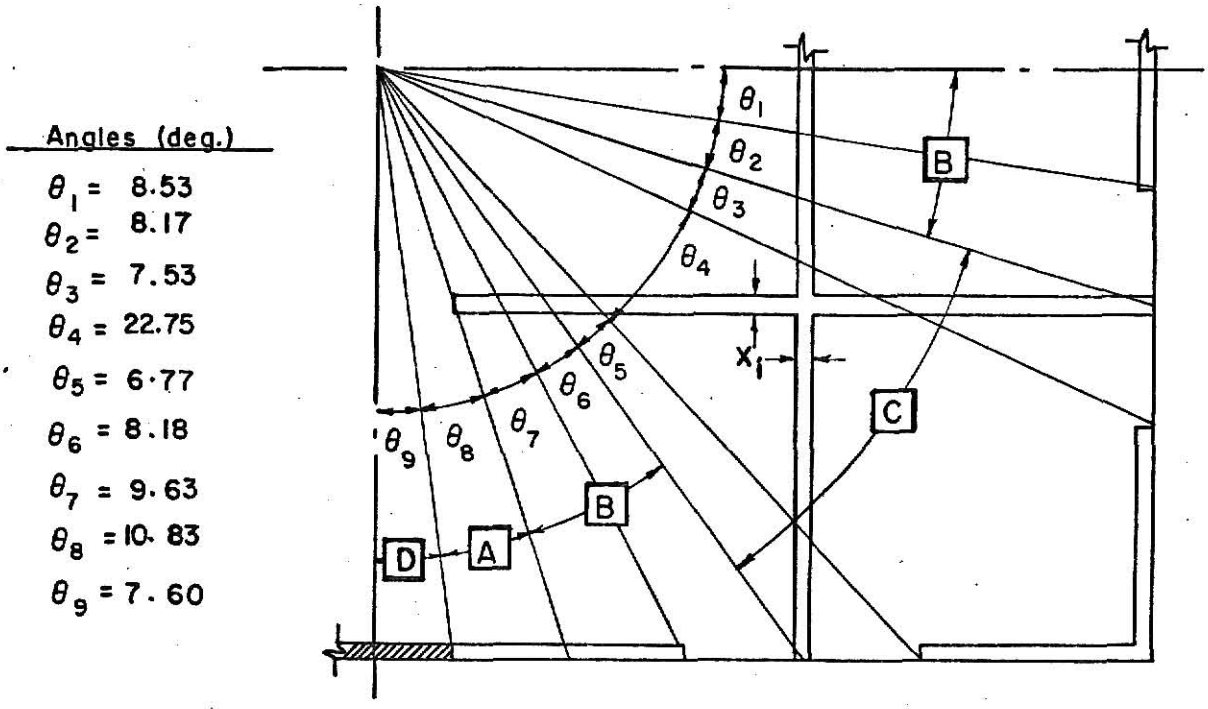

Figure A-5. Plan of one quarter of the test house with interior partitions.

$$\tilde{A}_{z_A} = A_{z_A}, \quad \tilde{A}_{z_B} = A_{z_B} B_i(X_i), \quad \tilde{A}_{z_C} = A_{z_C} B_i(2X_i).$$

The functional expressions are written here with the geometry factors as sums over the sectors with the appropriate weighting factors. Note that the contribution from the small wall sections above and below the doors are added in Eqs. (A-17), (A-18), (A-20), and (A-21). The expressions given are for a detector above the window sill and below the top of the window.

$$C_g^{D1} = [\sum{}^{*}\{[G_d(\omega_\ell',H) - G_d(\omega_\ell,H)]\ \tilde{A}_{z_i}\} + [G_d(\omega_\ell',H) - G_d(\omega_\ell,H)] \times A_{z_D}][1-S_w(X_w)]B_e(X_w,H)\ B_f(X_f) \tag{A-17}$$

$$C_g^{S1} = [\sum\{[G_s(\omega_\ell') - G_s(\omega_\ell)]\ \tilde{A}_{z_i}\} + [G_s(\omega_\ell') - G_s(\omega_\ell)]\ A_{z_D}] \times S_w(X_w)E(e)\ B_e(X_w,H)\ B_f(X_f) \tag{A-18}$$

$$C_g^{D2} = [\sum\ \{[G_d(\omega_\ell,H) - P_{a_i}\ G_d(\omega_{a\ell},H)]\ \tilde{A}_{z_i}\}][1-S_w(X_e)]B_e(X_e,H) \tag{A-19}$$

$$C_g^{S2} = [\sum\{[G_s(\omega_u) - P_{a_i} G_s(\omega_{au}) - P_{a_i}\ G_s(\omega_{a\ell}) + G_s(\omega_\ell)]\tilde{A}_{z_i}\} + [G_s(\omega_u) - G_s(\omega_{au})]\ A_{z_D}]\ S_w(X_e)\ E(e)\ B_e(X_e,H) \tag{A-20}$$

$$C_g^{A2} = [\sum\{[G_a(\omega_u) - P_{a_i}\ G_a(\omega_{au})]\ \tilde{A}_{z_i}\} + [G_a(\omega_u) - G_a(\omega_{au})]A_{z_D}] \times [1-S_w(X_e)]\ B_e(X_e,H) \tag{A-21}$$

* Summation symbol implies summation over i for i equal A, B, and C.

$$C_g^{D3} = B_e(0,H) \sum\{G_d(\omega_{a\ell},H)\ P_{a_i}\ \tilde{A}_{z_i}\} \tag{A-22}$$

$$C_g^{A3} = B_e(0,H) \sum\{G_a(\omega_{au})\ P_{a_i}\ \tilde{A}_{z_i}\} \tag{A-23}$$

The contributions through the doors are the same as in the non-partitioned cases. For certain combinations of floor height and low detector positions Eqs. (A-17) and (A-18) may be in error because some radiation from the exposed basement wall may reach the detector without intercepting an interior partition. No attempt is made to correct for this.

The skyshine contribution through the roof is formulated by differencing the contributions from rectangular areas on the ceiling. Refer to Fig. A-6. The dimensions and solid angle fraction for each rectangular area are tabulated below:

Dimensions	Solid angle fraction
12' × 22'	ω_1
4' × 30'	ω_2
4' × 12'	ω_3
22' × 30'	ω_4
12' × 40'	ω_5
30' × 40'	ω_u

$$C_g^{A4} = \{[A_a(\omega_1) + A_a(\omega_2) - A_a(\omega_3)] + [A_a(\omega_4) + A_a(\omega_5) - A_a(\omega_1) - A_a(\omega_2) + A_a(\omega_3)]\ B_i(X_i) + [A_a(\omega_u) - A_a(\omega_4) - A_a(\omega_5) + A_a(\omega_1)]\ B_i(2X_i)\ \ B'_o(X_r) \tag{A-24}$$

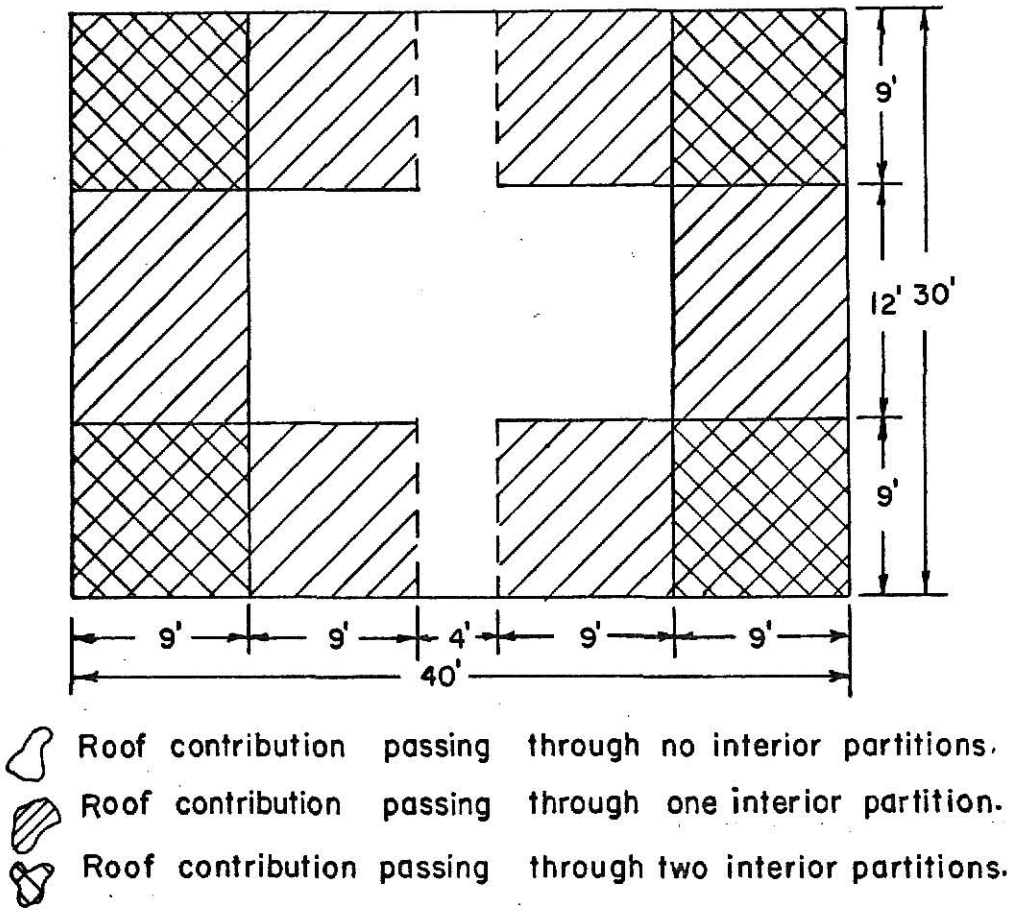

Figure A-6. Rectangular areas on the ceiling for the roof contribution in partitioned cases.

10.1.5 Basement Detector Locations

The general basement detector location is shown in Fig. A-7. The aperture fraction for the first story walls, A_p, is defined as the ratio of the window area to the first story wall area. The doors are considered in a separate azimuthal sector as in the first story cases. Refer to Fig. A-8 for this contribution.

$$C_g^{S1} = [G_s(\omega_u') - G_s(\omega_u)]\ S_w(X_w)\ E(e)\ B_e(X_w,3') \tag{A-25}$$

$$C_g^{A1} = [G_a(\omega_u') - G_a(\omega_u)][1-S_w(X_w)]\ B_e(X_w,3') \tag{A-26}$$

$$C_g^{S2} = \{G_s(\omega_u'') - G_s(\omega_u') - [G_s(\omega_d) - G_s(\omega_u')]A_{z_D}\}[1-A_p]S_w(X_e)$$

$$\times E(e)\ B_e(X_e,3')\ B_o'(X_f) \tag{A-27}$$

$$= \{G_s(\omega_u'') - A_{z_D} G_s(\omega_d) - [1-A_{z_D}]\ G_s(\omega_u')\}\ [1-A_p]S_w(X_e)$$

$$\times E(e)\ B_e(X_e,3')\ B_o'(X_f)$$

$$C_g^{A2} = \{G_a(\omega_u'') - A_{z_D}\ G_a(\omega_d) - [1-A_{z_D}]\ G_a(\omega_u')\}\ [1-A_p]$$

$$\times [1-S_w(X_e)]\ B_e(X_e,3')\ B_o'(X_f) \tag{A-28}$$

$$C_g^{A3} = \{G_a(\omega_u'') - A_{z_D}\ G_a(\omega_{ud}) - [1-A_{z_D}]\ G_a(\omega_u')\}\ A_p\ B_o'(X_f) \tag{A-29}$$

$$C_g^{A4} = A_a(\omega_u'')\ B_o'(X_o) \tag{A-30}$$

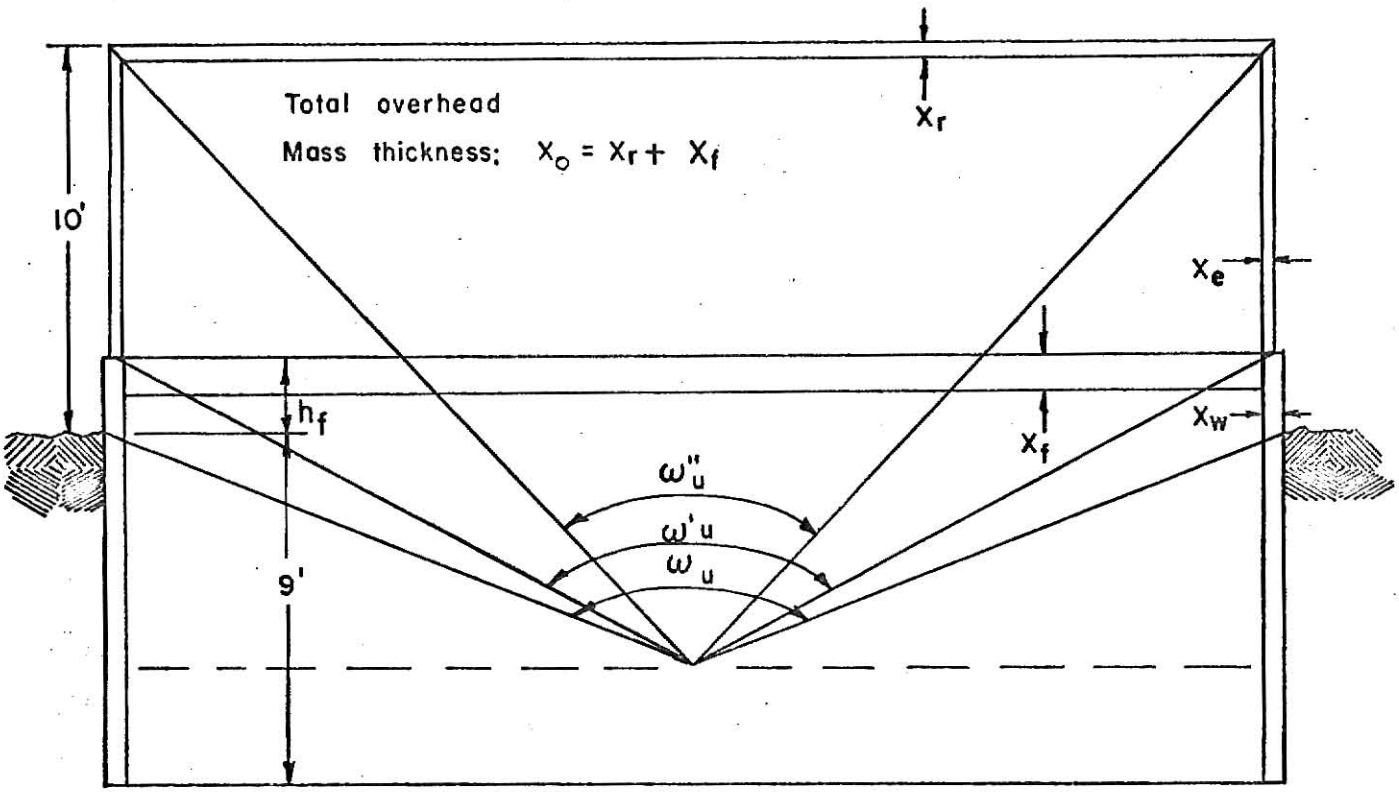

Figure A-7.. Elevation of the test house showing solid angle fractions for a basement detector location.

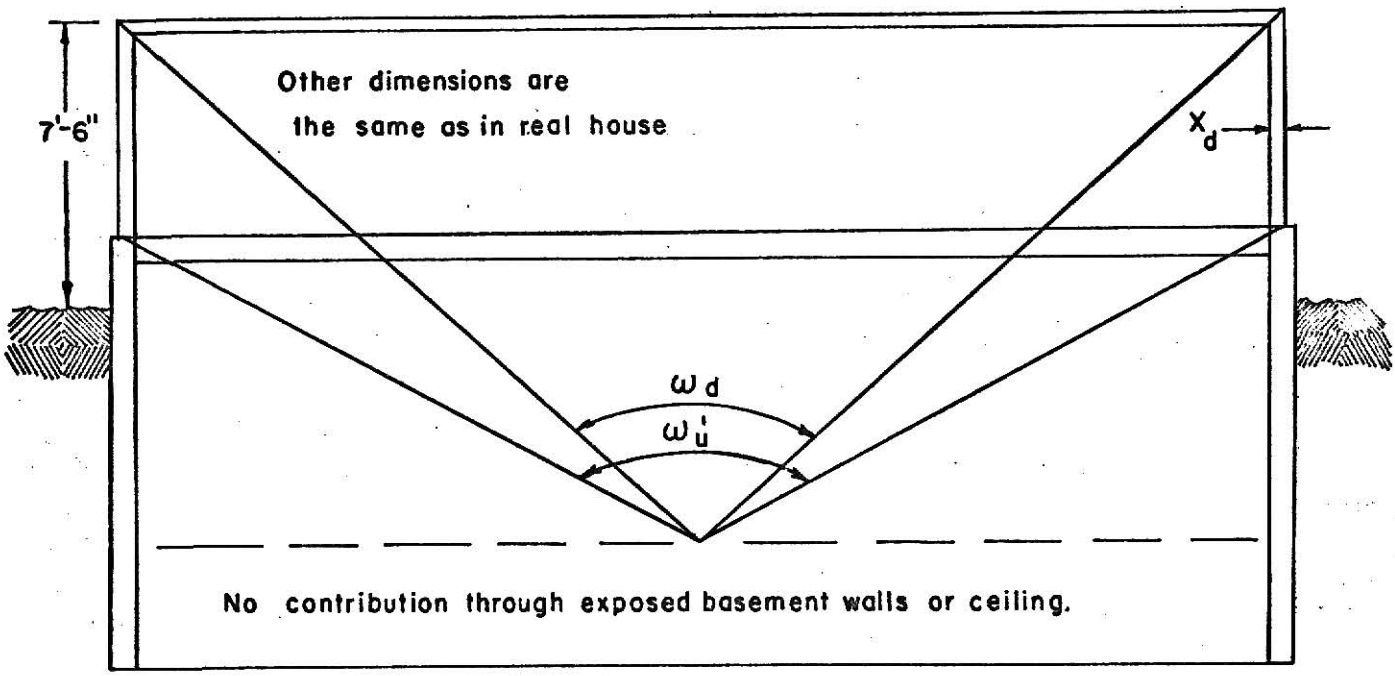

Figure A-8. Fictitious building for the contribution through the doors to a basement detector location.

$$C_g^{Sd} = [G_s(\omega_{ud}) - G_s(\omega_u')]\ S_w(X_d)\ E(e)\ B_e(X_d,3')\ B_o'(X_f)\ A_{z_D} \quad (A-31)$$

$$C_g^{Ad} = [G_a(\omega_{ud}) - G_a(\omega_u')][1-S_w(X_d)]\ B_e(X_d,3')\ B_o'(X_f)\ A_{z_D} \quad (A-32)$$

For cases where a detector is located in the basement and yet is above grade, shown in Fig. A-9, there is an additional contribution to C_g^{S1} and also a direct radiation component.

$$C_g^{S1} = [G_s(\omega_u') + G_s(\omega_\ell')]\ S_w(X_w)\ E(e)\ B_e(X_w,3') \quad (A-33)$$

$$C_g^{D1} = G_d(\omega_\ell',3')\ [1-S_w(X_w)]\ B_e(X_w,3') \quad (A-34)$$

The effects of interior partitions in the first story on the contributions to a basement detector are neglected. Although the partitions would act as a barrier to some of the radiation reaching a detector in the basement, the fraction of the geometry factor for which this occurs is small and requires much effort to determine. Some initial calculations showed that neglecting the partitions would result in errors of the order of five percent on the conservative side.

10.1.6 Off-center Detector Locations

Off-center detector locations, whether in the basement or upstairs, are treated, in general, by adding the contributions from four fictitious buildings. The fictitious buildings are formed by dividing the plan of the house into four sectors and reflecting each sector into the other three quadrants. Refer to Fig. A-10. The contributions are then determined for each fictitious building, summed, and divided by four. Note that the azimuthal sectors containing the

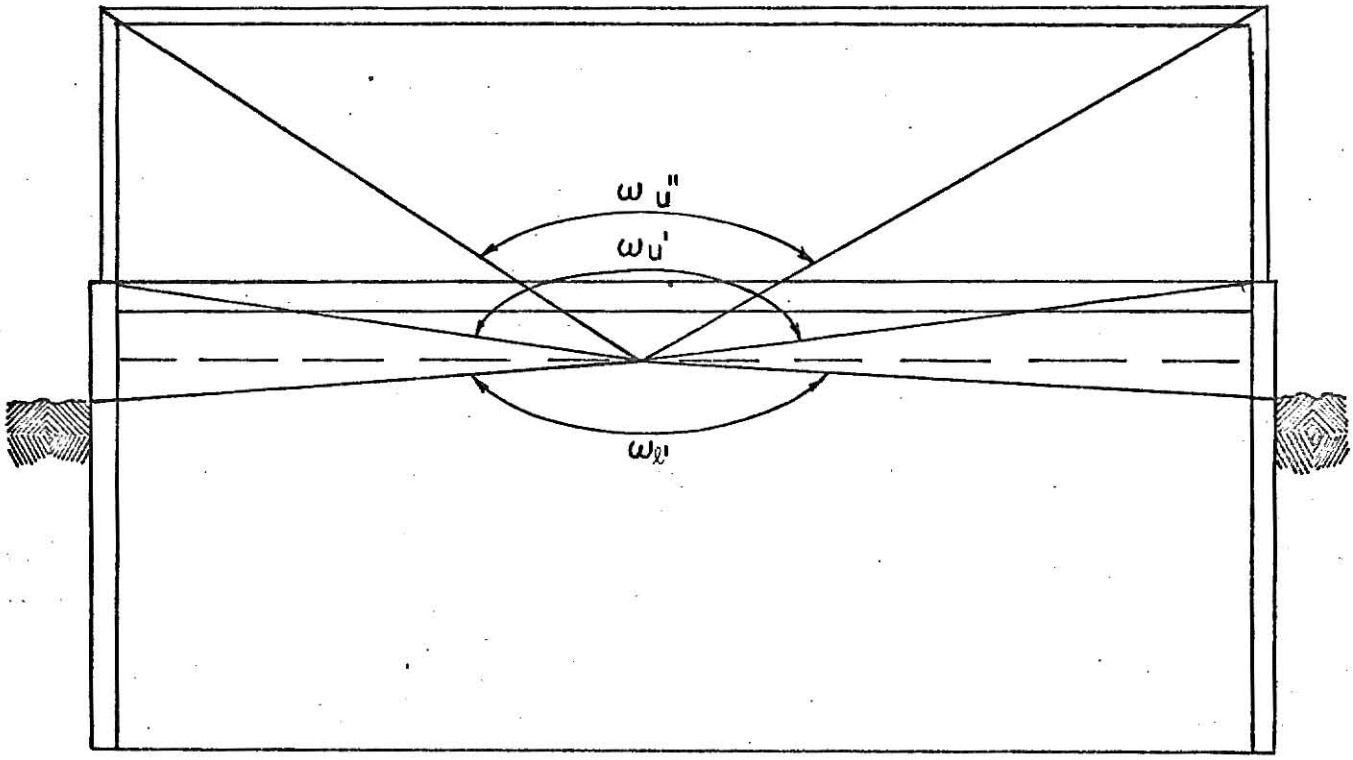

Figure A-9. Solid angle fractions for a basement detector location above grade.

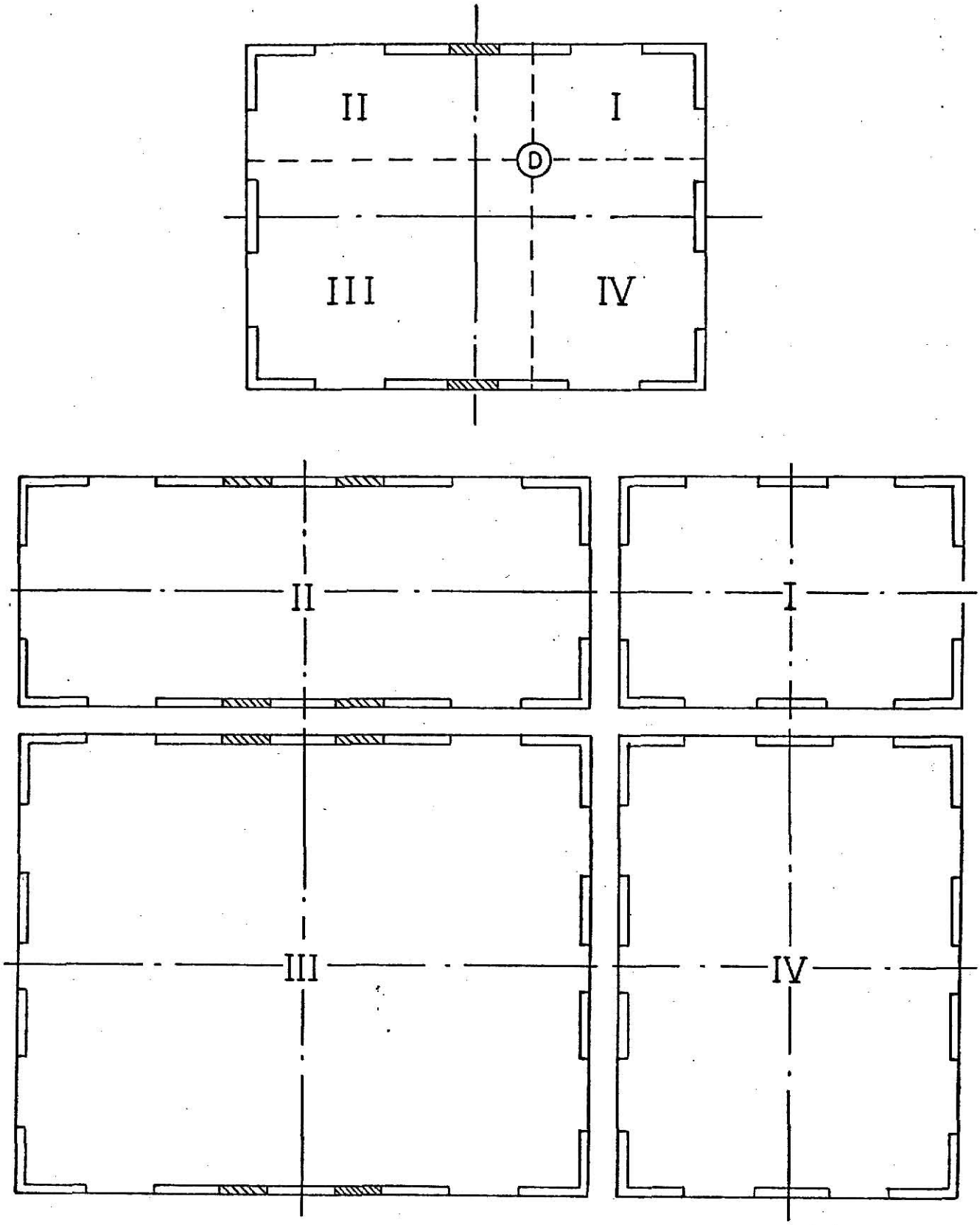

Figure A-10. Fictitious buildings required for a typical off-center detector location.

windows and the doors change radically in each fictitious building. If the detector should lie on either the north-south centerline or the east-west centerline of the house, only two fictitious buildings are required.

10.1.7 The Modified Ceiling Attenuation Factor

In the July 1969 edition of the EM, the ceiling attenuation factor $B'_o(X)$ has been replaced by a new function $B_c(X,\omega)$ which is solid angle dependent. This change affects the functional expressions for basement detector locations. If calculations are desired for this edition of the EM, the factor $B'_o(X_f)$ should be replaced by $B_c(X_f,\omega'_u)$ in Eqs. (A-27), (A-28), (A-29), (A-31), and (A-32).

10.1.8 The Computer Program ENGMAN

Since a large number of calculations were required and since inconsistencies can result from visual interpolation of the EM charts, the EM procedure was programmed to enable rapid and consistent calculations. The code ENGMAN features a number of options which should make it useful in future studies with the test house. The code was written in FORTRAN IV for the IBM 360/50 system at the Kansas State University Computing Center.

There are three groups of input data required by ENGMAN: 1) the EM chart data, 2) the house parameters, and 3) the detector position data. The EM charts are read in as tables and intermediate values are obtained by linear interpolation. The user may elect to use the EM functions for the fallout spectrum or an analogous set of functions for a ^{60}Co spectrum. Tabulated values for the former were taken from [15], while those for the latter were obtained by methods detailed in Appendix B. The over-all dimensions of the house and the positions of the doors and windows are fixed in the code. The

mass thicknesses of the barriers, the height of the floor, and the presence of interior partitions are read in as data to allow flexibility for parameter studies. A detector position is specified by three coordinates: the height above the floor of the detector, the distance north of center, and the distance east of center. The output list the reduction factors for each of the partial contributions listed above as well as the total.

A source listing of ENGMAN is presented here along with Table A-I, which defines each variable used in the code. The comment statements in the source listing should provide an adequate description of the program logic. A detector position may be specified anywhere in the basement of the house and, generally, anywhere below the top of the windows in the first story. For cases with interior partitions, the detector positions in the first story are limited to centerline locations.

A SOURCE LISTING OF ENGMAN

```
      DIMENSIONVAL1(18),VAL2(18),VAL3(18),VAL4(18),VAL5(18,7),VAL6(15),V
     CAL7(15),VAL8(15),VAL9(15),VAL10(15,7),WORK(7),VLN6(15),VLN7(15),VL
     CN8(15),VLN10(15,7),OMEGA(18),HTS(7),PSF(15),PARAM(20,4),AZP(3),PPR
     C(3),GPTS(300,2)
    1 FORMAT(1H1,10X,'HOUSE',I3,'    FLOOR HT.',F5.2,' FT.'/13X,'EFFECTI
     CVE MASS THICKNESSESS (PSF): XE=',F4.1,'  XW=',F4.1,'  XD=',F4.1,'
     C XF=',F4.1,'  XC=',F4.1,'  XR=',F4.1,'  XI=',F4.1)
    2 FORMAT(1HO,12X,'BARRIER FACTORS'/15X,'SW(XE)=',F5.3,'  SW(XW)=',F5
     C.3,'  SW(XD)=',F5.3/15X,'BE(XE,3FT.)=',F5.3,'  BE(XW,3FT.)=',F5.3,
     C'  BE(XD,3FT.)=',F5.3/15X,'BF(XF)=',F5.3,'  BO(XF)=',F5.3,'  BO(XO
     C)=',F5.3,'  BO(XR)=',F5.3)
    3 FORMAT(1HO,5X,'BASEMENT DETECTOR LOCATIONS')
    4 FORMAT(1HO,5X,'UPSTAIRS DETECTOR LOCATIONS')
    5 FORMAT(1HO,5X,'GRID POINT LOCATIONS (BASEMENT)')
    6 FORMAT(1HO,'FT. NORTH  FT. WEST    ELEVATION'/' OF CENTER  OF CENT
     CER     (FT.)')
    7 FORMAT(1H ,14X,'BI(XI)=',F5.3,'  BI(2*XI)=',F5.3)
    8 FORMAT(1HO,5X,'GRID POINT   ELEVATION(FT.)')
    9 FORMAT(1H+,38X,'SOURCE  GROUND DIRECT  WALL SCATTERED  SKYSHINE
     C      TOTAL')
   10 FORMAT(1H+,40X,'1',F15.6,F16.6,F13.6/41X,'2',15X,F16.6,F13.6/41X'3
     C',31X,F13.6/41X'4',31X,F13.6/41X,'D',15X,F16.6,F13.6/40X,'TOTAL',F
     C12.6,F16.6,F13.6,F14.6)
   11 FORMAT(1H+,40X,'1',F15.6,F16.6,/41X,'2',F15.6,F16.6,F13.6/41X,'3',
     CF15.6,16X,F13.6/41X,'4',31X,F13.6/41X'D',F15.6,F16.6,F13.6/40X,'TO
     CTAL',F12.6,F16.6,F13.6,F14.6)
   12 FORMAT(1H ,'. . . . . .
     C. . . . . .'/2X,3(F7.3,4X)
     C)
   13 FORMAT(1HO,5X,'KEY TO SOURCES FOR PARTIAL CONTRIBUTIONS'/11X,'1-EX
     CPOSED BASEMENT WALLS'/11X,'2-WALLS OF FIRST STORY'/11X,'3-WINDOWS
     COF FIRST STORY'/11X,'4-ROOF'/11X,'D-DOORS')
   14 FORMAT(5F7.4)
   15 FORMAT(I3/(8F7.4))
   16 FORMAT(6I3)
   17 FORMAT(1HO,5X,'ELEVATIONS ARE IN RELATION TO FLOOR OF DETECTOR'//)
   18 FORMAT(1HO,5X,'ENGINEERING MANUAL REDUCTION FACTORS FOR GROUD CONT
     CRIBUTION')
   19 FORMAT(10F7.4)
   87 FORMAT(1HO,20X,'CO-60 SPECTRUM')
   88 FORMAT(1HO,20X,'FALLOUT SPECTRUM')
   89 FORMAT(1HO,5X,'ENGINEERING MANUAL REDUCTION FACTORS FOR GROUND CON
     CTRIBUTION WITH MODIFIED FLOOR BARRIER FACTOR').
   90 FORMAT(1H ,'. . . . . .
     C. . . . . .'/I11,F15.3)
   91 FORMAT(1HO,5X,'THE DETECTOR POSITION SPECIFIED IS OUTSIDE THE BASE
     CMENT')
   92 FORMAT(1HO,5X,'THE DETECTOR POSITION SPECIFIED IS OUTSIDE THE FIRS
     CT STORY'/6X,'(OR ABOVE THE TOP OF THE WINDOWS)')
   93 FORMAT(1HO,5X,'THE SPECIFIED GRID ELEVATION IS ABOVE THE FIRST FLO
     COR')
```

```
   95 FORMAT(4F7.4)
   96 FORMAT(1H0,5X,'THE CODE CANNOT DO OFF CENTER CALCULATIONS FOR UPST
     CAIRS-PARTITIONS CASES')
C
C       READ IN EM CHART DATA
C
      READ(1,16)ISPEC,NOMG,NHTS,NPSF
      READ(1,14)(OMEGA(I),VAL1(I),VAL2(I),VAL3(I),VAL4(I),I=1,NOMG)
      READ(1,19)((VAL5(I,J),I=1,NOMG),J=1,NHTS)
      READ(1,19)(HTS(I),I=1,NHTS)
      READ(1,14)(PSF(I),VAL6(I),VAL7(I),VAL8(I),VAL9(I),I=1,NPSF)
      READ(1,19)((VAL10(I,J),I=1,NPSF),J=1,NHTS)
C
C       STORE LOGARITHMS OF BARRIER FACTOR FUNCTIONS
C
      DO101I=1,NPSF
      VLN6(I)=ALOG(VAL6(I))
      VLN7(I)=ALOG(VAL7(I))
      VLN8(I)=ALOG(VAL8(I))
      DO101J=1,NHTS
  101 VLN10(I,J)=ALOG(VAL10(I,J))
C
C       READ IN HOUSE PARAMETERS
C
      READ(1,95)((PARAM(I,J),J=1,4),I=1,20)
      READ(1,14)XD,XF,XO,XR,XI
      READ(1,19)(AZP(I),I=1,3),(PPR(I),I=1,3)
      READ(1,15)NGP,((GPTS(I,J),J=1,2),I=1,NGP)
C
C       CALL FOR THE VARIOUS BARRIER FACTORS FROM EM CHARTS WHICH ARE
C         CONSTANT FOR ALL HOUSES
C
      X2I=2*XI
      CALL TWIN(XD ,3.,BEXD  ,PSF  ,HTS,VLN10,NPSF,NHTS,WORK,1)
      CALL OWIN(XD ,PSF  ,VAL9,NPSF,SWXD ,1)
      CALL OWIN(XO ,PSF  ,VLN6,NPSF,BOXO ,1)
      CALL OWIN(XR ,PSF  ,VLN6,NPSF,BOXR ,1)
      CALL OWIN(XF ,PSF  ,VLN7,NPSF,BFXF ,1)
      CALL OWIN(XI ,PSF  ,VLN8,NPSF,BIXI ,1)
      CALL OWIN(X2I,PSF  ,VLN8,NPSF,BI2XI,1)
C
C       WEIGHT AZIMUTHAL FRACTIONS FOR INTERIOR PARTITIONS
C
      AZP(2)=AZP(2)*BIXI
      AZP(3)=AZP(3)*BI2XI
C
C       READ IN THE NUMBER OF HOUSES FOR WHICH CALCULATIONS ARE DESIRED
C
      READ(1,16)NHOUSE
      DO99NH=1,NHOUSE
C
C       READ IN THE HOUSE NUMBER AND OTHER PARAMETERS
C
      READ(1,16)IHOUSE,NU,NG,NB,MODE
```

```
C
C       LOCATE THE VARIABLE HOUSE PARAMETERS FOR THE HOUSE IN QUESTION
C
      FLHT=PARAM(IHOUSE,1)
      XE  =PARAM(IHOUSE,2)
      XW  =PARAM(IHOUSE,3)
      PART=PARAM(IHOUSE,4)
C
C       CALL FOR THE BARRIER FACTORS FOR THESE PARAMETERS
C
      CALL OWIN(XE ,PSF  ,VAL9,NPSF,SWXE ,0)
      CALL OWIN(XW ,PSF  ,VAL9,NPSF,SWXW ,0)
      CALL TWIN(XE ,3.,BEXE  ,PSF  ,HTS,VLN10,NPSF,NHTS,WORK,1)
      CALL TWIN(XW ,3.,BEXW  ,PSF  ,HTS,VLN10,NPSF,NHTS,WORK,1)
      CALL OWIN(XF ,PSF  ,VLN6,NPSF,BOXF ,1)
      WRITE(3,1)IHOUSE,FLHT,XE,XW,XD,XF,XO,XR,XI
      WRITE(3,2)SWXE,SWXW,SWXD,BEXE,BEXW,BEXD,BFXF,BOXF,BOXO,BOXR
      IF(PART.NE.1.)GOTO20
      WRITE(3,7)BIXI,BI2XI
   20 GOTO(110,111),MODE
  110 WRITE(3,18)
      GOTO(120,121),ISPEC
  111 WRITE(3,89)
      GOTO(120,121),ISPEC
  120 WRITE(3,88)
      GOTO221
  121 WRITE(3,87)
  221 WRITE(3,13)
      WRITE(3,17)
      IF(NU.EQ.0)GOTO44
      WRITE(3,4)
      WRITE(3,6)
      WRITE(3,9)
      IU=1
C
C       READ IN DETECTOR LOCATION COORDINATES
C
   21 READ(1,14)DN,DW,ELV
C
C       CHECK TO SEE THAT THIS LOCATION IS IN THE UPSTAIRS AND BELOW THE
C         TOP OF THE WINDOWS
C
      H=FLHT+ELV
      IF(DN.GT.20.)GOTO22
      IF(DW.GT.15.)GOTO22
      IF(H.GT.7.5)GOTO22
      GOTO23
   22 WRITE(3,92)
      GOTO42
C
C       ZERO ALL PARTIAL CONTRIBUTIONS
C
   23 CGS1=0.
      CGD1=0.
```

```
      CGS2=0.0
      CGA2=0.0
      CGD2=0.0
      CGA3=0.0
      CGD3=0.0
      CGA4=0.0
      CGAD=0.0
      CGSD=0.0
      CGDD=0.0
C
C       DEFINE Z DISTANCES FOR SOLID ANGLE FRACTIONS
C
      ZU=10.-H
      ZAU=7.5-H
      ZAL=ABS(H-3.)
      ZL=ELV
      ZL1=H
      IFB=0
C
C       DEFINE HALF-WIDTH AND HALF-LENGHT OF HOUSE
C
      SN=20.-DN
      SW=15.-DW
   26 CALL APE(SN,SW,FLHT,EC,E,AL,AP,PR,AZD)
C
C       CALCUCATE SOLID ANGLE FRACTIONS
C
      WU =SAF(E,AL,ZU )
      WAU=SAF(E,AL,ZAU)
      WAL=SAF(E,AL,ZAL)
      WL =SAF(E,AL,ZL )
      WL1=SAF(E,AL,ZL1)
C
C       CALL FOR GEOMETRY FACTORS AND HEIGHT DEPENDENT BARRIER FACTORS
C
      BH=H
      IF(H.LT.3.)BH=3.
      CALL TWIN(XE ,BH,BEXEH ,PSF  ,HTS,VLN10,NPSF,NHTS,WORK,1)
      CALL TWIN(XW ,BH,BEXWH ,PSF  ,HTS,VLN10,NPSF,NHTS,WORK,1)
      CALL TWIN(0.0,BH,BEOH  ,PSF  ,HTS,VLN10,NPSF,NHTS,WORK,1)
      CALL TWIN(XD ,BH,BEXDH ,PSF  ,HTS,VLN10,NPSF,NHTS,WORK,1)
      CALL OWIN(WU ,OMEGA,VAL1,NOMG,GSWU ,0)
      CALL OWIN(WAU,OMEGA,VAL1,NOMG,GSWAU,0)
      CALL OWIN(WAL,OMEGA,VAL1,NOMG,GSWAL,0)
      CALL OWIN(WL ,OMEGA,VAL1,NOMG,GSWL ,0)
      CALL OWIN(WL1,OMEGA,VAL1,NOMG,GSWL1,0)
      CALL OWIN(WU ,OMEGA,VAL2,NOMG,GAWU ,0)
      CALL OWIN(WAL,OMEGA,VAL2,NOMG,GAWAL,0)
      CALL OWIN(WAU,OMEGA,VAL2,NOMG,GAWAU,0)
      CALL OWIN(WU ,OMEGA,VAL3,NOMG,AAWU ,0)
      CALL TWIN(WL ,BH,GDWLH ,OMEGA,HTS,VAL5 ,NOMG,NHTS,WORK,0)
      CALL TWIN(WL1,BH,GDWL1H,OMEGA,HTS,VAL5 ,NOMG,NHTS,WORK,0)
      CALL TWIN(WAL,BH,GDWALH,OMEGA,HTS,VAL5 ,NOMG,NHTS,WORK,0)
C
```

```
C       COMPUTE PARTIAL CONTRIBUTIONS FROM FUNCTIONAL EXPRESSIONS
C
      TGS1=(GSWL1-GSWL)*SWXW*EC*BEXWH*BFXF
      TGD1=(GDWL1H-GDWLH)*(1.-SWXW)*BEXWH*BFXF
      CGDD=CGDD+GDWLH*(1.-SWXD)*BEXDH*AZD
      CGSD=CGSD+(GSWAU+GSWL)*EC*SWXD*BEXDH*AZD
      CGAD=CGAD+GAWAU*(1.-SWXD)*BEXDH*AZD
      IF(PART.NE.1.)GOTO225
C
C       THE INTERIOR PARTITIONS ARE IN PLACE IF PART=1.0
C
      IF(H.GE.3.)GOTO123
C
C       DETECTOR IS BELOW THE SILL HEIGHT IF H<3.0
C
      DO 122 I=1,3
      TGD2=GDWLH*AZP(I)
      TGS2=(GSWU+GSWL-PPR(I)*(GSWAU-GSWAL))*AZP(I)
      TGA2=(GAWU-PPR(I)*(GAWAU-GAWAL))*AZP(I)
      TGD3=0.0
  122 TGA3=(GAWAU-GAWAL)*PPR(I)*AZP(I)
      GOTO125
  123 DO124I=1,3
      TGD2=(GDWLH-PPR(I)*GDWALH)*AZP(I)
      TGS2=(GSWU+GSWL-PPR(I)*(GSWAU+GSWAL))*AZP(I)
      TGA2=(GAWU-PPR(I)*GAWAU)*AZP(I)
      TGD3=GDWALH*PPR(I)*AZP(I)
  124 TGA3=GAWAU*PPR(I)*AZP(I)
  125 CGS1=CGS1+TGS1*(AZP(1)+AZP(2)+AZP(3)+AZD)
      CGD1=CGD1+TGD1*(AZP(1)+AZP(2)+AZP(3)+AZD)
      CGD2=CGD2+TGD2*(1.-SWXE)*BEXEH
      CGS2=CGS2+(TGS2+(GSWU-GSWAU)*AZD)*SWXE*EC*BEXEH
      CGA2=CGA2+(TGA2+(GAWU-GAWAU)*AZD)*(1.-SWXE)*BEXEH
      CGD3=CGD3+TGD3*BEXH
      CGA3=CGA3+TGA3*BEXH
C
C       ROOF CONTRIBUTION FOR PARTITIONS CASES
C
      W1=SAF(.545,22.,ZU)
      W2=SAF(.133,30.,ZU)
      W3=SAF(.333,12.,ZU)
      W4=SAF(.733,30.,ZU)
      W5=SAF(.300,40.,ZU)
      CALL OWIN(W1 ,OMEGA,VAL3,NOMG,AAW1 ,0)
      CALL OWIN(W2 ,OMEGA,VAL3,NOMG,AAW2 ,0)
      CALL OWIN(W3 ,OMEGA,VAL3,NOMG,AAW3 ,0)
      CALL OWIN(W4 ,OMEGA,VAL3,NOMG,AAW4 ,0)
      CALL OWIN(W5 ,OMEGA,VAL3,NOMG,AAW5 ,0)
      CGA4=CGA4+(AAW1+AAW2-AAW3+BIXI*(AAW4+AAW5-AAW1-AAW2+AAW3)+BI2XI*(A
     CAWU-AAW4-AAW5+AAW1))*BOXR
      GOTO27
  225 CGS1=CGS1+TGS1
      CGD1=CGD1+TGD1
      IF(H.LT.3.)GOTO126
```

```
      CGD2=CGD2+(GDWLH*(1.-AZD)-PR*GDWALH)*(1.-SWXE)*BEXEH
      CGS2=CGS2+(GSWU-GSWAU*(PR+AZD)-GSWAL*PR+GSWL*(1.-AZD))*SWXE*EC*BEX
     CEH
      CGA2=CGA2+(GAWU-GAWAU*(PR+AZD))*(1.-SWXE)*BEXEH
      CGD3=CGD3+GDWALH*PR*BEOH
      CGA3=CGA3+GAWAU*PR*BEOH
      GOTO127
  126 CGD2=CGD2+GDWLH*(1.-SWXE)*BEXEH*(1.-AZD)
      CGS2=CGS2+(GSWU-GSWAU*(PR+AZD)+GSWAL*PR+GSWL*(1.-AZD))*SWXE*EC*BEX
     CEH
      CGA2=CGA2+(GAWU-GAWAU*(PR+AZD)+PR*GAWAL)*(1.-SWXE)*BEXEH
      CGD3=0.0
      CGA3=CGA3+(GAWAU-GAWAL)*PR
  127 CGA4=CGA4+AAWU*BOXR
   27 IFB=IFB+1
C
C       DETERMINE IF FICTITIOUS BUILDINGS ARE NEEDED
C         IF SO, THE DIMENSIONS ARE DETERMINED AND CONTROL IS RETURNED
C         TO THE FUNCTIONAL EXPRESSIONS
C
      IF(DN.NE.0)GOTO28
      IF(DW.NE.0)GOTO30
      GOTO37
   28 IF(PART.EQ.1.)GOTO38
      IF(DW.NE.0)GOTO32
C
C       TWO FICTITIOUS BUILDINGS ARE NEEDED
C
      GOTO(29,36),IFB
   29 SN=20.+DN
      GOTO26
C
C       TWO FICTITIOUS BUILDINGS ARE NEEDED
C
   30 IF(PART.EQ.1.)GOTO38
      GOTO(31,36),IFB
   31 SW=15.+DW
      GOTO26
C
C       FOUR FICTITIOUS BUILDINGS ARE NEEDED
C
   32 GOTO(33,34,35,36),IFB
   33 SW=15.+DW
      GOTO26
   34 SN=20.+DN
      GOTO26
   35 SW=15.-DW
      GOTO26
   36 CONTINUE
C
C       DIVIDE EACH CONTRIBUTION BY THE NUMBER OF FICTITOUS BUILDINGS
C
      CGS1=CGS1/IFB
      CGS2=CGS2/IFB
```

```
      CGD1=CGD1/IFB
      CGD2=CGD2/IFB
      CGD3=CGD3/IFB
      CGA2=CGA2/IFB
      CGA3=CGA3/IFB
      CGA4=CGA4/IFB
      CGSD=CGSD/IFB
      CGDD=CGDD/IFB
      CGAD=CGAD/IFB
C
C       SUM THE PARTIAL CONTRIBUTIONS
C
   37 CGS=CGS1+CGS2+CGSD
      CGA=CGA2+CGA3+CGA4+CGAD
      CGD=CGD1+CGD2+CGD3+CGDD
      CG=CGS+CGA+CGD
      WRITE(3,12)DN,DW,ELV
      WRITE(3,11)CGD1,CGS1,CGD2,CGS2,CGA2,CGD3,CGA3,CGA4,CGDD,CGSD,CGAD,
     CCGD,CGS,CGA,CG
      GOTO42
   38 WRITE(3,96)
   42 IU=IU+1
C
C       HAVE ALL UPSTAIRS LOCATIONS BEEN COMPUTED
C
      IF(IU.LE.NU)GOTO21
   44 IF(NG.EQ.0)GOTO54
      IR=0
      WRITE(3,5)
      WRITE(3,8)
      WRITE(3,9)
      JG=1
   45 IG=0
C
C       READ IN GRID ELEVATIONS
C
      READ(1,14)ELV
      IF(ELV.LE.FLHT+9.)GOTO46
      WRITE(3,93)
      GOTO47
   46 IG=IG+1
      IF(IG.GT.NGP)GOTO47
C
C       LOCATE COORDINATES FOR THE GRID POINT NUMBER
C
      DN=GPTS(IG,1)
      DW=GPTS(IG,2)
C
C       GO TO THE FUNCTIONAL EXPRESSIONS FOR BASEMENT CASES
C
      GOTO57
   47 JG=JG+1
C
C       HAVE ALL GRIDS BEEN COMPUTED
```

```
C
      IF(JG.LE.NG)GOTO45
   54 IF(NB.EQ.0)GOTO99
      IR=1
      WRITE(3,3)
      WRITE(3,6)
      WRITE(3,9)
      IB=0
C
C       HAVE ALL BASEMENT LOCATIONS BEEN COMPUTED
C
   56 IF(IB.GE.NB)GOTO99
C
C       READ IN DETECTOR LOCATION COORDINATES
C
      READ(1,14)DN,DW,ELV
C
C       CHECK TO SEE IF POINT IS IN THE BASEMENT
C
      IF(ELV.GT.FLHT+9.)GOTO157
      IF(DN.GT.20.)GOTO157
      IF(DW.GT.15.)GOTO157
      IB=IB+1
      GOTO57
  157 WRITE(3,91)
      IB=IB+1
      GOTO56
C
C       ZERO ALL PARTIAL CONTRIBUTIONS
C
   57 CGS1=0.0
      CGS2=0.0
      CGSD=0.0
      CGA1=0.0
      CGA2=0.0
      CGA3=0.0
      CGA4=0.0
      CGAD=0.0
      CGD1=0.0
C
C       DEFINE Z DISTANCES FOR SOLID ANGLE FRACTIONS
C
      IF(ELV.LE.9)GOTO58
C
C       THE DETECTOR IS ABOVE GRADE IF ELV>9.0
C
      ZU=0.0
      ZL1=ELV-9.
      GOTO59
   58 ZU=9.-ELV
   59 ZU1=9.-ELV+FLHT
      ZUD=9.-ELV+7.5
      ZU2=9.-ELV+10.
      IF8=0
```

```
C
C       DEFINE HALF-WIDTH AND HALF-LENGHT OF HOUSE
C
      SN=20.-DN
      SW=15.-DW
   60 CALL APE(SN,SW,FLHT,EC,E,AL,AP,PR,AZD)
C
C       CALCUCATE SOLID ANGLE FRACTIONS
C
      WU=SAF(E,AL,ZU)
      WU1=SAF(E,AL,ZU1)
      WUD=SAF(E,AL,ZUD)
      WU2=SAF(E,AL,ZU2)
      IF(ELV.LE.9)GOTO61
      WL1=SAF(E,AL,ZL1)
C
C       CALL FOR GEOMETRY FACTORS FROM EM CHARTS
C
      CALL OWIN(WL1,OMEGA,VAL1,NOMG,GSWL1,0)
      CALL OWIN(WL1,OMEGA,VAL4,NOMG,GDWL1,0)
   61 CALL OWIN(WU ,OMEGA,VAL1,NOMG,GSWU ,0)
      CALL OWIN(WU1,OMEGA,VAL1,NOMG,GSWU1,0)
      CALL OWIN(WU2,OMEGA,VAL1,NOMG,GSWU2,0)
      CALL OWIN(WUD,OMEGA,VAL1,NOMG,GSWUD,0)
      CALL OWIN(WU ,OMEGA,VAL2,NOMG,GAWU ,0)
      CALL OWIN(WU1,OMEGA,VAL2,NOMG,GAWU1,0)
      CALL OWIN(WU2,OMEGA,VAL2,NOMG,GAWU2,0)
      CALL OWIN(WUD,OMEGA,VAL2,NOMG,GAWUD,0)
      CALL OWIN(WU2,OMEGA,VAL3,NOMG,AAWU2,0)
C
C       IF MODE=2 THE MODIFIED FLOOR BARRIER FACTOR WILL BE USED
C
      GOTO(163,162),MODE
  162 CALL FLOOR(WU1,XF,BOXF,ISPEC)
C
C       COMPUTE PARTIAL CONTRIBUTIONS FROM FUNCTIONAL EXPRESSIONS
C
  163 CGS1=CGS1+(GSWU1-GSWU)*SWXW*EC*BEXW
      CGA1=CGA1+(GAWU1-GAWU)*(1.-SWXW)*BEXW
      IF(ELV.LE.9)GOTO63
      CGS1=CGS1+GSWL1*SWXW*EC*BEXW
      CGD1=CGD1+GDWL1*(1.-SWXW)*BEXW
   63 CGSD=CGSD+(GSWUD-GSWU1)*SWXD*EC*BEXD*BOXF*AZD
      CGAD=CGAD+(GAWUD-GAWU1)*(1.-SWXD)*BEXD*BOXF*AZD
      CGS2=CGS2+(GSWU2-AZD*GSWUD-(1.-AZD)*GSWU1)*(1.-AP)*SWXE*EC*BEXE*BO
     CXF
      CGA2=CGA2+(GAWU2-AZD*GAWUD-(1.-AZD)*GAWU1)*(1.-AP)*(1.-SWXE)*BEXE*
     CBOXF
      CGA3=CGA3+(GAWU2-AZD*GAWUD-(1.-AZD)*GAWU1)*AP*BOXF
      CGA4=CGA4+AAWU2*BOXO
      IFB=IFB+1
C
C       DETERMINE IF FICTITICUS BUILDINGS ARE NEEDED
C         IF SO, THE DIMENSIONS ARE DETERMINED AND CONTROL IS RETURNED
```

```
C          TO THE FUNCTIONAL EXPRESSIONS
C
      IF(DN.NE.0)GOTO68
      IF(DW.NE.0)GOTO70
      GOTO77
   68 IF(DW.NE.0)GOTO72
C
C       TWO FICTITIOUS BUILDINGS ARE NEEDED
C
      GOTO(69,76),IFB
   69 SN=20.+DN
      GOTO60
C
C       TWO FICTITIOUS BUILDINGS ARE NEEDED
C
   70 GOTO(71,76),IFB
   71 SW=15.+DW
      GOTO60
C
C       FOUR FICTITIOUS BUILDINGS ARE NEEDED
C
   72 GOTO(73,74,75,76),IFB
   73 SW=15.+DW
      GOTO60
   74 SN=20.+DN
      GOTO60
   75 SW=15.-DW
      GOTO60
   76 CONTINUE
C
C       DIVIDE EACH CONTRIBUTION BY THE NUMBER OF FICTITOUS BUILDINGS
C
      CGS1=CGS1/IFB
      CGS2=CGS2/IFB
      CGA1=CGA1/IFB
      CGA2=CGA2/IFB
      CGA3=CGA3/IFB
      CGA4=CGA4/IFB
      CGD1=CGD1/IFB
      CGAD=CGAD/IFB
      CGSD=CGSD/IFB
C
C       SUM THE PARTIAL CONTRIBUTIONS
C
   77 CGS=CGS1+CGS2+CGSD
      CGA=CGA1+CGA2+CGA3+CGA4+CGAD
      CG=CGS+CGA+CGD1
      IF(IR.NE.0)GOTO78
      WRITE(3,90)IG,ELV
      GOTO79
   78 WRITE(3,12)DN,DW,ELV
   79 WRITE(3,10)CGD1,CGS1,CGA1,CGS2,CGA2,CGA3,CGA4,CGSD,CGAD,CGD1,CGS,C
     CGA,CG
```

```
C
C       RETURN TO THE NEXT GRID POINT IF IR=0 OR TO THE NEXT BASEMENT
C        LOCATION IF IR=1
C
      IF(IR-1)46,56,56
   99 CONTINUE
      STOP
      END

C        END OF MAIN PROGRAM


      FUNCTION SAF(E,AL,Z)
C
C       THIS SUBPROGRAM COMPUTES SOLID ANGLE FRACTIONS
C
      IF(AL.EQ.0)GOTO2
      IF(E.EQ.0)GOTO2
      IF(Z.EQ.0)GOTO1
      AN=2.*Z/AL
      SR=SQRT(AN*AN+E*E+1.)
      SAF=2.*ATAN(E/(AN*SR))/3.1416
      RETURN
    1 SAF=1.0
      RETURN
    2 SAF=0.0
      RETURN
      END


      SUBROUTINE FLCOR(W,XF,BOXF,ISPEC)
C
C       THIS SUBROUTINE COMPUTES THE MODIFIED FLOOR BARRIER FACTOR
C
      GOTO(1,2),ISPEC
    1 A2=3.5*EXP(-2.3*W)
      BOXF=(1.-A2)*EXP(-0.1*XF)+A2*EXP(-0.04*XF)
      GOTO3
    2 A2=3.0*EXP(-2.3*W)
      BOXF=(1.-A2)*EXP(-0.12*XF)+A2*EXP(-0.042*XF)
    3 IF(BOXF-1.0)5,5,4
    4 BOXF=1.0
    5 RETURN
      END
```

```
      SUBROUTINE APE(SN,SW,FLHT,EC,E,AL,AP,PR,AZD)
C
C       THIS SUBROUTINE DOES THE FOLLOWING:
C          DETERMINES THE LENGTH OF THE BUILDING
C          CALCULATES THE ECCENTRICITY RATIO, W/AL
C          CALCULATES THE SHAPE FACTOR, E(E)
C          CALCULATES THE APERTURE FRACTION, AP, FOR BASEMENT CASES
C          CALCULATES THE AZIMUTHAL FRACTION FOR THE WINDOWS, PR, FOR
C            UPSTAIRS CASES
C          CALCULATES THE AZIMUTHAL FRACTION FOR THE DOORS, AZD
C
      ANG(S,X,Y,W,Z)=ATAN(Y/S)-ATAN(X/S)+ATAN(Z/S)-ATAN(W/S)
      IF(SW.EQ.0.0)GOTO18
      IF(SN.EQ.0.0)GOTO18
      IF(SN-SW)1,2,2
    1 AL=2.*SW
      W=2.*SN
      GOTO3
    2 AL=2.*SN
      W=2.*SW
    3 E=W/AL
      EC=(1.+E)/SQRT(1.+E*E)
      IF(SN.LT.34)GOTO4
      WN=12.
      WAW=ANG(SW,SN-34.,SN-28.,SN-12.,SN-6.)
      GOTO8
    4 IF(SN.LT.28)GOTO5
      WN=SN-22.
      WAW=ANG(SW,0.0   ,SN-28.,SN-12.,SN-6.)
      GOTO8
    5 IF(SN.LT.12.)GOTO6
      WN=6.
      WAW=ANG(SW,0.0   ,0.0   ,SN-12.,SN-6.)
      GOTO8
    6 IF(SN.LT.6)GOTO7
      WN=SN-6.
      WAW=ANG(SW,0.0   ,0.0   ,0.0   ,SN-6.)
      GOTO8
    7 WN=0.0
      WAW=0.0
    8 IF(SW.LT.24)GOTO9
      WW=12.
      WAN=ANG(SN,SW-24.,SW-18.,SW-12.,SW-6.)
      GOTO13
    9 IF(SW.LT.18)GOTO10
      WW=SW-12.
      WAN=ANG(SN,0.0   ,SW-18.,SW-12.,SW-6.)
      GOTO13
   10 IF(SW.LT.12)GOTO11
      WW=6.
      WAN=ANG(SN,0.0   ,0.0   ,SW-12.,SW-6.)
      GOTO13
   11 IF(SW.LT.6)GOTO12
      WW=SW-6.
```

```
      WAN=ANG(SN,0.0    ,0.0    ,0.0    ,SW-6.)
      GOTO13
   12 WW=0.0
      WAN=0.0
   13 PR=(WAW+WAN)*2./3.1416
   14 IF(SN.LT.22.)GOTO15
      WD=4.
      DAW=ANG(SW,SN-22.,SN-18.,0.0,0.0)
      GOTO17
   15 IF(SN.LT.18.)GOTO16
      WD=SN-18.
      DAW=ANG(SW,0.0,SN-18.,0.0,0.0)
      GOTO17
   16 WD=0.0
      DAW=0.0
   17 DA=WD*(7.5-FLHT)
      AP=4.5*(WN+WW)/((10.-FLHT)*(SW+SN)-DA)
      AZD=DAW*2./3.1416
      RETURN
   18 EC=1.0
      E=0.0
      AL=0.0
      AP=0.0
      PR=0.0
      AZD=0.0
      RETURN
      END
```

```
      SUBROUTINE TWIN(X,Y,Z,XT,YT,FCT,NX,NY,VAL,LN)
C
C       THIS SUBROUTINE PERFORMS TWO-WAY LINEAR INTERPOLATION
C          X IS AN ARGUMENT FOR WHICH INTERPOLATION IS REQUIRED
C          Y IS AN ARGUMENT FOR WHICH INTERPOLATION IS REQUIRED
C          Z IS THE INTERPOLATED FUNCTION VALUE
C          XT IS A VECTOR OF TABULATED X ARGUMENTS
C          YT IS A VECTOR OF TABULATED Y ARGUMENTS
C          FCT IS THE TWO-DIMENSIONAL TABLE OF VALUES
C          NX IS THE NUMBER OF TABULATED X ARGUMENTS
C          NY IS THE NUMBER OF TABULATED Y ARGUMENTS
C          VAL IS A STORAGE VECTOR
C          LN IS AN INDEX WHICH IF EQUAL TO 1 INDICATES THAT INTERPOLA-
C            TION IS PERFORMED ON THE LOGARITHMS OF THE FUNCTION VALUES
C            THE INTERPOLATED VALUE IS RETURNED AS THE ACTUAL VALUE
C
      DIMENSIONXT(1),YT(1),FCT(NX,NY),VAL(NY)
      IF(X.LT.XT(1))GOTO6
      IF(X.GT.XT(NX))GOTO6
      IF(Y.LT.YT(1))GOTO6
      IF(Y.GT.YT(NY))GOTO6
```

```
      DO5I=1,NX
      IF(XT(I)-X)5,1,3
    1 DO2J=1,NY
    2 VAL(J)=FCT(I,J)
      CALL OWIN1(Y,YT,VAL,NY,Z,LN)
      GOTO7
    3 DO4J=1,NY
    4 VAL(J)=(FCT(I,J)*(XT(I-1)-X)-FCT(I-1,J)*(XT(I)-X))/(XT(I-1)-XT(I))
      CALL OWIN1(Y,YT,VAL,NY,Z,LN)
      GOTO7
    5 CONTINUE
    6 WRITE(3,8)X,Y,XT(1),XT(NX),YT(1),YT(NY)
    7 RETURN
    8 FORMAT(' TWO WAY INTERPOLATION WAS REQUESTED FOR THE (X,Y) ARGUMEN
     CTS (',E10.3,',',E10.3,')'/'THIS IS EITHER OUTSIDE THE RANGE OF THE
     C TABULATED X VALUES:',E10.3,'-',E10.3/'OR OUTSIDE THE RANGE OF THE
     C TABULATED Y VALUES:',E10.3,'-',E10.3)
      END




      SUBROUTINE OWIN(X,ARG,VAL,NDIM,Y,LN)
C
C       THIS SUBROUTINE PERFORMS ONE-WAY LINEAR INTERPOLATION
C          X IS THE ARGUMENT FOR WHICH INTERPOLATION IS REQUIRED
C          ARG IS THE VECTOR OF TABULATED AGRUMENTS
C          VAL IS THE VECTOR OF TABULATED FUNCTION VALUES
C          NDIM IS THE NUMBER OF TABULATED POINTS
C          Y IS THE INTERPOLATED VALUE
C          LN IS AN INDEX WHICH IF EQUAL TO 1 INDICATES THAT INTERPOLA-
C            TION IS PERFORMED ON THE LOGARITHMS OF THE FUNCTION VALUES
C            THE INTERPOLATED VALUE IS RETURNED AS THE ACTUAL VALUE
C
      DIMENSIONARG(1),VAL(1)
      IF(X.LT.ARG(1))GOTO4
      IF(X.GT.ARG(NDIM))GOTO4
      ENTRY OWIN1(X,ARG,VAL,NDIM,Y,LN)
      DO3I=1,NDIM
      IF(ARG(I)-X)3,1,2
    1 Y=VAL(I)
      GOTO5
    2 Y=(VAL(I)*(ARG(I-1)-X)-VAL(I-1)*(ARG(I)-X))/(ARG(I-1)-ARG(I))
      GOTO5
    3 CONTINUE
    4 WRITE(3,6)X,ARG(1),ARG(NDIM)
      RETURN
    5 IF(LN.EQ.1)Y=EXP(Y)
      RETURN
    6 FORMAT(' INTERPOLATION WAS REQUESTED FOR THE ARGUMENT',E10.3/'WHIC
     CH IS OUTSIDE THE RANGE OF TABULATED ARGUMENTS:',E10.3,'-',E10.3)
      END
```

Table A-I. A description of FORTRAN variables used in ENGMAN.

Symbol	Definition
Two-dimensional arrays:	
GPTS	A table containing the distances north and west of center for the detector locations according to a predetermined grid
PARAM	A table containing the variable house parameters (row i of this table has the elements XE, XW, FLHT, and PART for house i)
VAL5	A two-dimensional table of values for the EM function $G_d(\omega,H)$
VAL10	A two-dimensional table of values for the EM function $B_e(X,H)$
VLN10	Natural logarithms of the values in VAL10
One-dimensional arrays:	
AZP	The azimuthal fractions for the sectors with interior partitions: A_{z_A}, A_{z_B}, A_{z_C}
HTS	The tabulated height arguments for the functions $G_d(\omega,H)$ and $B_e(X,H)$
ØMEGA	The tabulated solid angle fraction arguments for the geometry functions
PPR	The azimuthal aperture fractions for the sectors with interior partitions: P_{a_A}, P_{a_B}, P_{a_C}
PSF	The tabulated mass thickness arguments for the barrier factor
VAL1	The tabulated values of the EM function $G_s(\omega)$
VAL2	The tabulated values of the EM function $G_a(\omega)$
VAL3	The tabulated values of the EM function $A_a(\omega)$
VAL4	The tabulated values of the EM function $G_d(\omega,3')$
VAL6	The tabulated values of the EM function $B'_o(X)$

VAL7	The tabulated values of the EM function $B_f(X)$
VAL8	The tabulated values of the EM function $B_i(X)$
VAL9	The tabulated values of the EM function $S_w(X)$
VLN6	Natural logarithms of the values in VAL6
VLN7	Natural logarithms of the values in VAL7
VLN8	Natural logarithms of the values in VAL8
WØRK	A storage vector used in the interpolation subroutines

Integer variables:

IB, IFB, IG, IR, IU, JG	Cycling parameters
IHØUSE	The house number corresponding to the experimental house
ISPEC	An index denoting which set of EM charts is used (1 for fission charts, 2 for ^{60}Co charts)
MØDE	An index, which if equal to 1 causes BØXF to take the value interpolated from VAL6, or if equal to 2, causes BØXF to take the value computed in the subroutine FLØØR
NB	The number of basement detector locations for which calculations are required
NG	The number of grid elevations for which calculations are required
NGP	The number of points on the fixed grid
NHØUSE	The number of houses for which calculations are required
NHTS	The number of elements in the vector HTS
NØMG	The number of elements in the vector ØMEGA
NPSF	The number of elements in the vector PSF
NU	The number of upstairs detector locations for which calculations are required

Real variables:

AAWU	$A_a(\omega_u)$
AAWU2	$A_a(\omega_u'')$

AAW1	$A_a(\omega_1)$
AAW2	$A_a(\omega_2)$
AAW3	$A_a(\omega_3)$
AAW4	$A_a(\omega_4)$
AAW5	$A_a(\omega_5)$
AL	The length of the real or fictitious building
AP	A_p, the fraction of the first story wall area, exclusive of the doors, subtended by the windows
AZD	The azimuthal fraction of the sector containing the doors
BEXD	$B_e(X_d,3')$
BEXDH	$B_e(X_d,H)$
BEXE	$B_e(X_e,3')$
BEXEH	$B_e(X_e,H)$
BEXW	$B_e(X_w,3')$
BEXWH	$B_e(X_w,H)$
BEOH	$B_e(O,H)$
BFXF	$B_f(X_f)$
BH	The detector height above grade, H. If H is less than 3 ft, BH is set equal to 3 ft.
BIXI	$B_i(X_i)$
BI2XI	$B_i(2X_i)$
BØXF	$B'_o(X_f)$
BØXØ	$B'_o(X_o)$
BØXR	$B'_o(X_r)$
CG	C_g
CGA	C_g^A
CGAD	C_g^{Ad}
CGA1	C_g^{A1}

CGA2	C_g^{A2}
CGA3	C_g^{A3}
CGA4	C_g^{A4}
CGD	C_g^{D}
CGDD	C_g^{Dd}
CGD1	C_g^{D1}
CGD2	C_g^{D2}
CGD3	C_g^{D3}
CGS	C_g^{S}
CGSD	C_g^{Sd}
CGS1	C_g^{S1}
CGS2	C_g^{S2}
DN	A detector location coordinate, feet north of center
DW	A detector location coordinate, feet west of center
E	The ratio of width to length, e, for a real or fictitious building
EC	The shape factor, E(e), for wall-scattered radiation
ELV	A detector location coordinate, height (ft) above the floor
FLHT	The height (ft) of the top of the floor above grade
GAWAL	$G_a(\omega_{a\ell})$
GAWAU	$G_a(\omega_{au})$
GAWU	$G_a(\omega_u)$
GAWUD	$G_a(\omega_{ud})$
GAWU1	$G_a(\omega_u')$
GAWU2	$G_a(\omega_u'')$
GDWLH	$G_d(\omega_\ell, H)$
GDWL1	$G_d(\omega_\ell', 3')$

GDWL1H	$G_d(\omega_\ell', H)$
GSWAL	$G_s(\omega_{a\ell})$
GSWAU	$G_s(\omega_{au})$
GSWL	$G_s(\omega_\ell)$
GSWL1	$G_s(\omega_\ell')$
GSWU	$G_s(\omega_u)$
GSWUD	$G_s(\omega_{ud})$
GSWU1	$G_s(\omega_u')$
GSWU2	$G_s(\omega_u'')$
H	The detector height (ft) above grade
PART	An index which, if equal to 1, indicates that the interior partitions are in place
PR	The azimuthal fraction subtended by the windows
SN	Half the north-south dimension of the real or fictitious building
SW	Half the east-west dimension of the real or fictitious building
SWXD	$S_w(X_d)$
SWXE	$S_w(X_e)$
SWXW	$S_w(X_w)$
TGA2	An intermediate value of CGA2
TGA3	An intermediate value of CGA3
TGD1	An intermediate value of CGD1
TGD2	An intermediate value of CGD2
TGD3	An intermediate value of CGD3
TGS1	An intermediate value of CGS1
TGS2	An intermediate value of CGS2
WAL	$\omega_{a\ell}$

WAU	ω_{au}
WL	ω_{ℓ}
WL1	ω'_{ℓ}
WU	ω_{u}
WUD	ω_{ud}
WU1	ω'_{u}
WU2	ω''_{u}
W1	ω_{1}
W2	ω_{2}
W3	ω_{3}
W4	ω_{4}
W5	ω_{5}
XD	The effective mass thickness of the doors
XE	The effective mass thickness of the exterior walls
XF	The effective mass thickness of the floor
XI	The effective mass thickness of the interior partitions
XØ	The effective mass thickness of the floor plus roof
XR	The effective mass thickness of the roof
XW	The effective mass thickness of the exposed basement walls
X2I	Two times XI
ZAL	The vertical distance from the detector to the bottom of the windows for an upstairs location
ZAU	The vertical distance from the detector to the top of the windows for an upstairs location
ZL	The vertical distance from the detector to the top of the floor
ZL1	The vertical distance from the detector to grade for an upstairs location or a basement location above grade

ZU	Either the vertical distance from the detector to the top of the first-story walls for an upstairs location, or the vertical distance from the detector to grade for a basement location
ZUD	The vertical distance from the detector to the top of the doors for a basement location
ZU1	The vertical distance from the detector to the top of the floor for a basement location
ZU2	The vertical distance from the detector to the top of the first-story walls for a basement location

10.2 Appendix B: Preparation of Engineering Manual Charts for ^{60}Co Radiation

10.2.1 Introduction

The purpose of this section is to describe the mechanics used to convert the NBS-42 data [2] to the tabular data for the EM charts used in the computer code ENGMAN. The charts were constructed only for the ranges of the parameters required for the KSUNESF test house. No physical interpretation of the functions involved is given here nor is any justification given for their use.

10.2.2 General Methods

Spencer [2] has performed basic radiation transport calculations for three gamma-ray sources, 1.12 hour fission products, ^{60}Co, and ^{137}Cs. The data from the fission product spectrum were used to construct the EM charts as outlined in [3(Vol. II) and 4]. Here the identical procedures are used to construct the charts from the ^{60}Co data.

The following functions, which were calculated by Spencer and plotted in NBS-42, were used: $L(X)$, $S(d)$, $S'(X)$, $P^{(0)}(X)$, $P^{(S)}(X)$, $W(X,d)$, $L_a(X,\omega)$, $S_a(d,\omega)$. Values were read as accurately as possible from these curves for the ranges of interest and are listed in Tables B-I through B-III. The appropriate calculations (shown later) were carried out on these numbers to convert them to EM functions.

The data were then plotted and smooth curves drawn through the points to represent the EM functions, Figures B-1 through B-5. The tabular data were then read from these curves and are recorded in Tables B-IV through B-VII. It was hoped that this graphical smoothing process would diminish any errors arising from the reading of the NBS-42 curves.

It is noted that the parameters X and d both represent mass thickness. The units of X are pounds per square foot (psf), while the units of d are feet of

air. They are used interchangeably below, the relation between the two being: 1.0 psf = 13.3 feet of air.

10.2.3 Barrier Factors

Two EM functions are identical to NBS-42 functions:

$$B_f(X) = L(X) \tag{B-1}$$

and

$$B'_o(X) = S'(X). \tag{B-2}$$

The scattered fraction is defined here as the ratio of scattered to total dose rates from a point isotropic source:

$$S_w(X) = \frac{P^{(S)}(X)}{P^{(O)}(X) + P^{(S)}(X)} . \tag{B-3}$$

The wall barrier factor is defined by the approximate relationship

$$B_e(X,H) \simeq 2W(X,d), \tag{B-4}$$

where the EM variable H is equal to d. The NBS-42 function W(X,d) is for a detector imbedded thickness X in a semi-infinite wall. For low mass thicknesses, there is a significant contribution to the detector response from radiation which has been back-scattered in the wall material behind the detector. This is evidenced by the fact that $2\times W(0,3') = 1.1$. To correct for this effect in the function $B_e(X,H)$, the value for X = 0 and H = 3' was set equal to 1.0 and the curve was lowered slightly out to X ≃ 50 psf. Proportional corrections were made in the curves for H = 6' and H = 15'.

The barrier factor for interior partitions is set equal to the wall barrier factor at H = 3':

$$B_i(X) = B_e(X,3'). \tag{B-5}$$

10.2.4 Geometry Factors

The following definitions of the NBS-42 functions are required to formulate the EM functions:

$$L(X) = \int_{-1}^{1} d(\cos\theta)\ \ell(X,\cos\theta) \qquad \text{(B-6)}$$

$$L_a(X,\omega) = \frac{1}{L(X)} \int_{1-\omega}^{1} d(\cos\theta)\ \ell(X,\cos\theta) \qquad \text{(B-7)}$$

$$S_{(d)} = \int_{-1}^{0} d(\cos\theta)\ \ell(d,\cos\theta) \qquad \text{(B-8)}$$

$$S_a(d,\omega) = \frac{1}{S(d)} \int_{-1}^{-1+\omega} d(\cos\theta)\ \ell(d,\cos\theta). \qquad \text{(B-9)}$$

In addition, the following values are needed:

$$L(.2256) = 1.0$$

$$L(1.0) = 0.74$$

$$S(0) = 0.088$$

$$S(3') = 0.084$$

$$S(13.3') = 0.0755$$

3' (of air) = 0.2256 psf.

The EM geometry factors are now expressed in terms of these functions:

$$G_d(\omega,H) = \frac{\int_{0}^{1-\omega} d(\cos\theta)\ \ell(d,\cos\theta)}{\int_{-1}^{1} d(\cos\theta)\ \ell(d,\cos\theta)} \qquad \text{(B-10)}$$

$$= L_a(d,1) - L_a(d,\omega)$$

$$G_s(\omega) = \int_{-1+\omega}^{0} d(\cos\theta)\ \ell(3',\cos\theta) \qquad \text{(B-11)}$$

$$= 0.5\ [1-S_a(3',\omega)]$$

$$G_s(0) = 0.5$$

$$G_a(\omega) = S(3')[1-S_a(3',\omega][1 + 0.5\ S_a(3',\omega)] \qquad \text{(B-12)}$$

$$A_a(\omega) = \int_{1}^{-1+\omega} d(\cos\theta)\ \ell(0,\cos\theta) \qquad \text{(B-13)}$$

$$= S(0)\ S_a(0,\omega)\ .$$

In the construction of the original EM charts for the fission product spectrum, the functions $G_d(\omega,H)$ and $G_a(\omega)$ were arbitrarily normalized such that $G_d(0,3') = 0.9$ and $G_a(0) = 0.1$. No such round-off has been carried out here.

In the input tables for ENGMAN it was desired to have values for $B_e(X,H)$ and $G_d(\omega,H)$ for the same set of heights. Since $L_a(X,\omega)$ is only plotted for $X = 0.2256$ ($H = 3'$) and $X = 1$ ($H = 13.3'$), the functions $G_d(\omega,3')$ and $G_d(\omega,13.3')$ were constructed and linear interpolation was used to obtain values for the heights 6' and 15'.

The function $A_a(\omega)$ requires values of $S_a(d,\omega)$ for $d = 0$, whereas $S_a(3',\omega)$ is the lowest curve in NBS-42. However, the shape of this curve should be quite insensitive to such a small change in height.

Table B-I. Data taken from NBS-42 curves for the functions L(X), S'(X), $P^{(0)}(X)$, and $P^{(S)}(X)$ for ^{60}Co radiation.

X(psf)	L(X)	S'(X)	$P^{(0)}(X)$	$P^{(S)}(X)$
0	1.0[a]	1.0	0.360	0.0
5	0.43	0.54	0.320	0.040
10	0.305	0.347	0.277	0.069
15	0.237	0.245	0.240	0.090
20	0.193	0.180	0.210	0.103
25	0.160	0.139	0.181	0.111
30	0.131	0.109	0.160	0.120
40	0.095	0.070	0.120	0.126
50	0.069	0.046	0.091	0.121
60	0.051	0.030	0.070	0.113
70	0.038	0.0200	0.052	0.103
80	0.0286	0.0130	0.0400	0.092
90	0.0220	0.0086	0.0300	0.081
100	0.0164	0.0057	0.0230	0.069

[a]This value is actually for X = 0.2256

Table B-II. Data taken from NBS-42 curves for the function W(X,d) for ^{60}Co radiation.

	W(X,d)		
X(psf)	d = 3'	6'	15'
0	0.55	0.47	0.39
5	0.47	0.41	0.33
10	0.40	0.360	0.285
20	0.31	0.272	0.215
30	0.238	0.207	0.165
40	0.188	0.161	0.178
50	0.147	0.125	0.098
60	0.116	0.099	0.078
70	0.091	0.078	0.061
80	0.072	0.061	0.048
90	0.050	0.042	0.033
100	0.044	0.038	0.029

Table B-III. Data taken from NBS-42 curves for the functions $L_a(X,\omega)$ and $S_a(X,\omega)$ for ^{60}Co radiation.

ω	$L_a(.2256,\omega)$	$L_a(1.0,\omega)$	$S_a(3,\omega)$
0.0	0.0	0.0	0.0
0.05		0.0128	0.0148
0.10	0.0204	0.0280	0.0321
0.15	0.0314	0.0492	0.0538
0.20	0.0460	0.0615	0.0775
0.30	0.0745	0.099	0.126
0.40	0.108	0.144	0.179
0.50	0.146	0.198	0.250
0.60	0.191	0.264	0.331
0.70	0.253	0.352	0.428
0.80	0.344	0.470	0.56
0.85	0.403	0.550	0.67
0.90	0.49	0.64	0.73
0.95	0.61	0.76	0.85
1.00	0.916	0.898	0.00

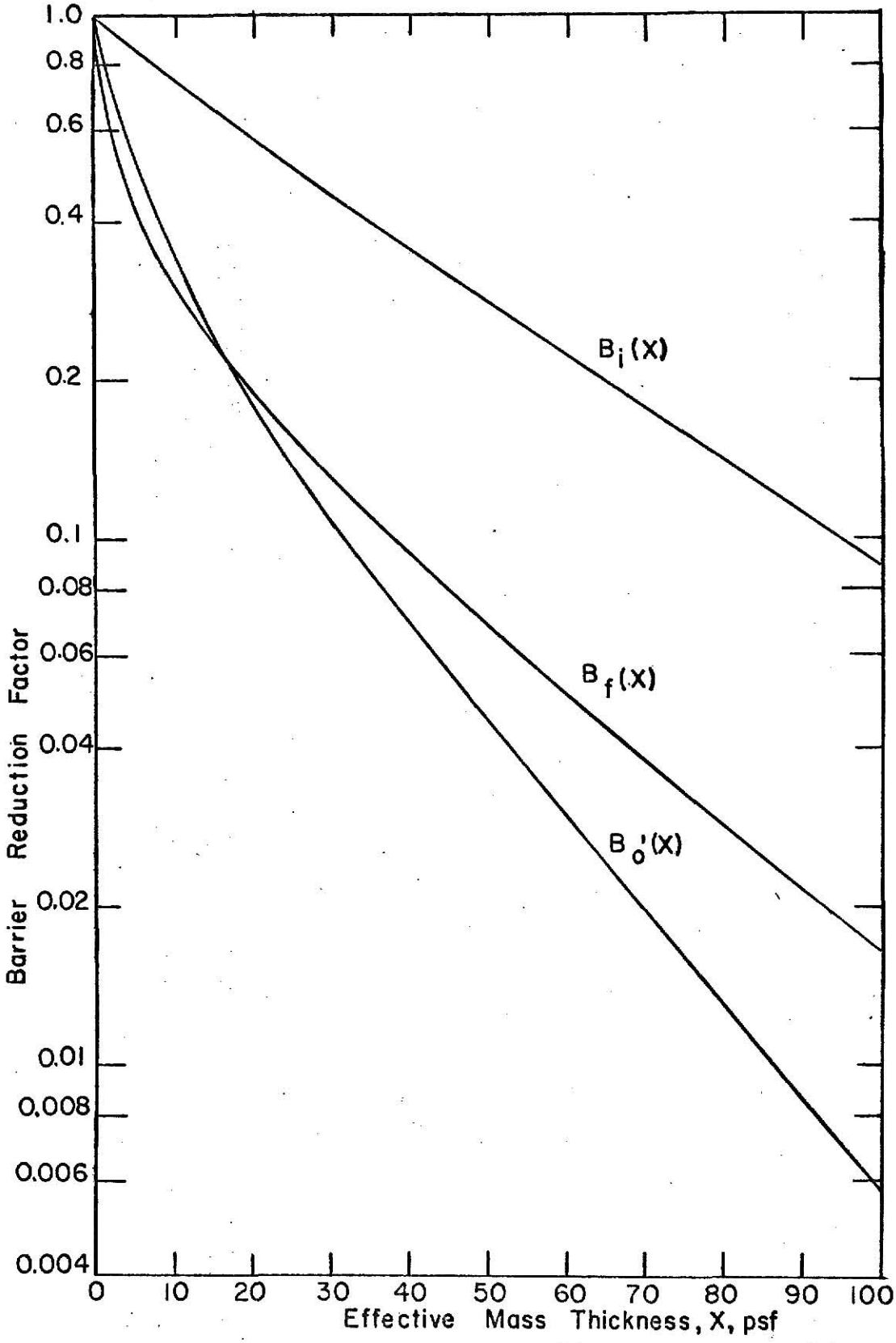

Figure B-1. The Engineering Manual functions $B_o'(X)$, $B_f(X)$, and $S_w(X)$ for ^{60}Co radiation.

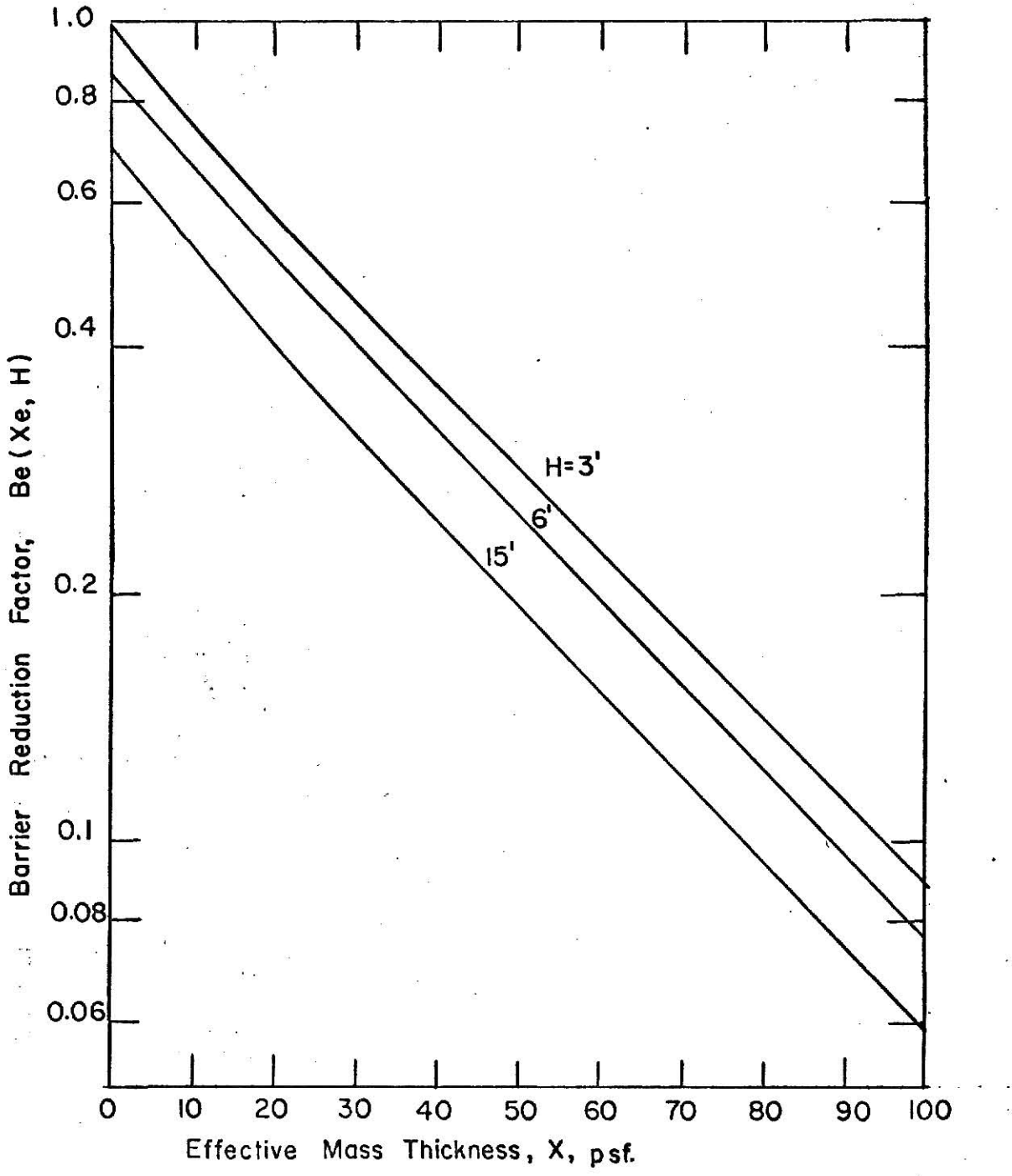

Figure B-2. The Engineering Manual function $B_e(X,H)$ for ^{60}Co radiation.

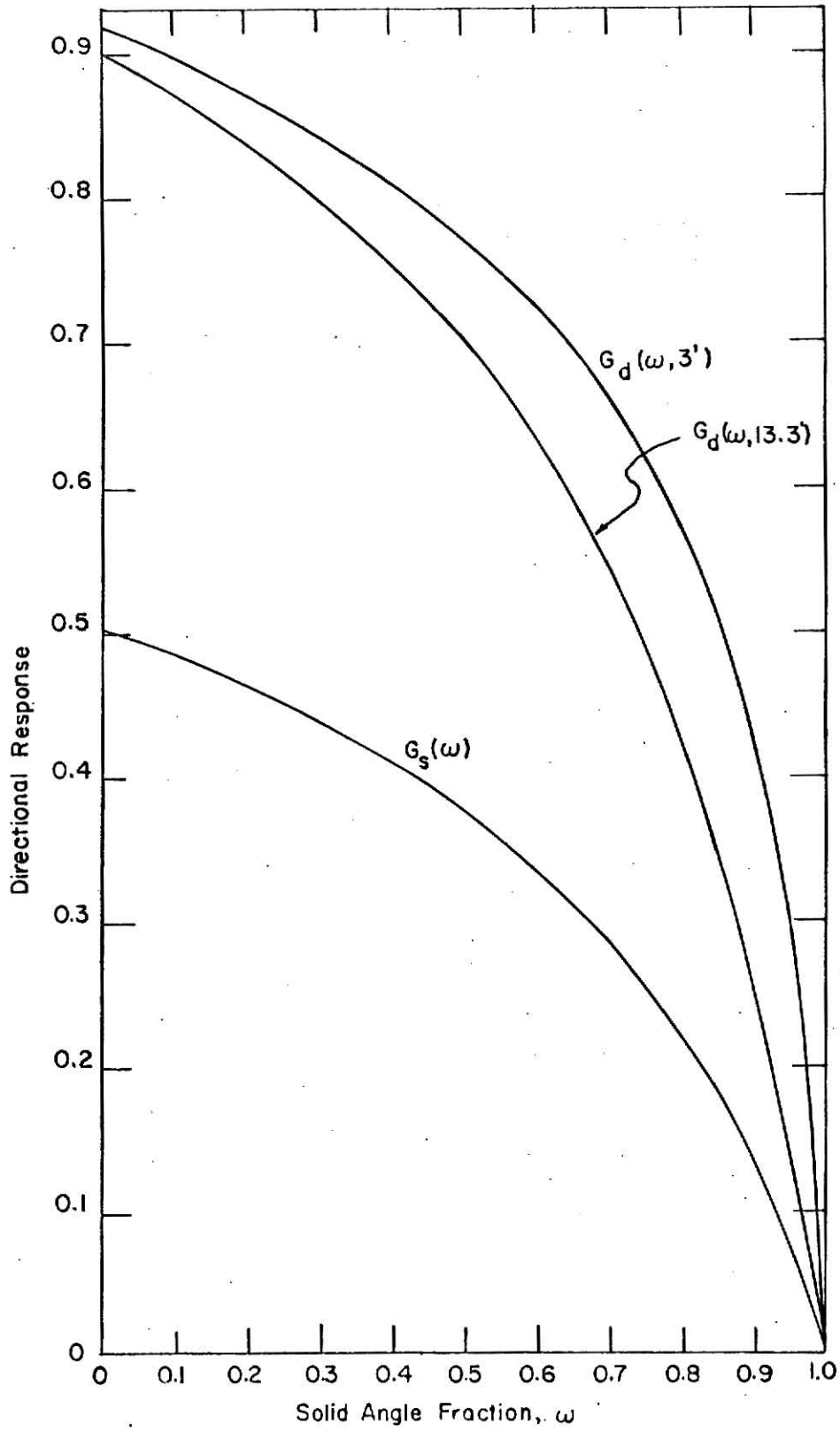

Figure B-3. The Engineering Manual functions $G_s(\omega)$ and $G_d(\omega,H)$ for ^{60}Co radiation.

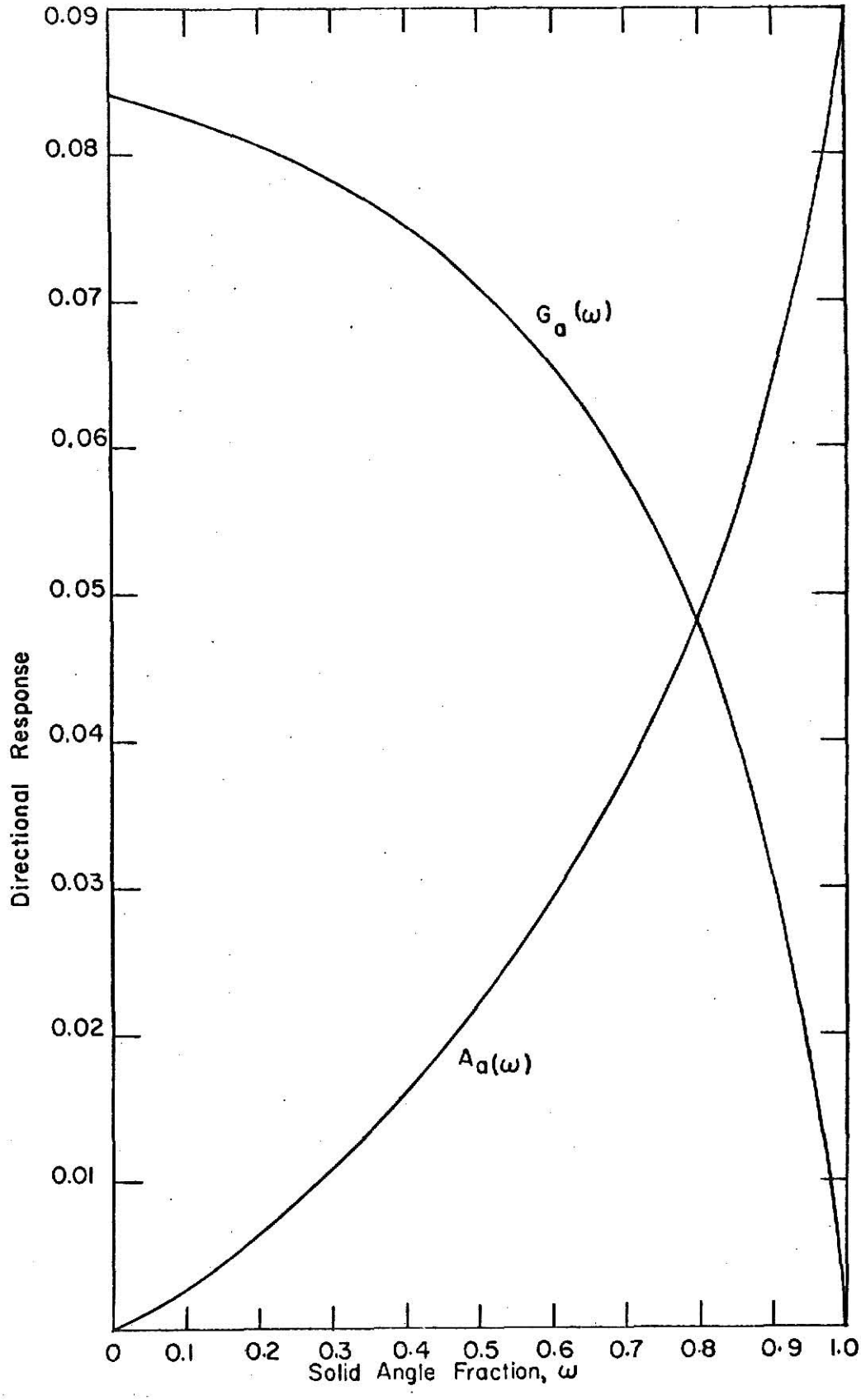

Figure B-4. The Engineering Manual functions $G_a(\omega)$ and $A_a(\omega)$ for ^{60}Co radiation.

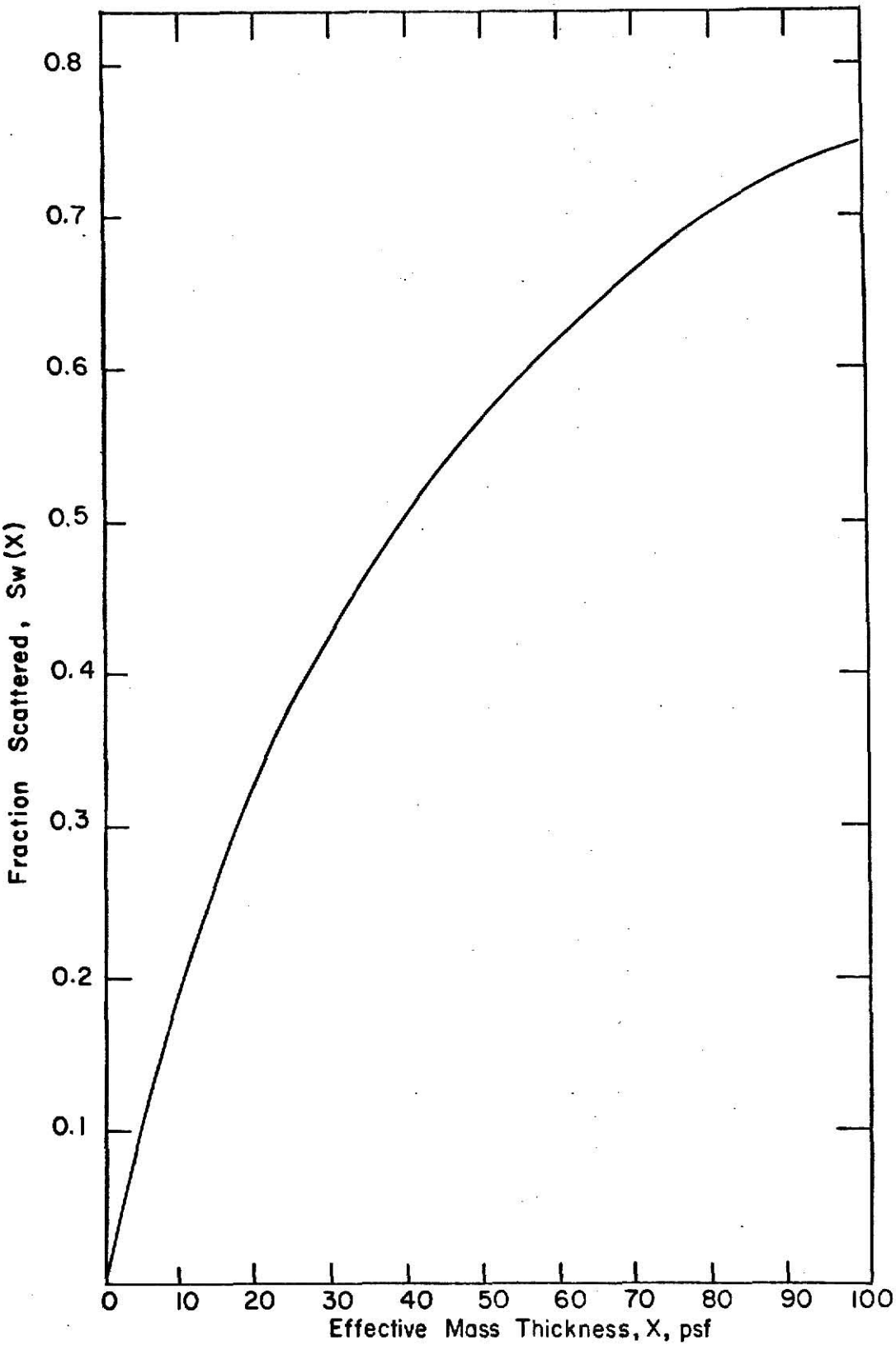

Figure B-5. The Engineering Manual function $S_w(X)$ for ^{60}Co radiation.

Table B-IV. Tabular ^{60}Co data for Engineering Manual functions $B'_o(X)$, $B_f(x)$, $B_i(X)$, and $S_w(X)$.

X(psf)	$B'_o(X)$	$B_f(X)$	$B_i(X)$	$S_w(X)$
0	1.0	1.0	1.0	0.0
5	0.54	0.43	0.870	0.110
10	0.350	0.305	0.757	0.199
15	0.245	0.240	0.662	0.272
20	0.180	0.193	0.585	0.330
25	0.139	0.160	0.516	0.382
30	0.109	0.131	0.458	0.429
40	0.070	0.095	0.360	0.505
50	0.0457	0.069	0.283	0.568
60	0.0298	0.051	0.224	0.620
70	0.0197	0.0382	0.179	0.665
80	0.0130	0.0288	0.141	0.702
90	0.0086	0.0218	0.112	0.731
95	0.0070	0.0188	0.100	0.741
100	0.0058	0.0164	0.089	0.749

Table B-V. Tabular ^{60}Co data for Engineering Manual function $B_e(X,H)$.

	$B_e(X,H)$		
X(psf)	H=3'	H=6'	H=15'
0	1.00	0.870	0.708
5	0.870	0.762	0.613
10	0.757	0.670	0.532
15	0.662	0.590	0.462
20	0.585	0.520	0.405
25	0.516	0.460	0.358
30	0.458	0.406	0.315
40	0.360	0.318	0.245
50	0.283	0.250	0.193
60	0.224	0.197	0.152
70	0.179	0.155	0.120
80	0.141	0.122	0.0945
90	0.112	0.0962	0.0743
95	0.0995	0.0851	0.0660
100	0.0885	0.0758	0.0585

Table B-VI. Tabular ^{60}Co data for Engineering Manual functions $G_s(\omega)$, $G_a(\omega)$, $A_a(\omega)$, and $G_d(\omega,3')$.

ω	$G_s(\omega)$	$G_a(\omega)$	$A_a(\omega)$	$G_d(\omega,3')$
0.0	0.500	0.0840	0.0	0.916
0.05	0.492	0.0834	0.0012	0.907
0.10	0.483	0.0826	0.0027	0.896
0.15	0.473	0.0816	0.0045	0.884
0.20	0.462	0.0806	0.0065	0.870
0.30	0.438	0.0782	0.0110	0.842
0.40	0.410	0.0751	0.0160	0.808
0.50	0.375	0.0709	0.0220	0.770
0.60	0.335	0.0655	0.0291	0.725
0.70	0.286	0.0583	0.0377	0.663
0.80	0.220	0.0476	0.0485	0.572
0.85	0.182	0.0409	0.0554	0.513
0.90	0.134	0.0310	0.0642	0.426
0.92	0.113	0.0263	0.0682	0.389
0.94	0.090	0.0213	0.0723	0.336
0.96	0.064	0.0156	0.0770	0.270
0.98	0.035	0.0086	0.0819	0.175
1.00	0.0	0.0	0.0880	0.0

Table B-VII. Tabular ^{60}Co data for Engineering Manual function $G_d(\omega,H)$.

	$G_d(\omega,H)$		
ω	H=3'	H=6'	H=15'
0.0	0.916	0.911	0.895
0.05	0.907	0.901	0.881
0.10	0.896	0.888	0.886
0.15	0.884	0.875	0.849
0.20	0.870	0.860	0.832
0.30	0.842	0.829	0.792
0.40	0.808	0.792	0.745
0.50	0.770	0.750	0.688
0.60	0.725	0.698	0.619
0.70	0.663	0.629	0.527
0.80	0.572	0.530	0.404
0.85	0.513	0.465	0.321
0.90	0.426	0.377	0.230
0.92	0.389	0.339	0.187
0.94	0.336	0.288	0.143
0.96	0.270	0.227	0.096
0.98	0.175	0.142	0.045
1.00	0.0	0.0	0.0

10.3 Appendix C: Calibration of the Dosimeters

This appendix describes briefly the experiment in which both types of dosimeters were calibrated. The equations used for determining the regression lines and associated statistics are cited but no derivation is given.

10.3.1 Experimental Procedure

The calibration experiment was conducted inside the instrument-storage building (a Butler-type building) at the KSUNESF. Two dosimeter racks were constructed of 1/2" plywood cut in the shape of a circular arc of radius 7 ft. Holes of 0.4" diameter were drilled in the racks with a spacing of four inches. The racks were suspended from the ceiling braces so that the centers of the racks were on opposite ends of the diameter of a circle of seven-feet radius. Each rack could accommodate up to twenty dosimeters of either type.

A point ^{60}Co source of nominally 0.3 Ci was used for the irradiations. The source was manipulated by means of a "gamma-ray projector." The projector consisted of a portable lead storage container with a flexible cable on one end of which the source was mounted. The cable was drawn through a flexible housing by a cranking mechanism which allowed the experimenter to stand some twenty-five feet from the storage container. When the source was fully exposed, it was located at the opposite end of the cable housing which also extended twenty-five feet from the storage container. By a system of lights on switches, the experimenter could tell whether the source was fully exposed, in an intermediate position, or stored.

When the dosimeters were in the racks and the tip of the source cable was positioned midway between the racks, the source-to-detector distance was seven feet with a maximum tolerance of $\pm$ 1/2". In this configuration the dosimeters received an approximate exposure-rate of 1 mR/min.

The exposure time was measured from the moment the source reached the fully exposed position to the moment the source was begun to be retracted. About two-thirds of the cable housing between the storage container and the exposed tip was shielded with lead bricks. However the dosimeters were still exposed to unwanted radiation as the source traveled from the storage container to the tip. This unwanted exposure was determined by measurement to be about 0.1/mR. Corrections were made for this in the data analysis.

The 10-mR chambers were charged to full voltage with the Tech/ops charger-reader and placed in the dosimeter rack. After irradiation they were recharged to full voltage while the meter on the charger-reader indicated a value proportional to the amount of charge neutralized by the ionizing radiation. The readings were recorded in microamperes. The exposure times varied from two to eight minutes.

The TL-12 dosimeters had to be zeroed by the read-out process before use since they were observed to accumulate a "background" dose of about 1 mR per day. There were 66 of these dosimeters and, as will be pointed out below, a separate regression line had to be determined for each. No less than ten exposures were taken for each dosimeter in the initial calibration. The exposure time varied from five to thirty-two minutes. The height of the glow curve was recorded for each reading in units of the scale divisions on the strip charts.

Since the response of the air-equivalent chambers is proportional to the density of the surrounding air medium, the chamber readings were normalized to the air density at 22° C and 760 mm of Hg. This was accomplished by multiplying the readings by an air-density correction factor β, given by

$$\beta = \frac{760(273 + T)}{295\ P} \qquad \text{(C-1)}$$

where T is the temperature in degrees centigrade and P is the pressure in millimeters of Hg.

10.3.2 Calculated Exposure Rate

The calculated exposure rate θ was determined from the following formula:

$$\theta = \frac{KS_c B e^{-\mu x} e^{-\lambda d}}{4 \pi x^2} ; \qquad \text{(C-2)}$$

where K = flux-to-dose conversion factor [$mR \cdot cm^2$ sec/min],

S_c = calibration source strength at the time of the source calibration [photons/sec],

B = dose build-up factor for air-scattering and floor reflection,

μ = total linear attenuation coefficient for 1.25 MeV photons in air [cm^{-1}],

d = time between the source calibration and the dosimeter calibration [days],

x = source to detector distance [cm],

λ = decay constant for ^{60}Co [$days^{-1}$].

One roentgen corresponds to an absorbed dose of 87.7 erg/g in air [16]. The absorbed dose rate from a unit flux of ^{60}Co photons is given by

$$\text{absorbed dose rate} = E_\gamma \hat{\mu}_d (E_\gamma) \phi_\gamma = 5.32 \times 10^{-8} \text{ [erg/g} \cdot \text{sec]}$$

where E_γ = 1.25 MeV = 2.00×10^{-6} erg,

$\hat{\mu}_d(E_\gamma)$ = 0.0266 cm^2/g, the linear attenuation coefficient for energy absorption of 1.25 MeV photons in air, divided by the density of air [17],

ϕ_γ = unit flux of 1.25 MeV photons [photon/sec·cm^2].

This absorbed dose rate would correspond to an exposure rate (for a unit flux) given by,

$$\text{exposure rate} = (5.32 \times 10^{-8} \text{ erg/g·sec})\ (1\text{R}/87.7 \text{ erg/g})\ (60\text{sec/min})$$
$$= 3.65 \times 10^{-8} \text{ R/min.}$$

The conversion factor K becomes

$$K = 3.65 \times 10^{-5} \text{ mR} \cdot \text{cm}^2 \cdot \text{sec/min},$$

which gives the exposure rate when multiplied by the flux in photons/ cm^2·sec.

The calibration source was calibrated in a previous experiment which yielded the following source strength as of August 10, 1965 [12];

$$S_c = 0.246 \pm 0.007 \text{ Ci}$$
$$= 1.82 \times 10^{10} \text{ photons/sec.}$$

There are two other contributions to the radiation incident on the detector besides the unscattered radiation. These are the radiation due to air scattering and the radiation which is reflected from the concrete floor. The build-up factor must therefore have the form

$$B = 1 + \frac{D_{\text{air scat.}}}{D_{\text{unscat.}}} + \frac{D_{\text{floor ref.}}}{D_{\text{unscat.}}}.$$

The first ratio is found from an expression for the build-up factor for a point source in an infinite air medium [18].

$$\frac{D_{\text{air scat.}}}{D_{\text{unscat.}}} = 0.92\ r\ e^{0.0632\ r} = 0.0135;$$

where $r = \mu x = \hat{\mu}\rho x = 0.0146$,

$\hat{\mu} = 0.0573$ cm^2/g,

$\rho = 0.001195\ g/cm^3$ (This is an average value for the atomospheric conditions observed during the experiments),

$x = 213.36\ cm = 7ft.$

The second ratio was taken from a report in which are tabulated the values of the ratios of the reflected dose rates for a source and detector in vacuum adjacent to a semi-infinite concrete slab [19]. The values are tabulated as a function of the source height and photon energy. The value for a source and detector six feet above a concrete slab and for 1.25MeV photons was taken to be 0.018. Hence,

$$B = (1 + 0.0135 + 0.018) = 1.032.$$

The attenuation in air is given by

$$e^{-\mu x} = e^{-\hat{\mu}\rho x} = 0.9855.$$

The product $Be^{-\mu x}$ has the value 1.017, and varied by less than 0.001 for any atmospheric changes observed during the experiments.

The decay constant for ^{60}Co in day^{-1} is given by

$$\lambda = \frac{\ell n\ 2}{(5.24)(365)} = 0.0003624\ day^{-1}.$$

When all these definitions as substituted into Eq. (C-2), the result is

$$\theta = \frac{(3.65\times10^{-5})(1.82\times10^{10})(1.017)\ e^{-0.0003624d}}{4\ \pi\ (213.36)^2} \qquad (C\text{-}3)$$

$$= 1.181\ e^{-0.0003624d}\ \ mR/min;$$

where the reference date for d is August 10, 1965.

10.3.3 Regression Analysis

It was assumed that the dosimeter response η is related to the true exposure ξ by the equation $\eta=\beta\xi$ and that the observations y_i are distributed normally about η. It was also assumed that there was no error in the calculated exposures. This was not exactly true since there was about a 0.5 percent uncertainty in the source-to-detector distance and some uncertainty in the exposure time (about one percent for two minutes and proportionately less for longer times.) However, these errors are considered as an additional spread in the observations. Although there was a 3.0 percent error in the calibration source strength S_c, this was a constant, rather than a random, error. It was treated as a systematic error, and its propagation is discussed in Appendix D.

For a given dosimeter, a set of k dosimeter readings; $y_1, y_2, \ldots y_k$, corresponding to the calculated exposures; $x_1, x_2, \ldots x_k$, was obtained by the procedure described above. The data were fitted by a least-squares line through the origin. The least-squares estimator b for the true value β is given by

$$b = \frac{\sum x_i \; y_i}{\sum x_i^2} \qquad \text{(C-4)}$$

where the summation symbol implies summation over i from one to k. To use the regression line in reverse, i.e., to determine the true exposure ξ from some new observation y', the observed reading is divided by the slope b. An estimate of the standard deviation s_ξ, is obtained from

$$s_\xi^2 = \frac{1}{b^2} \left[\sum y_i^2 - \frac{(\sum x_i \; y_i)^2}{\sum x_i^2} \right] \left[1 + \frac{y'^2}{b^2 \sum x_i^2} \right]. \qquad \text{(C-5)}$$

Eqs. (C-4) and (C-5) are taken from Brownlee [20].

10.3.4 Results

A sample of ten 10-mR chambers was used to determine if the responses of individual dosimeters were different. Eight readings were obtained from each dosimeter at various exposure times. A regression line was obtained for each dosimeter, and the slopes of each were compared. There was no significant difference in the results. On this basis one regression line was obtained from the data from all chambers.

The responses of the TL-12 dosimeters were quite different from one dosimeter to the next. A separate regression line was determined for each dosimeter. The slopes of the various regression lines varied by as much as fifteen percent from the average of all 66 dosimeters.

Figures C-1 and C-2 show the precision which could be expected in the readings from both types of dosimeters.

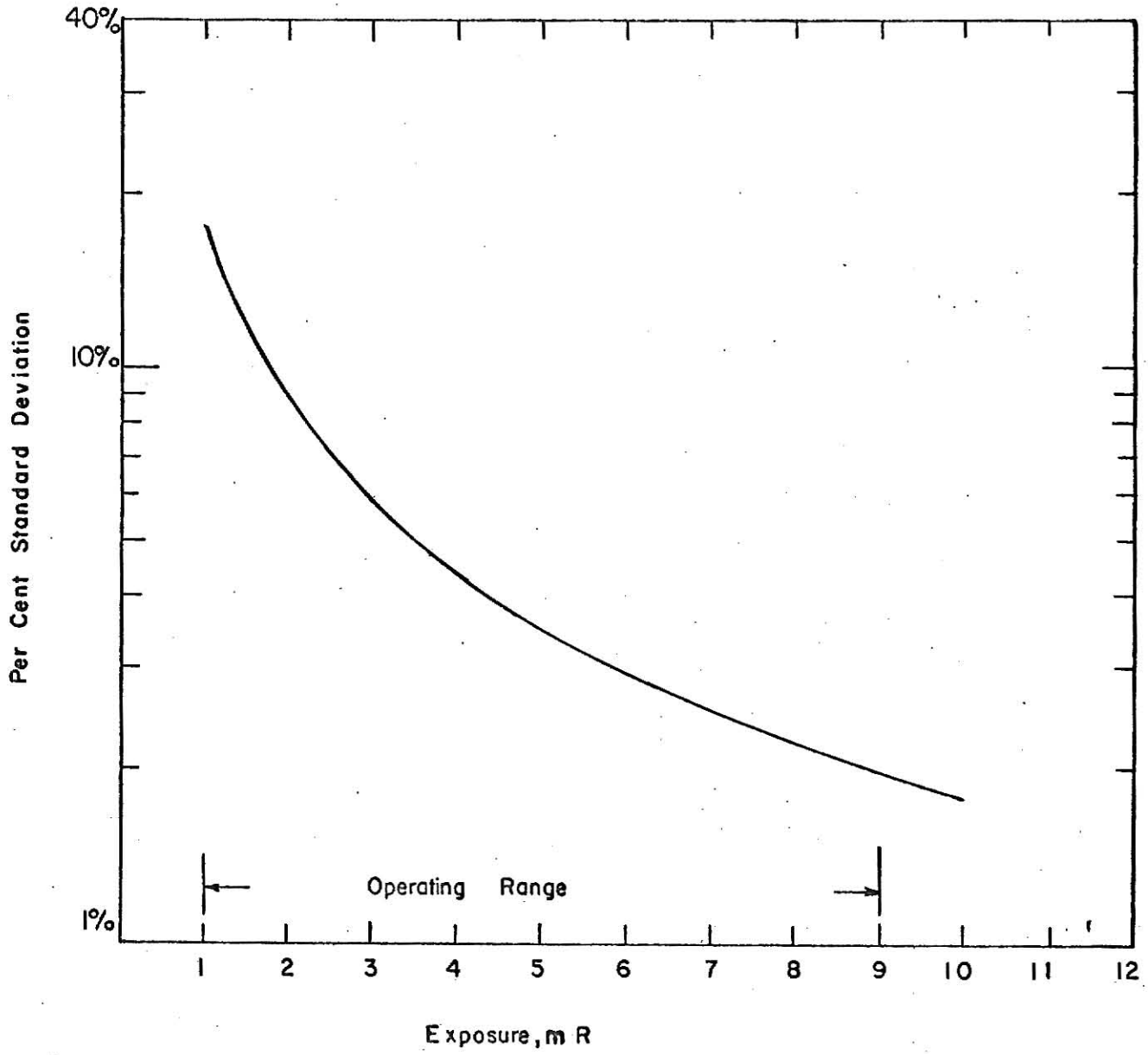

Figure C-1. Observed precision for the 10-mR ionization chambers.

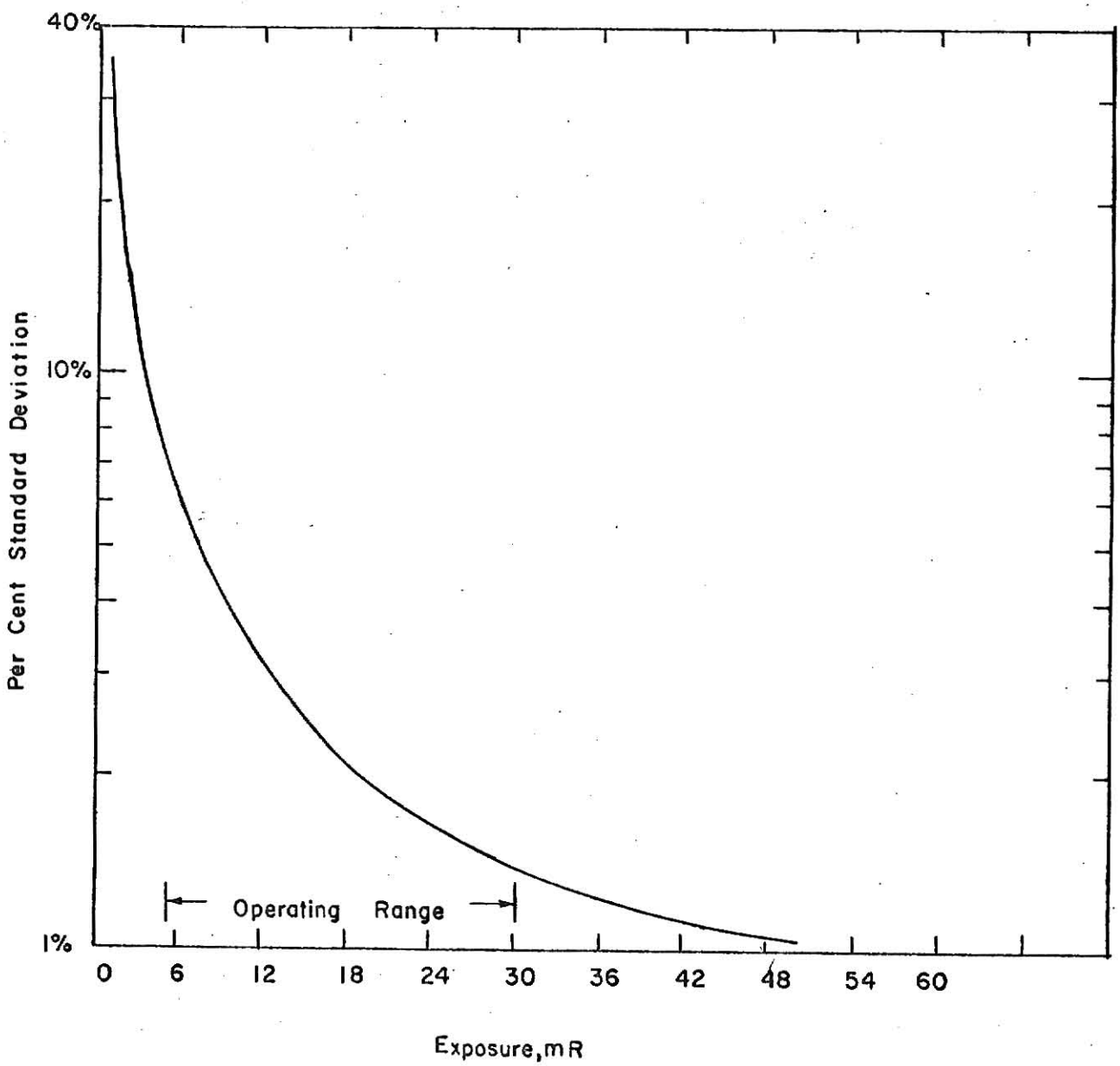

Figure C-2. Observed precision for a typical TL-12 dosimeter.

10.4 Appendix D: Data Reduction and Statistics

This appendix details all steps used in the reduction of the data. The propagation of all significant errors is fully discussed.

A brief review of the experimental procedure is necessary in order to understand the data reduction process. Calibration curves (regression lines) were determined for the dosimeters as described in Appendix C. An experiment in the test house consisted of placing the dosimeters in the house, circulating the pumped source in one of the three tubing areas of the test field, and reading and recording the accumulated doses. Generally, each experiment, or run, was repeated three times for each tubing area.

The first step in the data reduction is to convert the reading from each dosimeter D_m to a corrected exposure D_c in milliroentgens. This is done by dividing the dosimeter reading by the slope b, from Eq. (C-4), of the regression line for the dosimeter. An estimate of the standard deviation s_{D_c} is determined from Eq. (C-5). For the 10-mR chambers, the reading D_m is first multiplied by β, from Eq. (C-1), to correct for the density of air at the time of the measurement. The corrected dose is then converted to a reduction factor Q, for one-quarter symmetry, according to the following formula:

$$Q = \frac{A}{S_p T} \frac{D_c}{D_o} \qquad \text{(D-1)}$$

where A is the tubing area in square feet used in the run, S_p is the source strength in curies of the pumped source used in the run, T is the time in hours which elapsed while the source traversed the tubing area, and D_o is the reference dose rate. The value of D_o is taken to be 480×10^3 mR/hr for a point

located three feet in air from an air-ground interface at 22°C and 760 mm of Hg. The interface is the source plane with an intensity of one curie per square foot [14].

The factors A, T, and D_o are assumed to be without error. The fact that D_o may not be known accurately is irrelevant to the consideration of experimental errors. If one compares the results of these experiments with theory or with other experiments, the uncertainty in this factor is eliminated by normalizing both sets of data to the same reference dose rate. The corrected dose contains the factor S_c the calibration source strength, see Eq. (C-4), which has an associated standard deviation s_{S_c} which has not been included in s_{D_c}. Similarly the pumped source has an associated standard deviation in s_{S_p}. These are systematic errors and should not be propagated along with the random errors in the intermediate steps of the data reduction. It should be noted that the factor S_c/S_p is present and separable in all succeeding values in the data reduction. The standard deviation, not including source uncertainties, for the value Q is

$$s_Q = \frac{A}{S_p T D_o} s_{D_c}. \tag{D-2}$$

Since each experiment was repeated a number of times in the three tubing areas, the subscripts i and j are assigned to Q to differentiate the results of the various runs. The first subscript refers to the tubing area, while the second subscript refers to one of a series of runs from the same tubing area. Thus, Q_{ij} refers to the jth run in the ith tubing area. An average value $\bar{Q}_i$ is determined according to

$$\bar{Q}_i = \frac{1}{n} \sum_{j=1}^{n} Q_{ij} \tag{D-3}$$

where n is the number of times an experiment was repeated in the same area.

As an estimate of the standard deviation of $\bar{Q}_i$, one might use the formula

$$s'^2_{\bar{Q}_i} = \frac{1}{n^2} \sum_{j=1}^{n} s^2_{Q_{ij}}, \qquad \text{(D-4)}$$

since $s_{Q_{ij}}$ is the estimate of the standard deviation on each value Q_{ij}. However, the only uncertainty used to obtain $s_{Q_{ij}}$ was s_{D_c} which is a measure of the randomness of the dosimeter readings in the calibration experiment. In the experiments in which values of Q_{ij} were determined, a number of new variables were introduced which were not controllable and may have varied from one run to the next. Generally, the results from runs in the same area agreed within the precision indicated by $s_{Q_{ij}}$. There was, however, in some cases such poor agreement among the Q_{ij} that the validity of the $s_{Q_{ij}}$ was suspect; i.e., cases where, say, in comparing runs k and l that $Q_{ik} + 2s_{Q_{ik}} < Q_{il} - s_{Q_{il}}$, or in other cases where $Q_{ik} + s_{Q_{ik}} < Q_{il} < Q_{im} - s_{Q_{im}}$. To account for the spread of the data in those cases, another term is added to $s'_{\bar{Q}_i}$ to give a better estimate of the standard deviation on the average:

$$s^2_{\bar{Q}_i} = s'^2_{\bar{Q}_i} + \frac{1}{n(n-1)} \sum_{j=1}^{n} (Q_{ij} - \bar{Q}_i)^2. \qquad \text{(D-5)}$$

Reduction factors for full symmetry R_i are obtained by summing, over the symmetric points in each quadrant, the average values of the reduction factors for one-quarter symmetry. For a general off-center location, this sum is represented by

$$R_i = \bar{Q}_i^{NE} + \bar{Q}_i^{SE} + \bar{Q}_i^{SW} + \bar{Q}_i^{NW}, \qquad \text{(D-6)}$$

where the superscripts differentiate the four quadrant points. For a location along the east-west (north-south) center line of the house, the following formula is used:

$$R_i = 2\,[\bar{Q}_i^{N} + \bar{Q}_i^{S}] \quad (R_i = 2\,[\bar{Q}_i^{E} + \bar{Q}_i^{W}]\,), \qquad \text{(D-7)}$$

where the superscripts differentiate the symmetric points on the respective centerlines. The full-symmetry value for a point along the vertical centerline is just four times the quarter-symmetry value. The estimates of the standard deviation $s_{\bar{Q}_i}$ are propagated accordingly to obtain s_{R_i}.

The method used to obtain the far-field reduction factor R_f and its associated standard deviation s_{R_f} is detailed in Appendix E. It should be noted that the ratio S_c/S_p can be factored from R_f, see Eqs. (E-2), (E-9), and (E-10). The total experimental reduction factor R_T is given by

$$R_T = R_f + \sum_{i=1}^{3} R_i, \qquad \text{(D-8)}$$

and the estimate of the variance by

$$s_{R_T}^2 = s_{R_f}^2 + \sum_{i=1}^{3} s_{R_i}^2. \qquad \text{(D-9)}$$

The estimate s_{R_T} indicates the precision of the experimental values. It may be used in comparing values from similar experiments using the sources S_c and S_p. However, if one wishes to compare these results with theoretical values or values obtained from experiments using different sources, the systematic

error in the source strengths must be included. The standard deviation in the final results, including the systematic errors, is labeled σ_{R_T} even though it is an estimate. This value is obtained from the preceding values according to the following derivation:

$$R_T = \frac{S_c}{S_p} \hat{R}_T \tag{D-10}$$

$$s_{R_T} = \frac{S_c}{S_p} s_{\hat{R}_T} \tag{D-11}$$

$$\sigma^2_{R_T} = R_T^2 \left[\left(\frac{s_{S_c}}{S_c}\right)^2 + \left(\frac{s_{S_p}}{S_p}\right)^2 + \left(\frac{s_{\hat{R}_T}}{\hat{R}_T}\right)^2 \right] \tag{D-12}$$

$$= R_T^2 \left[\left(\frac{s_{S_c}}{S_c}\right)^2 + \left(\frac{s_{S_p}}{S_p}\right)^2 \right] + s^2_{R_T} .$$

All uncertainties quoted in this work refer to this value, σ_{R_T}.

10.5 Appendix E: Far Field Contribution and Associated Statistics

Since measurements could only be obtained from a simulated contaminated field of finite radius, the contribution from the contaminated area beyond that radius (to infinity) has to be estimated. This estimate is referred to as the far-field, or far-field contribution. The method of Kaplan [13] was used to obtain the far-field contribution. A basic description of this method and a means for estimating the uncertainty in the far-field is given here.

10.5.1 Theory

Kaplan's method is based on the equation

$$R_i = \alpha_D D_i + \alpha_S S_i \qquad \text{(E-1)}$$

where R_i is the measured dose rate from the ith annular area in the contaminated plane; α_D and α_S are the structure attenuation coefficients for the direct and skyshine radiation, respectively; and D_i and S_i are the direct and skyshine free-field dose rates, respectively. A free-field dose rate is defined here as the dose rate that is obtained from an unshielded detector which is three feet above the center of the source annulus. These numbers can be obtained from theoretical calculations. Direct radiation refers to unscattered plus up-scattered radiation with respect to the detector. The structure attenuation coefficients are simply quantities which satisfy the equation. Although the quantities R_i, α_D, and α_S are functions of the detector position inside the structure, it is assumed that one particular location is under consideration; therefore no functional dependence is indicated.

The fundamental assumption of the method is that the quantities α_D and α_S are invariant with respect to the dimensions of the source annulus. Kaplan states

that this is true as long as the separation between the source and the structure is greater than the dimensions of the structure. If one has measurements from at least two annular source areas, then, under this assumption the quantities α_D and α_S can be determined from Eq. (E-1). With these values the far-field contribution R_f is given by

$$R_f = \alpha_D D_f + \alpha_S S_f; \qquad \text{(E-2)}$$

where D_f and S_f are the free-field dose rates from the far-field area.

If each term in Eqs. (E-1) and (E-2) is divided by the reference dose rate D_o, then α_D and α_S relate the measured reduction factors to the free-field reduction factors. In this work, reduction factors rather than dose rates are dealt with.

10.5.2 Calculations

The values α_D and α_S are computed from a system of three equations of the form of Eq. (E-1) corresponding to the three source annuli:

$$\begin{aligned} R_1 &= \alpha_D D_1 + \alpha_S S_1 \\ R_2 &= \alpha_D D_2 + \alpha_S S_2 \qquad \text{(E-3)} \\ R_3 &= \alpha_D D_3 + \alpha_S S_3 \ . \end{aligned}$$

The left hand side of each equation has an independently determined variance $s^2_{R_i}$. In the determination of the variances of α_D and α_S, it is desirable to have a set of data in which all points have the same variance. Since one point with variance σ^2 is equivalent to n points with variances $n\sigma^2$, a set of weighting factors is obtained which will transform the system of equations into an

equivalent set in which the left-hand side of each equation has equal variance. The weighting factor for the ith equation is given by

$$W_i = \frac{\prod_{i=1}^{3} s_{R_i}}{s_{R_i}} \tag{E-4}$$

The weighted equations are of the form

$$\hat{R}_i = \alpha_D \hat{D}_i - \alpha_S \hat{S}_i ; \tag{E-5}$$

where $\hat{R}_i = w_i R_i$, $\hat{D}_i = w_i D_i$, and $\hat{S}_i = w_i S_i$. The variance of each member of the left hand side of the weighted equations is

$$\hat{s}_R^2 = \prod_{i=1}^{3} s_{R_i}^2 . \tag{E-6}$$

In matrix notation the system can be written as $\bar{\bar{R}} = \bar{\bar{A}}\ \bar{X}$; where $\bar{\bar{R}}$ is the three-element vector of measured reduction factors, $\bar{\bar{A}}$ is the three-by-two matrix of free-field reduction factors, and $\bar{X}$ is the two-element vector of unknowns. The least squares solution of the overdetermined system is given by

$$\bar{X} = (\bar{\bar{A}}^T \bar{\bar{A}})^{-1} \bar{\bar{A}}^T \bar{\bar{R}}. \tag{E-7}$$

The expressions for α_D and α_S, the elements of $\bar{X}$, can be written in terms of the elements of $\bar{\bar{A}}$ and $\bar{\bar{R}}$ with the aid of the following definition:

$$\gamma = 1/\ [\ \sum \hat{D}_i^2 \sum \hat{S}_i^2 - (\sum \hat{D}_i\ \hat{S}_i)^2] \tag{E-8}$$

where the summation symbol implies summation over i from one to three.

$$\alpha_D = \gamma[\sum \hat{S}_i^2 \sum \hat{D}_i\ \hat{R}_i - \sum \hat{D}_i\ \hat{S}_i \sum \hat{S}_i\ \hat{R}_i] \tag{E-9}$$

$$\alpha_S = \gamma[\sum \hat{D}_i^2 \sum \hat{S}_i \hat{R}_i - \sum \hat{D}_i \hat{S}_i \sum \hat{D}_i \hat{R}_i] \qquad \text{(E-10)}$$

From the principle of maximum likelihood, it can be shown that the variance of the estimators α_D and α_S are the diagonal elements of the matrix $(\bar{\bar{A}}^T \bar{\bar{A}})^{-1}$ times the variance $\hat{s}_R^2$ [21]. Explicitly, these values are

$$s_{\alpha_D}^2 = \hat{s}_R^2 \gamma \sum \hat{S}_i^2 \qquad \text{(E-11)}$$

$$s_{\alpha_S}^2 = \hat{s}_R^2 \gamma \sum \hat{D}_i^2. \qquad \text{(E-12)}$$

The estimate of the far-field is then determined from Eq. (E-2). The variance of R_f is obtained by propagation of the s_{α_D} and s_{α_S}:

$$s_{R_f}^2 = D_f^2 s_{\alpha_D}^2 + S_f^2 s_{\alpha_S}^2. \qquad \text{(E-13)}$$

The free field reduction factors were determined from moments method calculations of Rubin [12]. The numbers used are tabulated below:

Annulus	Inner radius	Outer radius	D	S
1	19'*	80'	0.2513	0.007662
2	80'	125'	0.07246	0.005791
3	125'	169'	0.04608	0.005381
f	169'	∞	0.2017	0.06433

*Since, in the actual test field, the inner boundary of the first tubing area was a 30' × 40' rectangle, an effective radius for this area was determined. It was defined as the radius of the disk which subtends the same solid angle as the rectangular area at a height of three feet above the center.

Using the data from the first tubing area apparently violates the condition that the source should be a distance away from the structure at least as large as the dimensions of the structure. However, after some initial calculations, it was decided that the inclusion of this data helped to balance the effects of random errors in the data from the second and third areas. Two sets of the values α_D and α_S were computed for a number of detector locations. One set was determined from the first two equations of Eqs. (E-3), while the other set was determined from the last two equations of Eqs. (E-3). The discrepancies between the two sets of values seemed to be random which indicated that no systematic error was introduced by including the data from the first area.

A COMPARISON OF THEORETICAL AND EXPERIMENTAL REDUCTION FACTORS FOR LOCATIONS IN THE BASEMENT OF A TYPICAL HOUSE

by

CHARLES ARTHUR BURRE

B.S., University of Kansas, 1967

AN ABSTRACT OF

A MASTER'S THESIS

submitted in partial fulfillment of the

requirements for the degree

MASTER OF SCIENCE

Department of Nuclear Engineering

KANSAS STATE UNIVERSITY

Manhattan, Kansas

1970

ABSTRACT

This work is a study of the reduction factor for fallout radiation at points in the basement of a typical house. The Engineering Manual theory for determining the reduction factor is discussed along with the proposed modifications of French, Kaplan, and Batter and Starbird. A 30 ft × 40 ft test house has been constructed at the Kansas State University Nuclear Engineering Shielding Facility. The design of the house is discussed and a computer code which can perform reduction factor calculations for the test house is presented.

The reduction factor was measured at nineteen locations in the basement for two wall thicknesses (5.5 and 45.5 psf) of the test house. The fallout field was simulated out to a radius of 169 ft with a point ^{60}Co source and a hydraulic source-circulation system. Exposures were measured with air-equivalent ionization chambers and thermoluminescent detectors.

With the exception of the original Engineering Manual theory, the various methods yielded similar results for the calculated reduction factors. The agreement between the magnitudes of the theoretical and experimental reduction factors was within a factor of two. However, the variation of the measured reduction factors with the distance below the basement ceiling was incorrectly predicted by all theoretical methods.